A Modified Adaptive Hill Climbing Maximum Power Point Tracking (MPPT) Control Method For Photovoltaic Power Systems

Weidong Xiao

BESc., Shenyang Polytechnic University, 1991

A THESIS SUBMITTED IN PARTIAL FULFILLMENT OF THE REQUIREMENTS FOR THE DEGREE OF

MASTER OF APPLIED SCIENCE

in

The Faculty of Graduate Studies

Department of Electrical and Computer Engineering

We accept this thesis as conforming

to the required standard

THE UNIVERSITY OF BRITISH COLUMBIA

July 2003

Department of electrical and computer Engineering

The University of British Columbia
Vancouver, Canada

Date July, 11, 2003

Abstract

A powerful attraction of photovoltaic (PV) power systems is that they produce electric power without harming the environment, by directly transforming a free inexhaustible source of energy, solar irradiation, into electricity. This fact, together with the continuing decrease in PV array cost and increase in efficiency, implies a promising role for PV generation systems in the near future.

The study started with the requirement that photovoltaic power systems should be integrated with specific control algorithms to deliver maximum possible power. In this thesis, the PV power system was introduced at the beginning, and a simple maximum power point tracking (MPPT) system was presented and analyzed. Next, different existing MPPT control approaches were discussed and a proposed control algorithm, namely modified adaptive hill climbing (MAHC) method, was introduced. Then, the results of simulation proved that the performance could be improved in both transient and steady state of the suggested control system. Finally, a simple test bed system with digital signal processor (DSP) was designed and implemented with optimized control software to verify the proposals.

Table of Contents

List of Figures

List of Tables

Acknowledgements

First of all, I would express my sincere gratitude to my advisor, Dr. William G. Dunford. His kind guidance, thorough comments and constant support have made it possible for me to make my dissertation complete. In 2002, he helped me to setup a small photovoltaic power system at home for research.

During my M.A.Sc program, I have been associated with my colleagues working in a research group. I would like to thank Victor Goncalves, P.Eng, the director of engineering department, who gave me a great opportunity to further my study in this area.

I would like to show my great appreciation to my wonderful parents, brother and sisters for their encouragement and support until I obtain this degree. I want to dedicate this dissertation to my wife, June, and my 8-month-old baby, William.

Chapter 1 Introduction

As energy needs are growing around the world, humanity tends to outgrow the fossil energy capacities. In order to satisfy the increasing demand, alternative energy resources have become an important issue for our time.

1.1 Solar Energy

Solar energy is important because of the benefits it provides. The key benefits are:

- Environmental Benefits
  - No noise
  - No pollution
- Energy for human's future
  - Renewable
- Energy independence
  - Solar energy comes directly from natural sunlight
- Acceptable application price

1.2 Photovoltaic

Photovoltaic (PV) converts sunlight directly into electricity, shown in Figure 1.1.

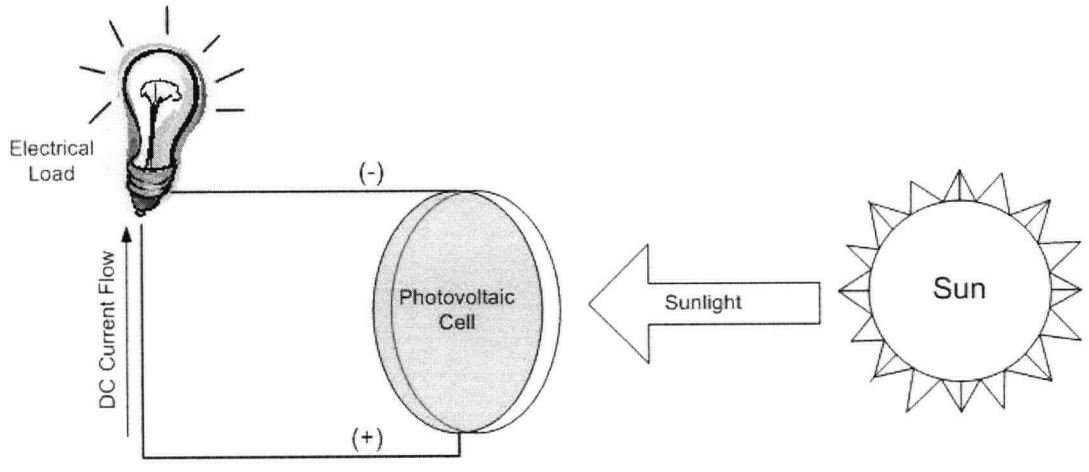

Figure 1.1 How Photovoltaic Works

PV cells are made of semi-conducting materials similar to those used in computer chips. When these materials absorb sunlight, the solar energy knocks electrons loose from their atoms, allowing the electrons to flow through the material to produce electricity [1].

1.3 Maximum Power Point Tracking

The performance of a PV cell or array is measured in terms of its efficiency at turning sunlight into electricity [2]. Only sunlight of certain energies will work efficiently to create electricity, and much of it is reflected or absorbed by the material that makes up the cell [2].

Every photovoltaic cell or module has an optimal operating point, called the maximum power point (MPP), which varies depending on cell temperature and present insolation level. Figure 1.2 shows a typical *current-voltage* curve to represent PV cell's output characteristics under a certain cell temperature and solar insolation level. Maximum power point is the operating point *A*, as shown in this figure, at which the power delivered by PV cell is maximum: $P_{max} = I_A * V_A$. Ideally, the PV cell is operated exactly at this point to guarantee maximum power output.

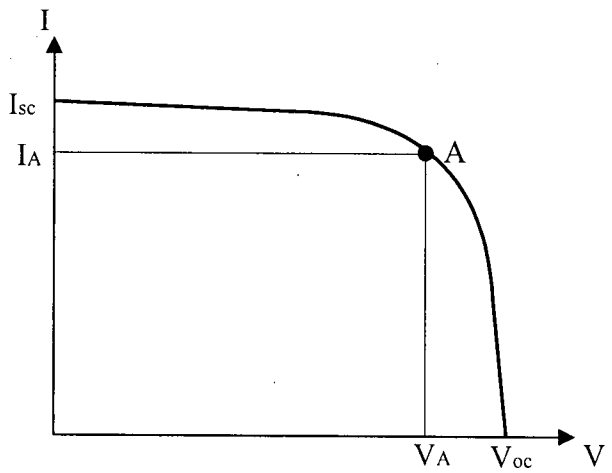

Figure 1.2 Typical Current-Voltage Curve of PV Cell Output

Maximum Power Point Tracking, frequently referred to as MPPT, is a control system that frequently adjusts the electrical operating point of the modules so that the photovoltaic modules are able to deliver maximum available power. Additional solar power extracted from the modules is made available to increase load consumption power.

The goal of this thesis is to find the effective MPPT control algorithm better suited for employment in extracting the maximum possible power from the PV modules. A MPPT control algorithm, namely modified adaptive hill climbing method (MAHC) will be introduced and evaluated. The other chapters will support to better-understand this dissertation and are organized as follows:

Chapter 2 covers a broad range of background knowledge and mathematical models of photovoltaic modules and switching mode DC/DC buck converters. Chapter 3 is a survey on a wide variety of existing MPPT techniques.

Chapter 4 discusses the possible modification and improvements on one available MPPT technology, adaptive hill climbing method (AHC). A modified adaptive hill climbing (MAHC) MPPT control algorithm will be presented in this section in detail.

In Chapter 5, the MPPT power system is modeled with Simulink® and the performance of proposed control algorithm is evaluated. Chapter 6 includes hardware and software design of a simple PV power system. This system is used as a test bed for verification of different MPPT control algorithms.

Conclusions and recommendations will be given in Chapter 7. Appendix A represents the comparison between different existing MPPT techniques. Appendix B gives some additional experimental results.

Chapter 2 The Photovoltaic Power Systems

Although a PV array produces electric power when exposed to sunlight, other components are required to properly conduct, control, convert, distribute, and store the energy produced by the array. They are photovoltaic power systems.

2.1 The Photovoltaic Power Systems

Photovoltaic power systems are generally classified according to their functional and operational requirements, their component configurations, and how the equipment is connected to other power sources and electrical loads. The two principal classifications are stand-alone systems and grid-connected or utility-interactive systems. [3]

2.1.1 Stand-Alone Systems

Stand-alone PV systems are designed to operate independent of the electric utility grid, and are generally designed and sized to supply certain DC and/or AC electrical loads. In some remote areas, they may be more cost-effective than extending power lines.

2.1.2 Grid-connected Systems

Grid-connected or utility-interactive PV systems are designed to operate in parallel with and interconnected with the electric utility grid and supply the solar power through grid to utility. In some countries, utilities allow net metering, which allows the PV system owner to sell excess power to the utilities.

2.1.3 A Simple Maximum Power Point Tracking System

In this thesis, a simple MPPT-PV stand-alone power system is presented, analyzed and installed, which consists of an array of photovoltaic modules (power source), a resistive load and a step-down switching mode DC/DC converter to act as the power interface

between the PV array and the load (Figure 2.1). The system will be used as a test bench to verify the effectiveness of the proposed MPPT control algorithms.

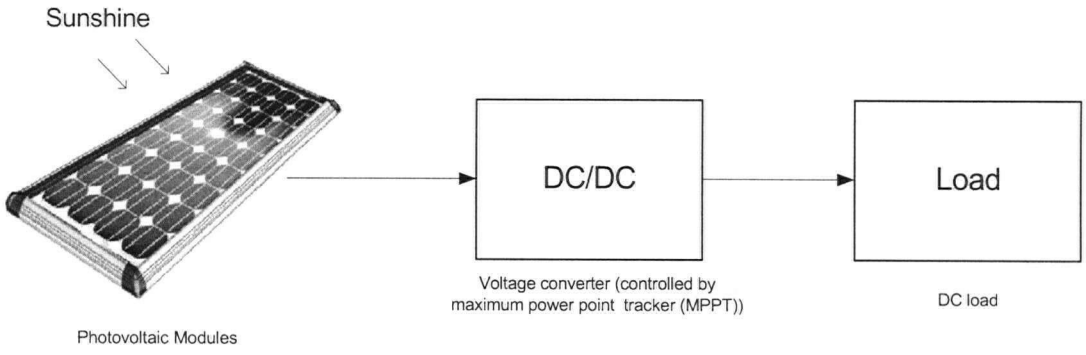

Figure 2.1 Block Diagram of the Proposed MPPT-PV System

The following paragraphs will introduce the elements of such a photovoltaic power system and derive the mathematical models necessary to represent its behavior in a complete system simulation. In Chapter 5 and Chapter 6, the proposed MPPT control algorithm called modified adaptive hill climbing (MAHC) method, will be simulated and evaluated based on such a PV power system.

2.2 Photovoltaic Cells, Modules and Solar Arrays

The PV cells are the basic units of a PV system. A group of solar *cells* are electrically connected together and mechanically mounted in a support structure or frame to form a *module* or *panel*. Panels are wired together to form an *array* that can be used to meet the power requirement of loads.

2.2.1 PV Cell

For a PV cell, a thin semiconductor wafer is specially treated to form an electric field, positive on one side and negative on the other. When light energy strikes the solar cell, electrons are knocked loose from the atoms in the semiconductor material. If electrical conductors are attached to the positive and negative sides, forming an electrical circuit, the electrons can be captured in the form of an electric current -- that is, electricity [4].

During darkness, the solar cell is not an active device. It works as a diode, i.e. a p-n junction. It produces neither a current nor a voltage. However, if it is connected to an external supply (large voltage) it generates a current I_D, called diode current or dark current [5].

2.2.1.1 Cell Model

A solar cell is usually represented by an electrical equivalent one-diode model [5], shown in Figure 2.2.

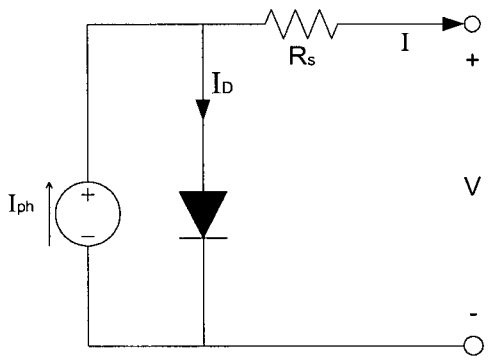

Figure 2.2 Model of a Single Solar Cell

The model contains a current source *Iph*, one diode and series resistance *Rs*, which represents the resistance inside each cell and in the connection between the cells. The net current *I* is the difference between the photocurrent *Iph* and the normal diode current I_D:

$$I = I_{ph} - I_D = I_{ph} - I_0\left[e^{\frac{q(V+IR_s)}{mkT_c}} - 1\right] \qquad (2.1)$$

The variable definitions are described in Table 2-1.

Table 2-1 Parameter Definitions

Symbols	Description
m	It is the idealizing factor
k	It represents the Boltzmann's constant
Tc	It is the absolute temperature of the cell
q	It represents the electronic charge
V	It is the voltage imposed across the cell

I_o	It represents the dark saturation current, which is strongly depending on temperature

2.2.1.2 PV Cell Characteristics

Figure 2.3 shows the *Current-Voltage* characteristic of the solar cell under the standard condition, which is described in Table 2-2.

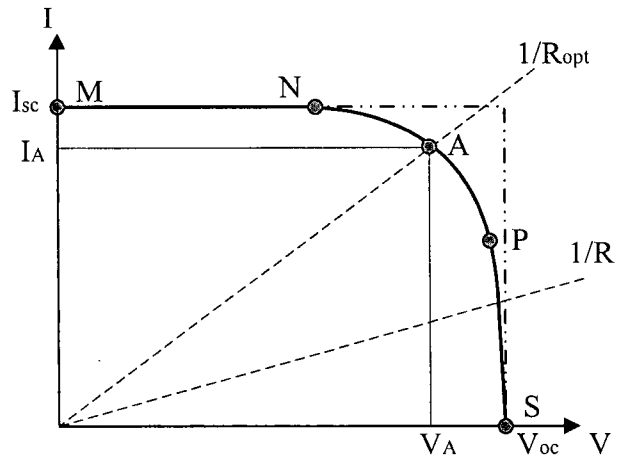

Figure 2.3 A Typical Current-Voltage Curve of a PV Cell under Standard Condition

When the cell's terminals are connected to a variable resistance *R*, the operating point is determined by the intersection of the *current-voltage* characteristic of the solar cell with the load *I-V* characteristic. For a resistive load, the load characteristic is a straight line with a slope *I/V=1/R*, shown in the figure. A typical solar cell can be characterized by some fundamental parameters, which are sketched in Figure 2.3 and summarized in Table 2-2.

Table 2-2 Fundamental Parameters of a Standard Photovoltaic Cell

Parameters	Symbols	Descriptions
Short circuit current	*Isc*	It is the PV output current under short circuit conditions. Its value is equal to photocurrent *Iph*.
Open circuit voltage	*Voc*	It is the voltage value of a PV cell when its output current is zero.
Maximum power point	*MPP*	It represents the maximum power level of a PV's output under a specific condition. The point A in Figure 2.3 shows this point.
Standard Condition	*SC*	It represents the condition when the insolation level is 1000W/m^2 and the Cell temperature is 25°C

2.2.1.3 Influence of Ambient Irradiation and Cell Temperature on Characteristics

In Figure 2.3, the *I-V* characteristic of a solar cell only for a certain insolation *Ga* and a certain cell temperature *Tc* is illustrated. The influence of the insolation *Ga* and the cell temperature *Tc* on the cell characteristics is presented in Figure 2.4 and Figure 2.5.

Figure 2.4 shows that the open circuit voltage increases slightly with the ambient irradiation, while the short circuit current is a linear function of the ambient irradiation [5]. The influence of the cell temperature on the *I-V* characteristics is illustrated in Figure 2.5. The dominant effect with increasing cell's temperature is the linear decrease of the open circuit voltage. The short circuit current slightly increases with cell temperature [5].

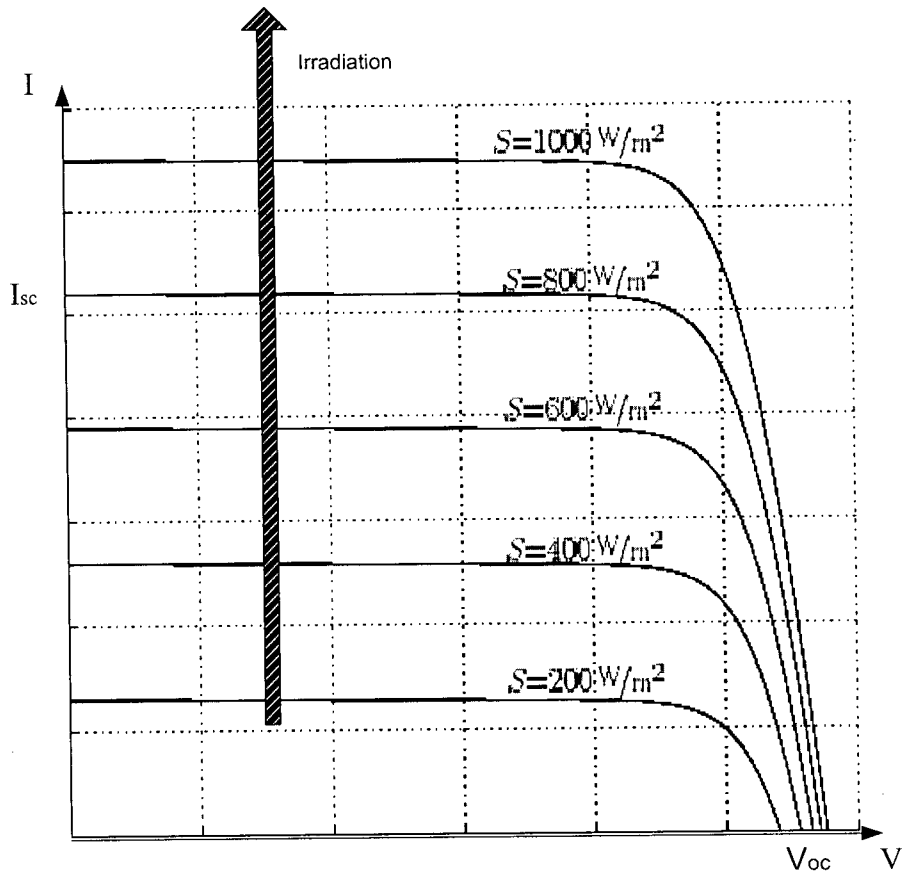

Figure 2.4 Influence of the Ambient Irradiation on a PV Cell's Characteristics

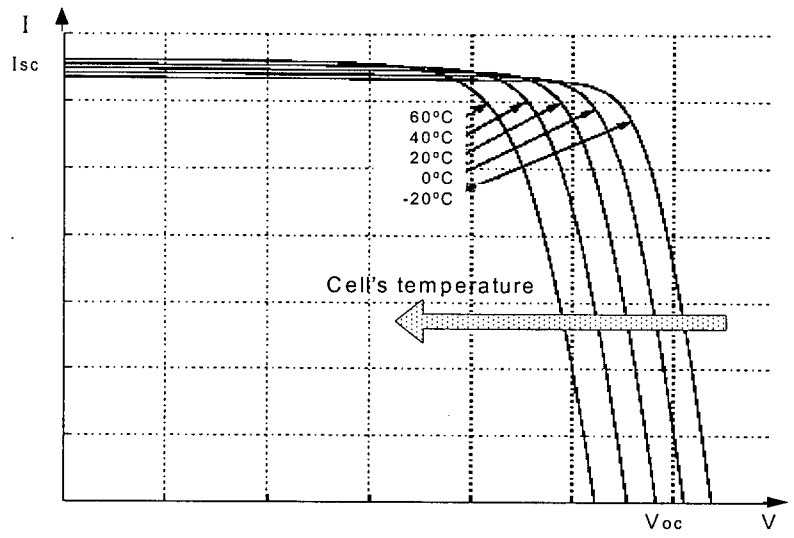

Figure 2.5 Influence of the Cell Temperature on the Cell's Characteristics

2.2.1.4 Cell Connections

The solar cells are electrically connected in series or parallel. Figure 2.6 presents how the *I-V* curve is modified in the case when two identical cells are connected in series and in parallel.

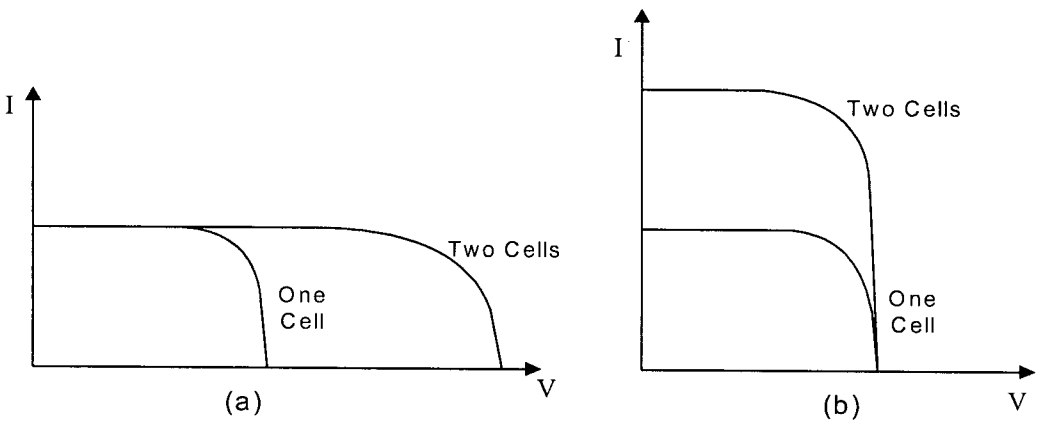

Figure 2.6 Series (a) and Parallel (b) Connections of Identical Cells

It is seen that *I-V* characteristics of series interconnected cells can be found by adding, for each current, the different voltages of the individual cells [5]. On the other hand, for parallel cells the currents of the individual cells must be added at each voltage in order to find the overall *I-V* curve [5].

2.2.2 PV Module

Cells are normally grouped into "modules" or "panels", which are encapsulated with various materials to protect the cells and the electrical connectors from the environment [5]. The manufactures supply PV cells in modules, consisting of N_{PM} parallel branches, each with N_{SM} solar cells in series, as shown in Figure 2.7.

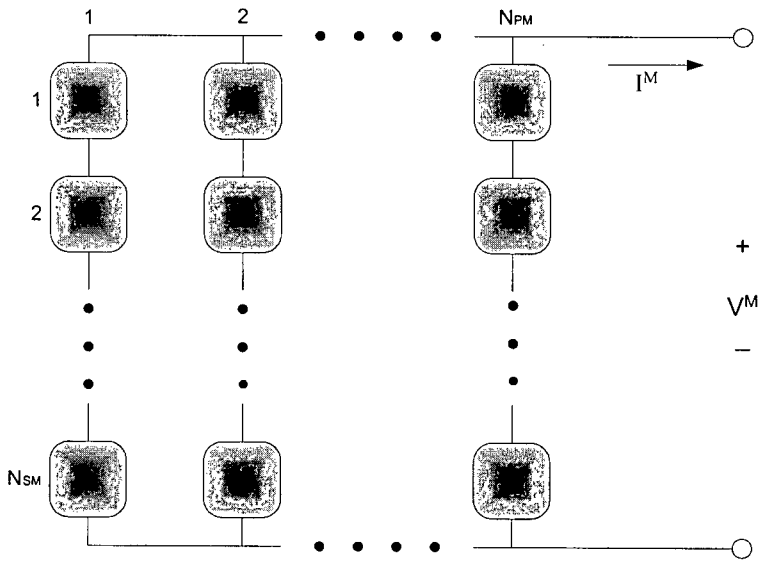

Figure 2.7 The Structure Diagram of a PV Module

2.2.2.1 Mathematical Model of PV Modules

The model for the PV module is obtained by replacing each cell in Figure 2.7, by the equivalent diagram from Figure 2.2.The mathematical model of a PV module, suggested by [5], is represented as Equation 2.2.

$$I^M = I_{SC}^M \left[1 - e^{\left(\frac{V^M - V_{OC}^M + R_s^M \cdot I^M}{N_{SM} V_t^C} \right)} \right] \tag{2.2}$$

The variables used in Equation 2.2 are defined in Table 2-3.

Table 2-3 Variable Definition of Equation 2.2

Symbols	Definitions
I^M	The output current of the module
V^M	The module voltage

N_{SM}	The number of solar cells in series
N_{PM}	The number of solar cells in parallel
I_{SC}^{M}	The short circuit current of the module
V_{OC}^{M}	The open circuit voltage of the module
R_{S}^{M}	The equivalent serial resistance of the module
V_{t}^{C}	$V_{t}^{C} = \frac{mkT_{c}}{q}$, the thermal voltage in the semiconductor of a single cell

2.2.2.2 Essential Components in PV Panels

Besides photovoltaic cells, there are other important components in PV panel application, one is the bypass diode and another is the blocking diode. The blocking diode could be replaced by some kind of switches in case. Figure 2.8 shows these diodes.

Bypass diode--A diode connected across one or more solar cells in a photovoltaic module such that the diode will conduct if the cell(s) become reverse biased [6]. Alternatively, diode connected anti-parallel across a part of the solar cells of a PV module. It protects these solar cells from thermal destruction in case of total or partial shading, broken cells, or cell string failures of individual solar cells while other cells are exposed to full light [6].

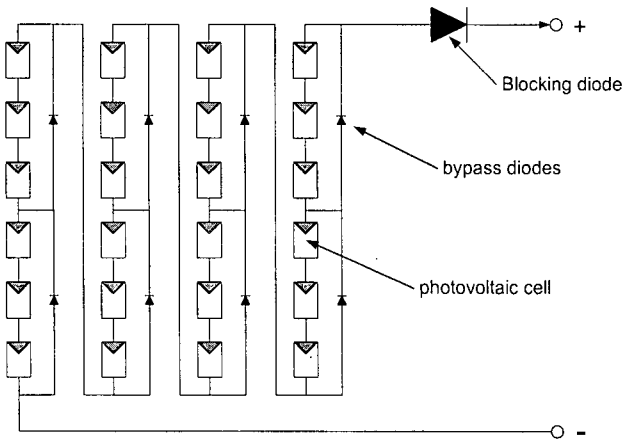

Figure 2.8 Schematic Representation of a 24-cell Solar Panel

Blocking diode--A diode used to restrict or block reverse current from flowing backward through a module. Alternatively, diode connected in series to a PV string; it

protects its modules from a reverse power flow and, thus, against the risk of thermal destruction of solar cells [6].

PV modules are usually connected in series and parallel to form an array. Therefore, the total available power is increased to meet the requirement of a particular application. A photovoltaic module or array acts as neither a voltage source nor current source [15]. However, in most applications the load may require a steady voltage or current that the photovoltaic is not capable of. Furthermore, the electrical characteristics (voltage and current relationship) of the photovoltaic module vary with the changes in insolation level and temperature.

2.3 Switching Mode DC-DC Buck Converter

In an ordinary photovoltaic power system, it is often necessary to adapt the module characteristics to meet that of the variable load by applying a power conditioner. Several advantages i.e., high efficiency, and high stability, make the buck converter an ideal choice for the load interface of PV power systems. Following paragraphs will introduce the operating principles of switching mode dc-dc converters.

2.3.1 Ideal Buck Converter

The fundamental schematic circuit for an ideal buck (step-down) converter is shown in Figure 2.9.

The Buck converter uses a switch that alternately connects and disconnects the input voltage to an inductor. The switches could be MOSFETs, power transistors or IGBTs etc. When the switch turns on, the input voltage is connected to the inductor. The difference between the input and output voltages is then forced across the inductor, causing current through the inductor to increase [7,8].

During the on time, the inductor current flows into both the load and the output capacitor (the capacitor charges during this time). When the switch is turned off, the input voltage applied to the inductor is removed. However, since the current in an inductor cannot change instantly, the voltage across the inductor will adjust to hold the current constant [7,8].

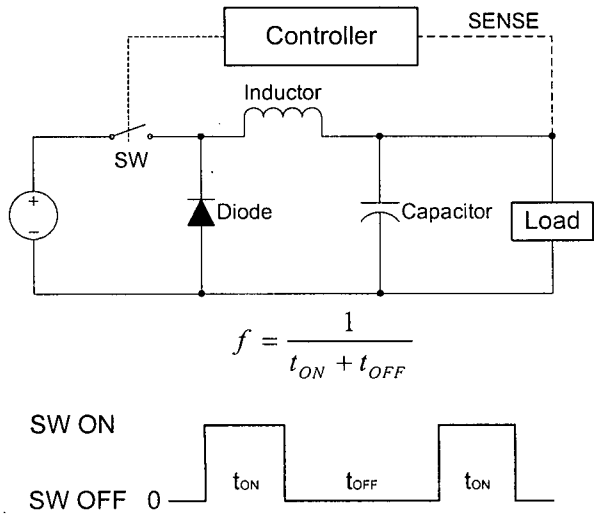

Figure 2.9 Basic Schematics of a Standard DC/DC Buck Converter

The input end of the inductor is forced negative in voltage by the decreasing current, eventually reaching the point where the diode is turned on. The inductor current then flows through the load and back through the diode [7,8].

The capacitor discharges into the load during the off time, contributing to the total current being supplied to the load (the total load current during the switch off time is the sum of the inductor and capacitor current) [7,8]. The actual waveforms associated with the buck converter are shown in Figure 2.10.

If a steady-state condition exists, the basic relationship between the input and output voltage may be derived by inspecting the inductor current waveform and writing:

$$\frac{V_{IN} - V_{OUT}}{L} \bullet t_{on} = \frac{V_{OUT}}{L} \bullet t_{off}$$

Solving for V_{OUT}:

$$V_{OUT} = V_{IN} \bullet \frac{t_{on}}{t_{on} + t_{off}} = V_{IN} \bullet D \qquad (2.3)$$

where D is the switch duty cycle, defined as the ratio of the switch on-time (t_{on}) to the total switch cycle time (t_{on}+t_{off}).

This discussion so far has assumed the regulator is in the *continuous-mode* of operation, defined by the fact that the inductor current never goes to zero. If the output load current is decreased, there comes a point where the inductor current will go to zero

between cycles, and the inductor current is said to be discontinuous [7,8]. Waveforms for discontinuous operation are shown in Figure 2.11.

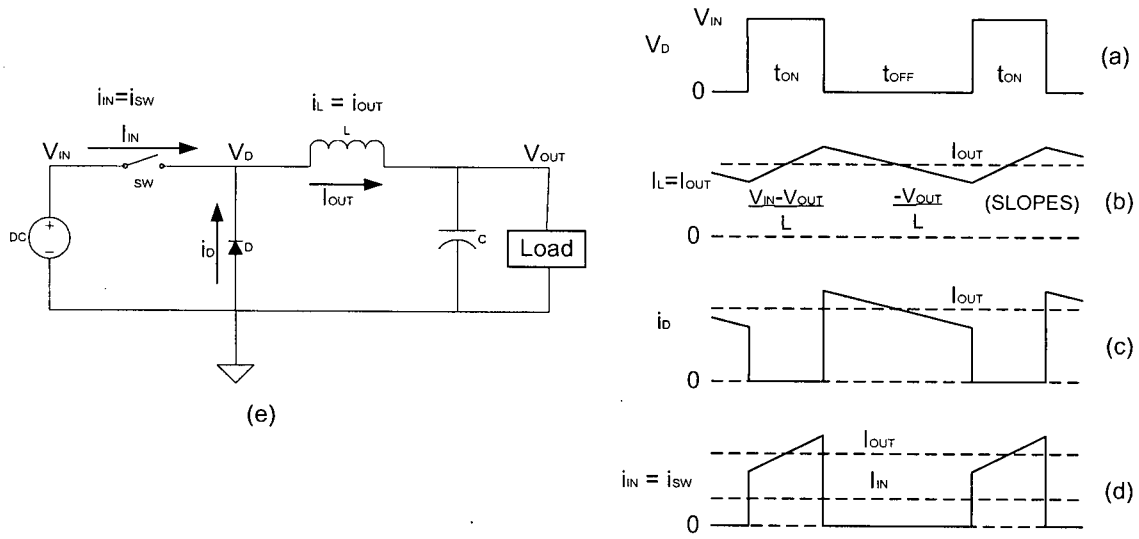

Figure 2.10 Basic Waveforms of a Buck Converter Operating at Continuous Mode

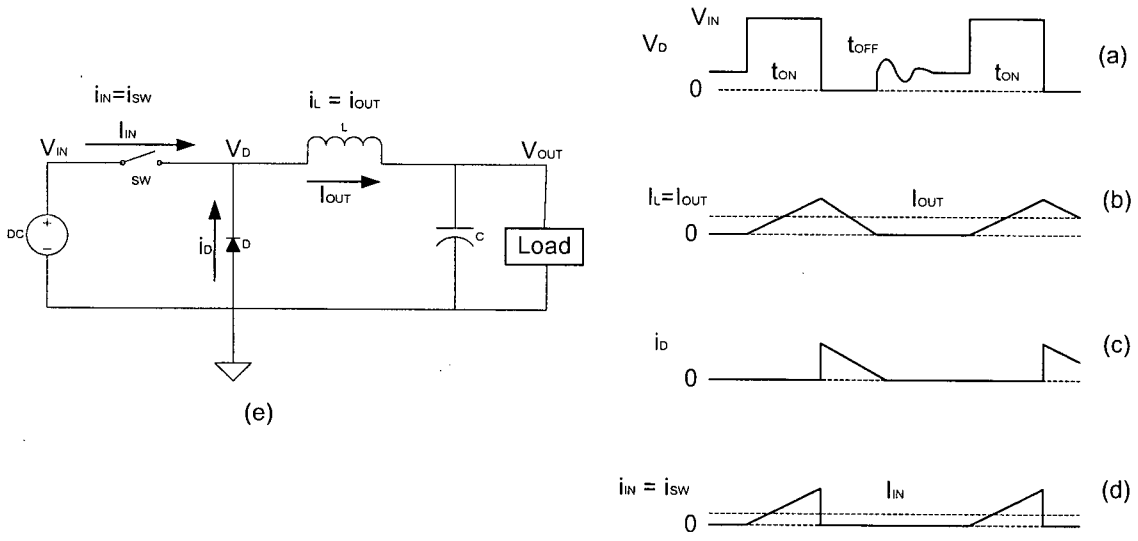

Figure 2.11 Basic Waveforms of a Buck Converter Operating at Discontinuous Mode

2.3.2 Modeling of DC-DC Converter

In this thesis, a switching-mode DC-DC buck converter acts as executive unit of the MPPT-PV system. It is important to know the dynamic behavior of this converter with easy-to-use and accurate model. The major analytical methods are known as state-variable-averaging methods [9].

The state-variable-averaging method [9] presented by Middlebrook and S. Cuk in 1976 was the first approach to result in a complete linear model of a switching mode dc-dc converter. It was a major contribution to the dynamic analysis of switching structures and has been adopted by other investigators. Many recent developments are still based on this method.

In this section the state-variables-averaging method is introduced in general for any dc-dc switching converter [9].

The basic dc-to-dc level conversion function of switching converters is achieved by repetitive switching between two linear networks consisting of ideally loss-less storage elements, inductances and capacitances. In practice, this function may be obtained by used of transistors and diodes, which operate as synchronous switches. On the assumption that the circuit operates in the so-called "Continuous conduction" mode in which the instantaneous inductor current does not fall to zero at any point in the cycle, there are only two different "states" of the circuit. Each state, however, can be represented by a linear circuit model or by a corresponding set of state-space equations. Even though any set of linearly independent variables can be chosen as the state variables, it is customary and convenient in electrical networks to adopt the inductor currents and capacitor voltages. The total number of storage elements thus determines the order of the system. Let us denote such a choice of a vector of state variable by x.

It then follows that any switching dc-to-dc converter operating in the continuous conduction mode can be described by the state space equations for the two switched models as shown in Figure 2.12.

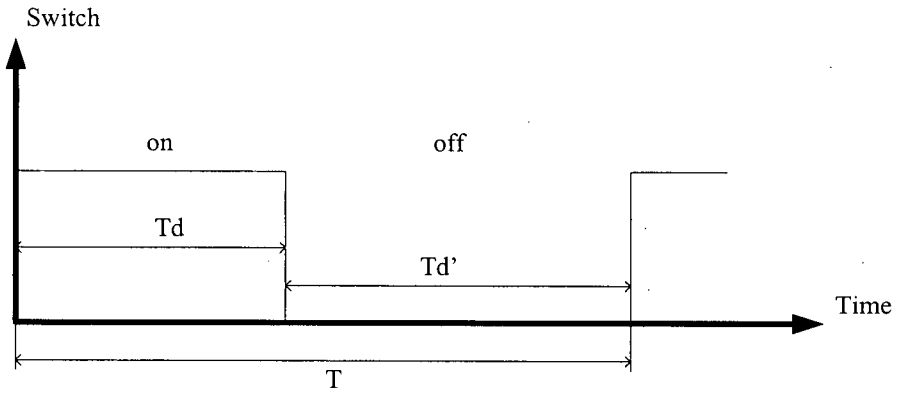

Figure 2.12 Definitions of the two Switched Intervals *Td* and *Td'*

a) interval *Td*

$$\begin{aligned} \dot{x} &= A_1 x + b_1 v_{in} \\ y_1 &= c_1 x \end{aligned} \tag{2.4}$$

b) interval *Td'*

$$\begin{aligned} \dot{x} &= A_2 + b_2 v_{in} \\ y_2 &= c_2 x \end{aligned} \tag{2.5}$$

where T is time period representing one switching cycle, Td denotes the interval when the switch is in the "on" state and $T(1-d) \equiv Td'$ is the interval for which it is in the "off" state.

Our objective now is to replace the state-space description of the two linear circuits emanating from the two successive phases of the switching cycle T by a single state-space description, which represents approximately the behavior of the circuit across the whole period of T. We therefore propose the following simple averaging step: take the average of both dynamic and static equations for the two switched intervals (2.4)(2.5), by summing the equations for interval Td multiplied by d (duty cycle) and the equations for interval Td' multiplied by d' *(d'=1-d)*. The following linear continuous system results:

$$\begin{aligned} \dot{x} &= d(A_1 x + b_1 v_{in}) + d'(A_2 x + b_2 v_{in}) \\ y &= dy_1 + d'y_2 = (dc_1 + d'c_2)x \end{aligned} \tag{2.6}$$

after rearranging (2.6) into the standard linear continuous system state-space description, we obtain the basic averaged state space description (over a single period T):

$$\dot{x} = (dA_1 + d'A_2)x + (db_1 + d'b_2)v_{in}$$
$$y = (dc_1 + d'c_2)x \tag{2.7}$$

This model (2.7) is the basic averaged model, which is the starting model for all other derivations.

Chapter 3 Maximum Power Point Tracking

One significant problem in PV power system is the probable mismatch between the operating characteristics of the load and the PV array [10]. Maximum power point tracking is specifically designed to remove the mismatch.

Shown in Figure 2.3 is a standard *I-V* curve for a PV panel, with *X*-axis representing voltage and the *Y*-axis representing current. When a PV array is connected to a load directly, the system's operating point will be at the intersection of *I-V* curves of PV array and load. Under most conditions, this operating point may not be at the PV array's maximum power point (MPP), which is clearly shown in Figure 2.3. Furthermore, the output characteristics of photovoltaic cells are non-linear, and the value for the optimum operating point varies constantly with changes in the environmental conditions of solar irradiation and cell temperature. The relations between power and voltage (*P-V* curves) are shown in Figure 3.1.

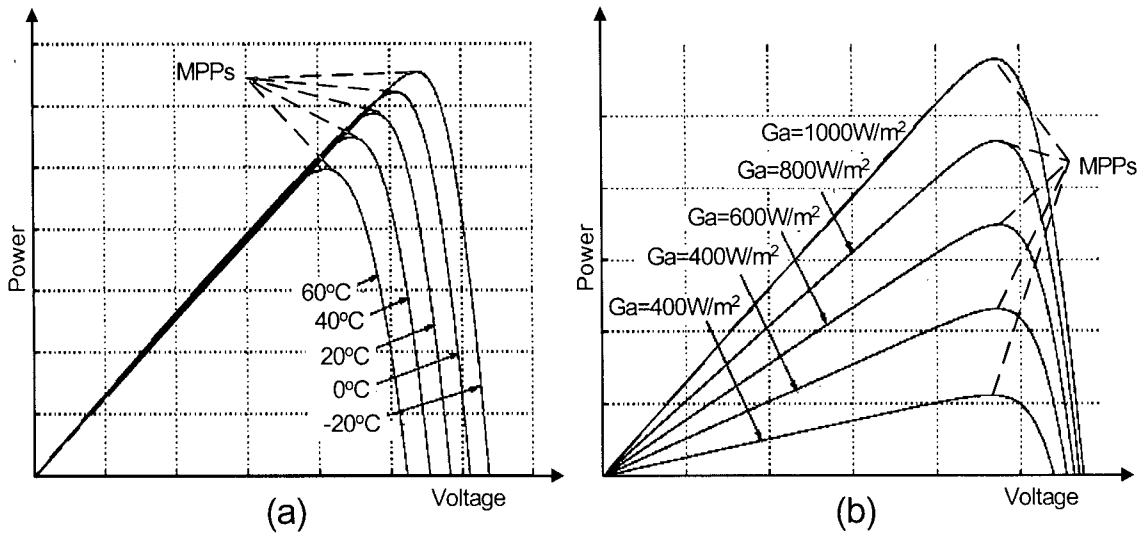

Figure 3.1 (a) P-V Characteristics of a Photovoltaic Array for Various Values of Temperature at Constant Irradiation (b)P-V Characteristics of a Photovoltaic Array for Various Values of Insolation at Constant Temperature

Figure 3.1(a) shows the MPP shifts with cell temperature change, and Figure 3.1(b) represents that it moves with insolation change. In reality, the change of array temperature moves the MPP in a large range along X-axis and changing irradiation varies array power output dramatically with little maximum operating voltage (V_{MPOP}) shift.

In previous analysis, solar insolation and photovoltaic array temperature were considered separately. In reality, it is impossible to encounter one without the other because they are highly coupled under ordinary operating conditions. This statement implies that an increase in the insolation on PV module will be accompanied by an increase in the module temperature as well. Therefore, it seems the tracking control of maximum power point is even complicated.

To overcome these problems, a power interface (such as DC/DC converter or DC/AC inverter) controlled by maximum power point tracking (MPPT) controller can be used to maintain the PV array's operating point at the maximum power operating point (MPOP). However, the location of the MPP in the *I-V* curve plane is not known a *prori* [10]. One way to calculate it is using a model of the PV array and measurements of insolation and array temperature, but making such measurements is usually too expensive for this application, and often the required parameters for the PV array model are not known adequately [10]. Thus, a good way is that MPPT searches for the MPP continuously by way of other measurements [10].

In the past years, several MPP search algorithms have been proposed that make use of different characteristics of solar panels and the location of the MPP. In this chapter, the different available approaches operating a solar panel close to its maximum power point are analyzed. Table 3-1 lists the variable symbols often used in the following sections.

Table 3-1 Variables Definition

Symbols	***Description***
AHC	Adaptive Hill Climbing Method
Vref	Reference voltage
MPOP	Maximum power operating point
MPP	Maximum Power Point
MPPT	Maximum Power Point Tracking

MAHC	Modified Adaptive Hill Climbing Method
Ppv	PV array output power
Vmpop	PV array voltage at its maximum power operating point
Pmpop	PV output power at its maximum power operating point
a	Incremental step of duty cycle in switching mode DC/DC converter
c	Incremental step on PV reference voltage of voltage regulation
Ga	Solar Insolation value
Tc	Cell absolute temperature

3.1 Performance Specification of Maximum Power Point Tracking Control Systems

Considering the MPPT as a control system, the following requirements are important for a successful system design.

3.1.1 Stability

The most fundamental design requirement of a dynamic control system is system stability. Switching mode dc-dc converters are serious nonlinear systems, which were introduced in Chapter 2 and behave very differently from linear systems. The output characteristic of solar array is also nonlinear. So stability is a very important factor to evaluate a PV-MPPT control systems dealing with non-linearity.

3.1.2 Dynamic Response

A good MPPT control algorithm needs response quickly to rapidly changing atmospheric conditions, i.e. array temperature and insolation. The faster the tracking, the less loss of solar energy is.

3.1.3 Steady State Error

When MPP is found, it is ideal to keep the system operate exactly on this point statically. In actual MPPT system, it is impossible because of the active MPPT control algorithm and the continuous variation in insolation and temperature. So small output

power fluctuation is preferred. It is related directly to the efficiency value of system power conversion.

3.1.4 Robustness to Disturbances

The MPPT control systems need accurate response under uncertain conditions. Usually, the disturbances of control systems, which are mainly from the input noise, measurement error and parameter variation can cause the system to become unstable. It is important to design a MPPT control system robust to any kind of disturbances.

3.1.5 Efficient In a Large Power Range

The ratio between the actual PV array power and the delivered power to load is an indication of how successful the PV generation facility is used. The efficiency at low light level is a serious problem for many MPPT designs. Many products only work efficiently during nominal power delivery. But in reality, in a day period, the PV array output power varies in a large range. A successfully designed MPPT control system shall show good performance in different power levels.

3.2 Recent Researches on Maximum Power Point Tracking Methods

In past years, many control algorithms were proposed for photovoltaic power system to achieve maximum power output and high efficiency. These are introduced in the following paragraphs.

3.2.1 Simple Panel-Load Matching

The simple PV battery chargers are available on the market. They use photovoltaic cells packaged in structurally and environmentally protective polymer and designed for indoor/outdoor equipment using 6V, 12V or 24V batteries. There is not any control circuitry inside. Such PV panels are usually designed such that the average battery voltage is close to the average maximum power operating point (*Vmpop*) in most cases. But the maximum power point tracking is unavailable for these simple configurations.

For example, the products designed for Florida may not work efficiently in Alaska. Another issue is that the battery voltage is not truly constant.

3.2.2 Load Switching Method

A method for optimizing the power output of a PV array was presented by Huang Yongji and Lin Deheng [11] in 1993. The MPPT is based on reconfigurations of battery cells in series or parallel to meet the requirement of load matching. Figure 3.2 shows the experimental system block diagram.

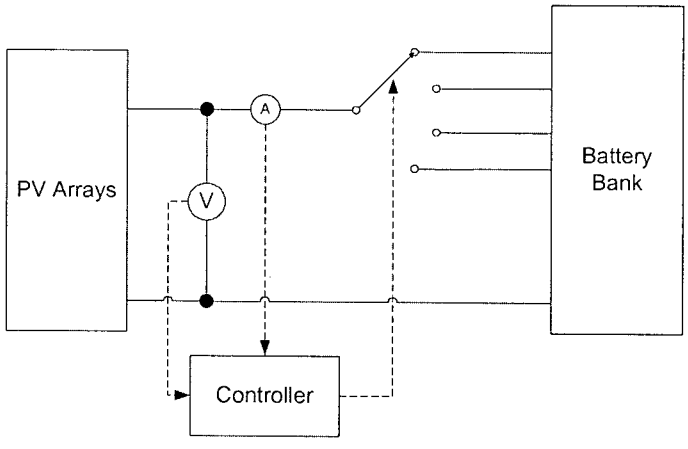

Figure 3.2 Schematic Block Diagram of the Experimental Load-Switching System

The power from the photovoltaic array is stored in a group of batteries. The controller detects the output power of the solar cell array in real time, finds out the optimal operating point, and keeps this point by switching the battery connection.

The drawbacks of this method are clear:

a) "The stepwise switching operating voltage can't guarantee accurate tracking of MPP" [12].

b) "Furthermore, it is difficult to keep an equal charge level on all the battery cells which in the long term degrades battery life" [12].

3.2.3 The Voltage Feedback Methods

A simple and cheap MPPT method is to keep the array near the maximum power point by regulating the array voltage and matching it to a reference voltage, which represents the maximum power operating point (*Vmpop)*. Many researchers lead to maximum power point tracking based only on a simple PV voltage measurement.

3.2.3.1 Using Fixed Reference Voltage

A very common MPPT technique [12,13,15] is to use standard feedback control technology to regulate the PV array voltage following a constant reference voltage (Figure 3.3). This predetermined reference voltage can be derived from monitoring the PV module characteristics and selecting a single value that would best represent the module operation under normal operating conditions regarding maximum power delivery. The resulting difference signal (error signal) is used to feed the controller (i.e. PID). The controller generates control signals (such as PWM drive signals) to drive a power conditioner, which interfaces the PV array to the load.

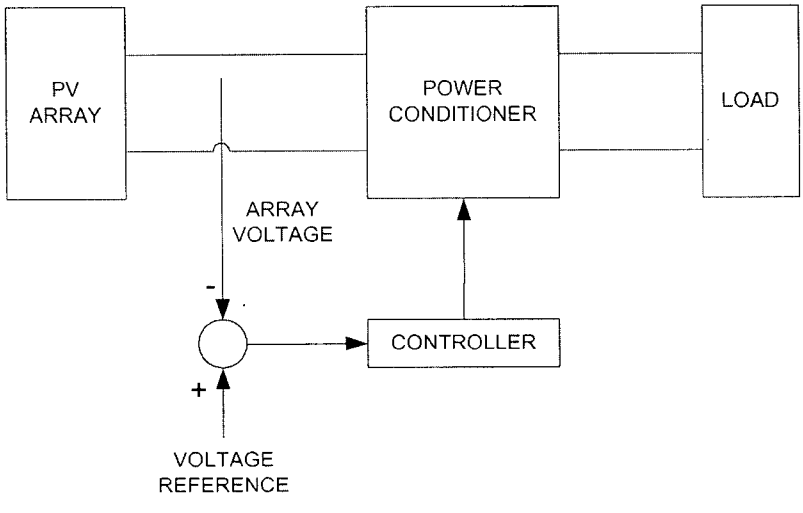

Figure 3.3 Voltage Feedback MPPT Control System With Constant Voltage Reference

It is very clear that such a system cannot automatically track the variations in the maximum power point of the array, because the influence of environmental change is ignored.

3.2.3.2 Reference Voltage Varying With Array Open-Circuit Voltage Measurement

The control method can be modified by varying the array reference voltage according to variations in array temperature and insolation. One way to get information related to array temperature and irradiation is to measure the array's open-circuit voltage.

In 1998, Wernher Sweigers and Johan H.R. Enslin proposed a MPPT method to be integrated with the panel during manufacturing [14]. The system block diagram is illustrated in Figure 3.4.

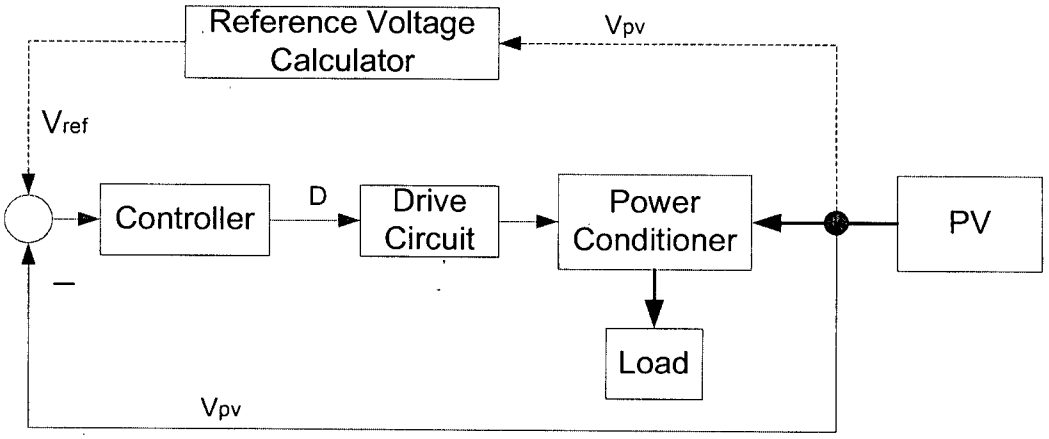

Figure 3.4 Block Diagram of Voltage Feedback System with Controllable Reference

The upper loop control action is defined as the way in which the maximum power point reference operating point (*Vref*) is generated. Inner loop operation is defined as the way in which the reference voltage is followed as a standard voltage regulator. The experiments showed that the maximum power point voltage of a solar panel is always very close to a fixed percentage of the panel's open circuit voltage.

The maximum power point tracking algorithms used, samples the open circuit voltage of the panel regularly (say every 60 sec) by switching the converter off and allowing the MPPT's input voltage to rise to the panel's open circuit voltage. This method is very easy to implement because only simple voltage measurement is needed. Usually, the maximum power point reference voltage is set to 70-80% of the open-circuit voltage.

There are several drawbacks of this implementation:

a) The actual open-circuit array voltage is measured by momentarily interrupting the normal operation of the array and MPPT. The energy not transferred by the sampling of the open circuit voltage is wasted due to stopping power conversion.
b) If aging and dust accumulation on the cell surface are taken into account, the fixed percentage cannot hold true [12]. Losses are caused by the inaccuracy in finding the actual MPP.

3.2.3.3 Using a Small Open Circuited Reference Cell

In the control algorithm mentioned above, the energy is wasted by a frequent interruption of the system operation for the measurement of open-circuit voltage *Voc*. The problem can be solved easily by using a small open circuited reference cell (test cell or pilot cell), electrically separated from the rest of the array [17,18].

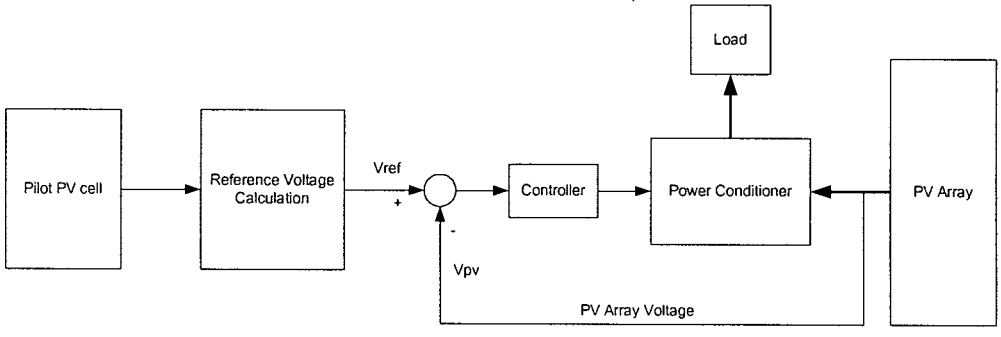

Figure 3.5 Block Diagram of MPPT Control System with Reference Cell

The system block diagram is shown in Figure 3.5. The system uses a pilot PV cell, which is electrically independent of the rest of array. Its open circuit voltage *Voc* is constantly measured and therefore provides the reference information of maximum power point voltage. The operating voltage set-point (*Vref*) is also a fixed percentage of the PV panels' open circuit voltage.

The disadvantages of this implementation are:

1) In most cases, a reference cell is difficult to use because of the requirement of leaving space and installation for it on the solar array. Another issue is that it may

not be an adequate representative of the entire array. It also increases the cost on PV cells and system installation.

2) Since this method still uses a fixed factor to estimate the optimal operating point voltage from a measured value of *Voc*, the MPP is still not truly tracked [12].

3.2.4 Power Feedback Methods

A controller that directly finds the actual maximum power point, instead of estimating it from measurements of other quantities has the advantage of being independent of any a *priori* knowledge of the array characteristics. Thus it can be depended upon to work properly even with an array that has not been previous tested, or with an array whose characteristics have changed. Such a controller needs to have a measurement indicative of the array power, and an algorithm implemented in software or hardware to find a local maximum in the power indication [19]. This method is so called "true" maximum power point tracking. Several algorithms based on power feedback control are introduced and analyzed in following paragraphs.

3.2.4.1 Perturbation and Observation Method (P&O)

By investigating the *P-V* curve shown in Figure 3.1, the maximum power operating point can always be tracked if we keep *dP/dV* equal to zero mathematically, no matter what situation of solar insolation and array voltage are. All local maximum power points have the same mathematical tributes: $dP/dV = 0$. And the power slope *dP/dV* can be calculated digitally by sampling the PV array output current I and voltage V at consecutive time intervals $(n-1)$ and (n) as follows.

$$\frac{dP}{dV}(n) = \frac{P(n) - P(n-1)}{V(n) - V(n-1)} \qquad (3.1)$$

where

$$P(n) = V(n) \bullet I(n)$$

The Perturbation and Observation (P&O) method [20] is a widely used digital approach to MPPT. The P&O operation is to make *dP/dV* oscillate around zero by periodically incrementing or decrementing the solar array voltage. If a given perturbation leads to an increase (decrease) in array power, the subsequent perturbation is made in the

same (opposite) direction. In this manner, the peak power tracker continuously hunts or seeks the maximum power operating point (*Vmpop*) [20,21]. The block diagram of such control system can be illustrated as Figure 3.6.

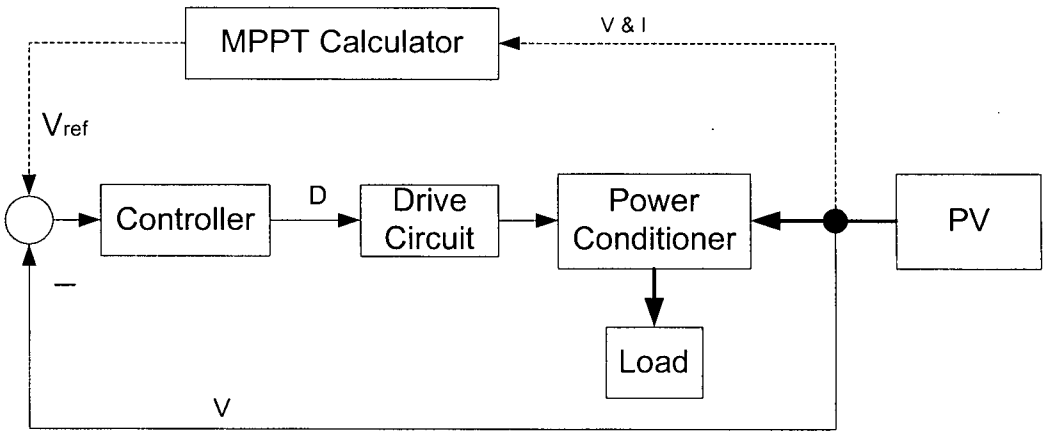

Figure 3.6 Block Diagram of Power Feedback Control System

Two control loops are required. The MPPT control algorithm is based on the calculation of the PV output power and of the power change is detected by comparing the present and previous voltage levels, in order to calculate a reference voltage (*Vref*), which is used as the voltage set point for PV voltage regulation. The second loop controls the array voltage according to the reference voltage set. The control flow chart of P&O is shown in Figure 3.7.

The P&O tracking method is very easy for digital control implementation. But the array voltage is perturbed every control cycle based on this method. Therefore, the P&O algorithm will oscillate around the optimal operating voltage when the maximum power operating point is reached. This results in a waste in PV power delivery, which depends on the step width "*c*", a constant perturbation. If the step width is selected large, this MPPT algorithm will respond quickly to the sudden changes in operating conditions with the trade-off of poor steady state performance. If the step width is very small, the losses under stable or slowly changing conditions will be reduced, but the system cannot respond to rapid changes in insolation or temperature. The value of the suitable step width needed be tuned experimentally in the specific systems and environment.

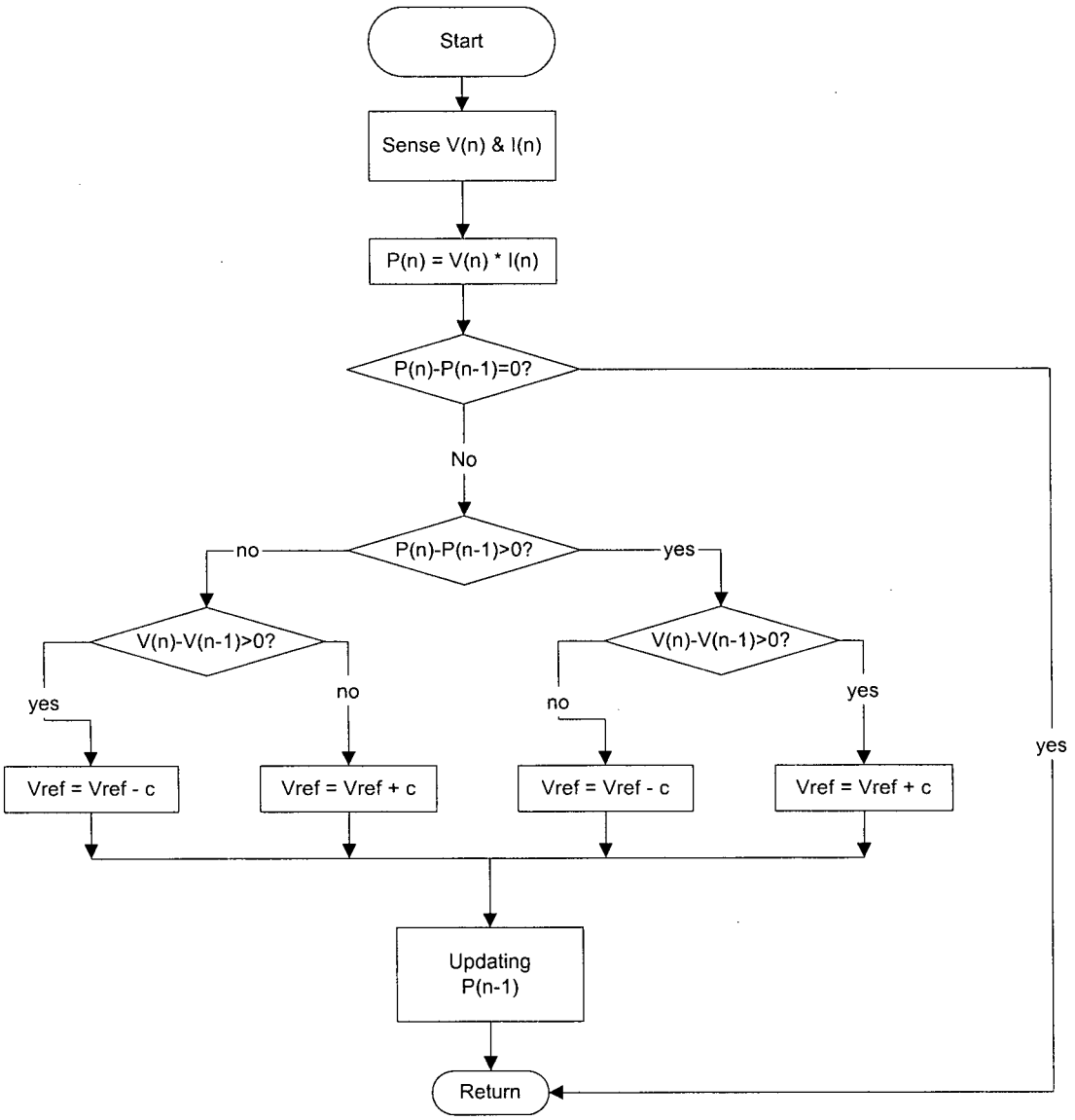

Figure 3.7 Flow Chart of the P&O MPPT Algorithm

In [12, 22], the drawback of P&O method is discussed and analyzed further that the dynamic response is slow in cases of rapidly varying atmosphere conditions. When a sudden increase in insolation, The P&O algorithm reacts as if the increase occurred as a result of the previous perturbation of the array operation voltage. The next perturbation, therefore, will be in the same directions as the previous one. Assuming that the system has been oscillating around the MPP, it can be seen in Figure 3.8 that a continuous

perturbation in one direction will lead to an operating point far away from the actual MPP. This process continues until the increase in insolation slows down or ends. The reason for this problem is that the output power increase is dominated by solar insolation over control signal, and at this moment the control goes to wrong direction.

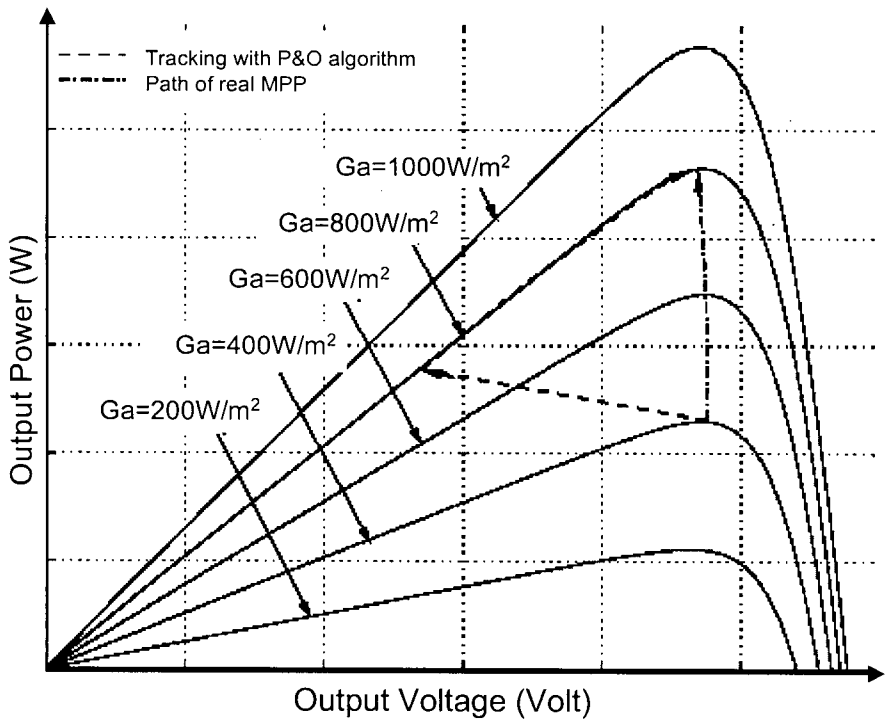

Figure 3.8 Deviation From the MPP Caused by P&O Algorithm under Rapid Increasing Irradiation Levels

3.2.4.2 The improved P&O algorithm

In 2001, a modified P&O algorithm was presented [23]. It can be defined as improvement based on the basic P&O algorithms, which fails to track the maximum power point quickly.

Figure 3.9 shows the flowchart of control algorithm. An additional insolation control loop is proposed in this modified version. If there is a large and sudden change in the array output current, it can be supposed that this is due to a sudden change in insolation, which is caused by fast moving clouds. A current change threshold "*e*" needs to be defined as a system parameter. The direction of the array output current is used to directly control the perturbation direction of the array reference voltage. With this additional

control loop, fast tracking was achieved. But the difficulties in choosing the voltage incremental step "*c*" and current change threshold "*e*" remain unsolved.

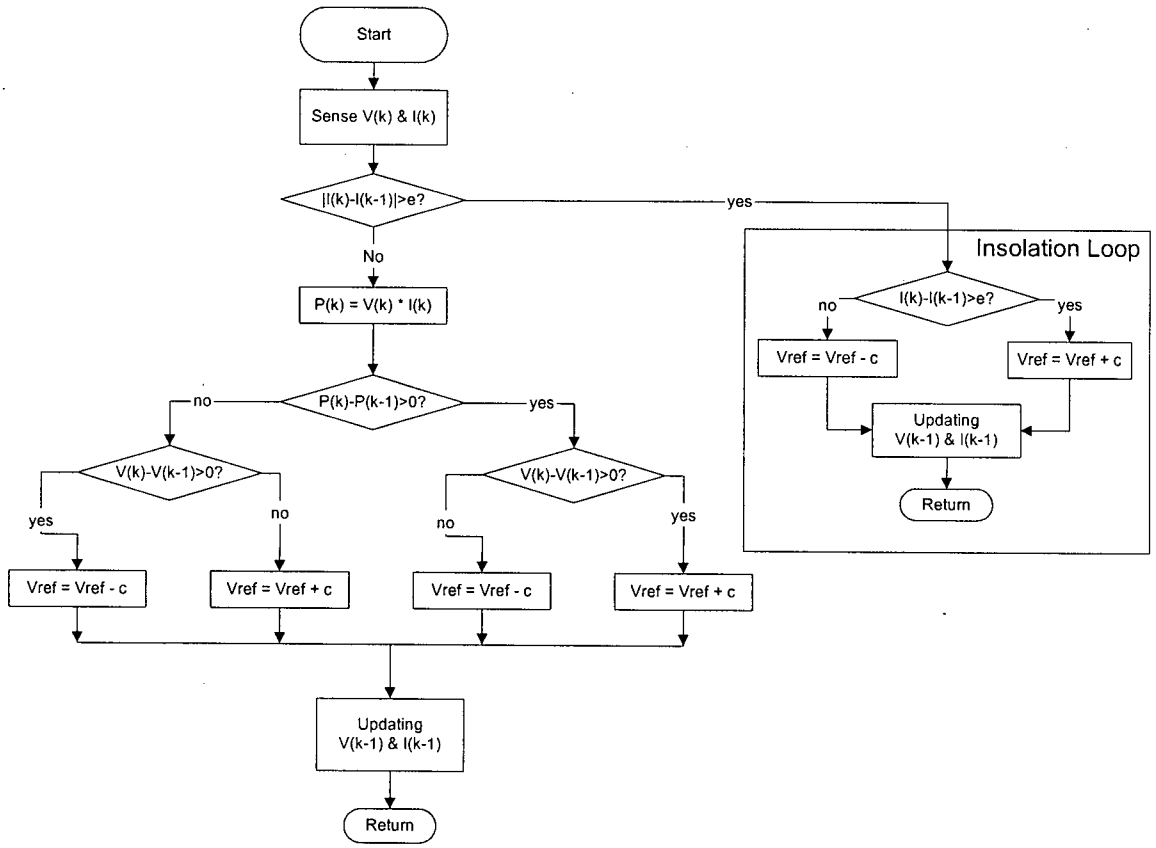

Figure 3.9 Flow Chart of the Improved P&O MPPT Algorithm

3.2.4.3 Incremental Conductance Method

The Incremental Conductance (IncCond) algorithm was developed in 1995 [22]. It is also based on the fact that the derivative of the output power P with respect to the panel voltage V is equal to zero at the maximum power point (MPP). The PV array P-V characteristics in Figure 3.1 show further that to the left of the MPOP the power is increasing with the voltage, i.e. $dP/dV>0$, and it is decreasing to the right of the MPOP, i.e. $dP/dV<0$. This can be written in the following simple equations:

$dP/dV = 0$ at the MPOP

$dP/dV > 0$ at the left of MPOP

$dP/dV < 0$ at the right of MPOP

and, P = V*I

These relations can further be written in terms of the array current and voltage using:

$$\frac{dP}{dV} = \frac{d(VI)}{dV} = I\frac{dV}{dV} + V\frac{dI}{dV} = I + V\frac{dI}{dV} \qquad (3.2)$$

to keep $dP/dV = 0$, we get

$$\frac{dI}{dV} = -\frac{I}{V} \qquad (3.3)$$

It seems that the equation (3.3) provides enough information to determine the relative location of the MPP by measuring the incremental and instantaneous array conductance, dI/dV and I/V, respectively. The control system structure is the same as shown in Figure 3.6. The detailed operation of the IncCond algorithm can be followed with reference to the flow chart of Figure 3.10.

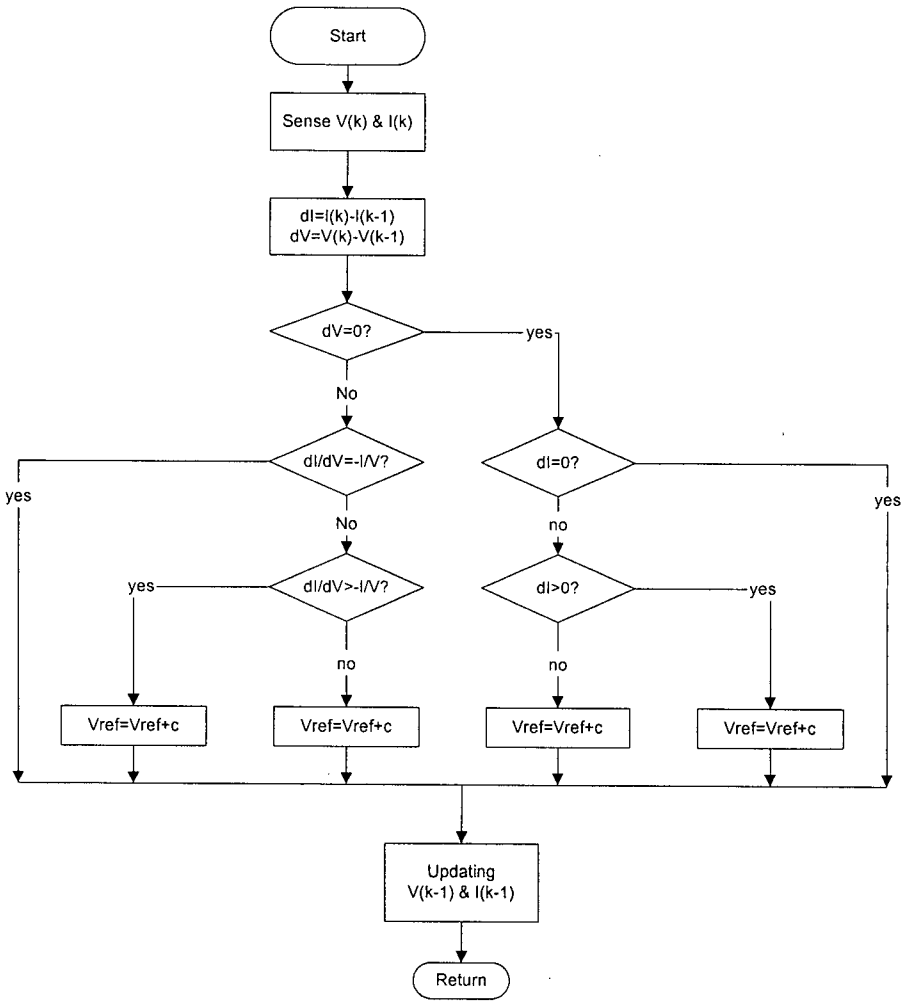

Figure 3.10 Flow Chart of IncCond MPPT Method

The main purpose of this IncCond MPPT algorithm is to make the operating point not oscillate around the MPP. In theory, the conditions of $dI/dV=-I/V$ and $dI = 0$ provide enough information to bypass the perturbation step and maintain a constant operating voltage V when the MPP is found. But the experiments [12,22] show that there were still oscillations under stable environmental conditions, because the maximum power condition $dP/dV = 0$ (which is equivalent to $dI/dV = -I/V$) only rarely occurred. The chosen perturbation step width "c" is also difficult with the consideration of the trade-off between steady-state performance and fast dynamic response.

3.2.4.4 Hill-Climbing Maximum Power Point Tracking Method

Most of the preceding MPPT design methods to the problems of finding a local maximum of output power by regulating the PV array output voltage are to sense the derivative, dP/dV, and used feedback to force this quantity to zero. P is the PV array output power and V is PV array voltage. In most of applications, PWM type dc-dc converters and dc-ac inverters are used as the power interface between PV arrays and loads. The switching duty cycle or duty ratio is the control variable of such kind of systems. So a variation of these methods is to directly use the duty cycle of switching mode converter or inverter as a MPPT control parameter and force dP/dD to zero, where P is the PV array output power and D is the switching duty cycle. It is so called hill-climbing maximum power point tracking method. In such control system, only one control loop is required. The control structure and algorithm are even simpler. Figure 3.11 presents the system structure block diagram.

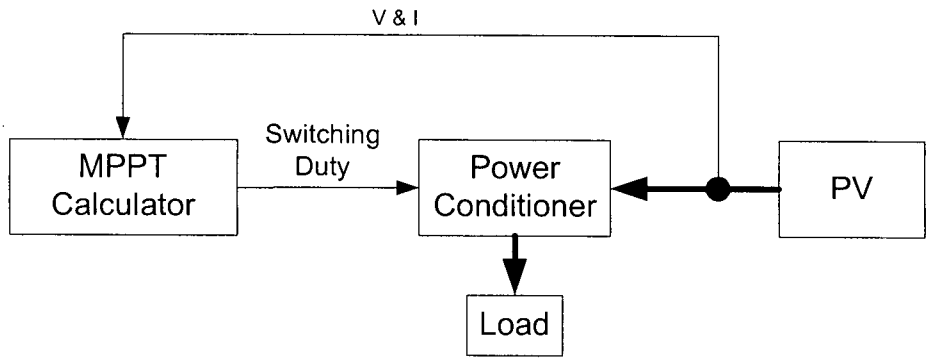

Figure 3.11 Block diagram of the Hill Climbing MPPT control system

In [19] an analog controller is proposed, where dc-dc converter is controlled so that *dIout/dD* equals zero because of relatively stable output voltage of the battery, where *Iout* is the dc/dc converter output current. This assumes the voltage across battery is constant. The simplicity of this MPPT method makes analog controller available too.

In [24] a digital implementation of this method is presented. Figure 3.12 shows a simplified flow diagram of the algorithm. Every duty ratio is decided by comparison of the current power value and history value. If $dP>0$, then make $dD>0$. And if $dP<0$, then make $dD<0$. "a" shown in Figure 3.12 is the incremental step of duty cycle.

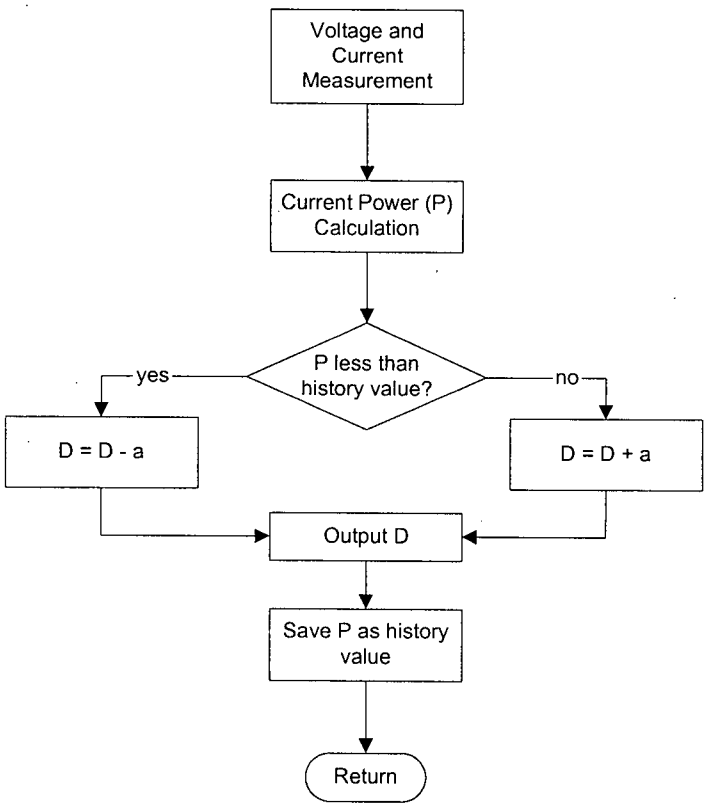

Figure 3.12 Flow Chart of the Hill Climbing MPPT Control Algorithm

But there is a fatal problem in this algorithm through the following detailed analysis. If we consider the simple maximum power point tracking system shown in Figure 2.1, we could draw the *P-D* curve, where *P* represents the PV output power and *D* is the duty cycle of switching mode DC-DC converter. Figure 3.13 shows the relationship of *P* and *D* in the PV power system with a switching mode buck converter as power conditioner. Duty cycle usually varies from 0% to 100% for a switching mode buck converter. The

maximum power point (MPP) is also indicated. If the system starts in the left area, keeping $dP/dD > 0$ can access MPP. But if the original operating point is in the right-hand area, we need keep $dP/dD<0$ to reach maximum power delivery. According to this simple hill climbing algorithm mentioned above, the algorithm always keep $dP/dD >0$ for higher power tacking. In most cases, it holds true that system always starts from a duty cycle equal to zero percent. But it is also possible for the operating point to shift to the right side. If this happens, the tracking will fail.

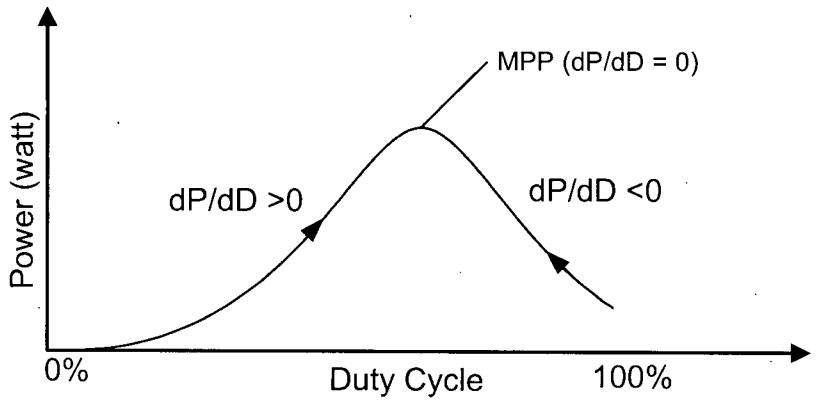

Figure 3.13 *P-D* curve with switching mode buck converter as power interface

Adaptive Hill Climbing Method

The defect of the hill climbing method was corrected by [26] in 2001, which introduced a more adaptive, but simpler solution, namely, adaptive hill climbing method (AHC). The flowchart of the control program is shown in Figure 3.14. "Slope" is a program variable with values either "1" or "-1", indicating the direction that must followed on the hill-shaped *P-D* curve in order to increase the output power. While "a" represents the increment step of duty cycle, which is a constant number between 0 and 1. The current power is compared to its value calculated in previous iteration and according to the result of the comparison, the sign of "Slope" is either complemented or remains unchanged. Then, the PWM duty cycle is changed accordingly until operating point oscillates around the MPP. This method is simple and flexible to keep tracking direction correctly.

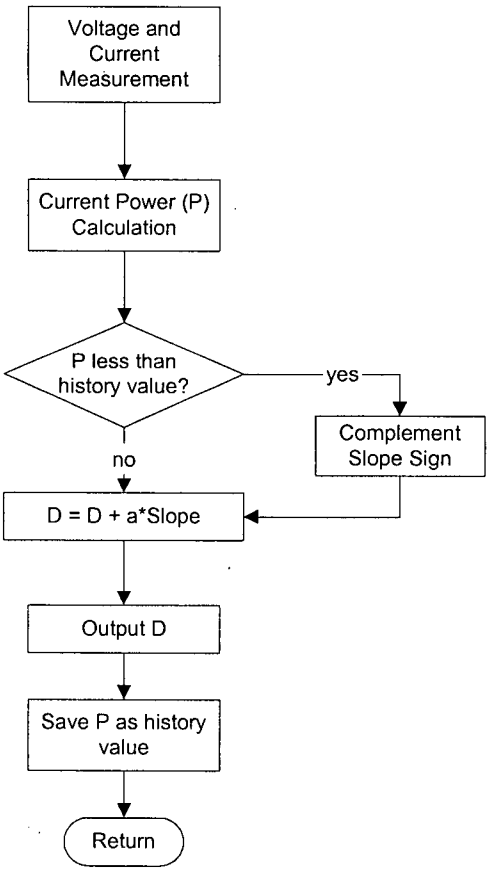

Figure 3.14 Flow Chart of Adaptive Hill Climbing MPPT Control Algorithm

Adaptive Hill Climbing with Fuzzy Logic Automatic tuning

The disadvantages of the adaptive hill climbing (AHC) method with constant incremental step on switching duty cycle were easily proved by analysis or experiment results [25]. If the incremental step of the duty factor "a" is small, the tracking time is long. It is not good in dynamic response. Otherwise, if it is chosen large, the output power fluctuating in a large range results in energy waste. It gives bad steady-state performance. If the changes of solar insolation and array temperature are taken into account, the value of duty cycle increment is very difficult to choose or tune in the adaptive hill climbing algorithm implementation. So the fuzzy logic tuning on increment "a" is introduced to maximum power point tracking [25].

Based on detailed analysis on PV output characteristics, the linguistic rules can be described as [25]:

[RULE 1]. IF the power decrease is small, then the absolute value of "a" is small

[RULE 2]. IF the power decrease is large AND the change of solar insolation is small, THEN the absolute value of "a" is big.

[RULE 3]. IF the power decrease is large AND the change of solar insolation is large, THEN the absolute value of "a" is small.

[RULE 4]. IF the power increase is small, then the absolute value of "a" is small

[RULE 5]. IF the power increase is large AND the change of solar insolation is small, THEN the absolute value of "a" is big.

[RULE 6]. IF the power increase is large AND the change of solar insolation is large, THEN the absolute value of "a" is small.

This method of maximum power point tracking using fuzzy control can be treated as an extension of the adaptive hill climbing method. The experimental results mentioned in [25] show improvements in both dynamic response (quick tracking) and steady-state condition (low power fluctuation).

It is not difficult to find that both [RULE 3] and [RULE 6] are wrong statements. In [25], it is explained that the large change of insolation doesn't move the operating point in a large range but changes the array output power significantly. If we investigate the *Power-Voltage* curve of PV output, shown in Figure 3.1(b), this assumption is correct. If we study the *P-D* relationship of a PV power system with switching mode converter, the controller needs to increase (decrease) the switching duty cycle in a large range to track a fast and large change on insolation or a big variation in load condition. The hill-climbing method is based on *P-D* curve instead of *P-V* curve. In [25], the simulation results only show good dynamic performance during the tracking start-time. And there is not any indication about improvement dealing with rapid insolation change.

3.2.5 Other Methods

The following methods can also be used in maximum power point tracking.

3.2.5.1 Feed-forward current-mode control topology

The advantage of using input and output parameters to achieve optimum or near-optimum control of dc-dc converters are broadly recognized [28].

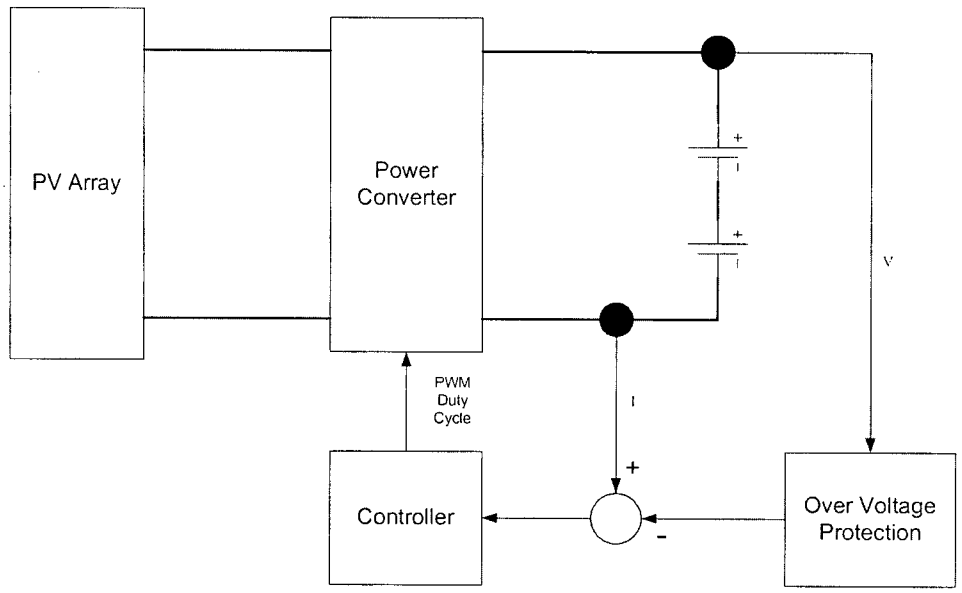

Figure 3.15 System Structure of Feed-forward Current-mode MPPT Control

For battery charging applications, where dc/dc converter output voltage can be assumed almost constant, a simplified feed-forward MPPT controller [27,29] may be applied, as shown in Figure 3.15. Feed-forward control for maximum power point tracking in PV systems need only the output converter current as a feed-forward parameter. The value of the battery charging current is used to directly control the duty cycle of the PWM control signal applied to the dc/dc converter. An output power increase results in both higher output current and higher PWM control signal duty cycle, until the maximum power is transferred to the load. The voltage regulation loop is converted into an over-voltage protection loop. This over-voltage protection loop becomes only active when the output voltage rises above a predetermined high level to avoid any damage on batteries. When it is active, no maximum power point tracking can be achieved and the charging current will be reduced to keep the battery voltage under limit.

The limitation of this method is that it can be used only in applications where the output voltage remains relatively constant, such as battery charging. Actually, the battery voltage changes significantly during charge and the discharge period. Further, although the output current is the only parameter used for control law, an additional measurement of output voltage is also essential in this implementation. It is very convenient to derive power feedback control mentioned in section 3.2.4, which can be treated as true maximum power point tracking.

3.2.5.2 Mathematical Model Based Maximum Power Point Tracking Control

A voltage-based maximum power point tracking method was presented by Mummadi Veerachary, Tomonobu Senjyu and Katsumi Uezato in 2002 [30]. Without relatively expensive current detection, the method can perform MPPT with an intermediate interleaved dual boost converter (IDB).

A mathematical model $Ppv = f(V_A, d)$ is derived from applicable PV power system. Ppv is PV output power, V_A is PV voltage and d is duty ratio of IDB. With these relationships, the maximum power point $Pmpop$ and current power condition Ppv can be calculated relatively. By comparing $Pmpop$ and Ppv, the control signal on duty ratio d can be easily generated for next step. The algorithm seems very simple, but the mathematical model is very complicated.

The disadvantage and limitation are very clear. The mathematical model is based on fixed and accurate system parameters including load impedance. In reality, it is almost impossible to reach accurate system parameters in variable environment, and the load is not always constant. Furthermore, the modeling method of switching-mode dc-dc converter has been a problem for decades due to its special characteristics.

3.2.5.3 Application of Modern Control Theories

A robust controller for MPPT in a photovoltaic power system is presented in 2002 [31]. The H_∞ robust control is adopted in array voltage regulation of MPPT system to improve the control performance. The experimental results obtained from the proposed system reduce the fluctuation of regulated power.

The fuzzy logic implementation was also applied successfully in MPPT control system [17,18,25,32]. In [33,34], an artificial neural network was used in MPPT system to improve system robustness to disturbances. All these modified algorithms are still based on fundamental theories of maximum power point tracking and not far from the basic P&O or IncCond MPPT control algorithm.

Chapter 4 The Modified Adaptive Hill Climbing Method (MAHC)

In this chapter, two important issues on MPPT techniques are analyzed, control bandwidth and power measurement. Further, based on ordinary adaptive hill climbing (AHC) control algorithm, a modified adaptive hill climbing method (MAHC) is introduced and derived, which is designed to overcome the existing drawbacks of traditional adaptive hill climbing (AHC) control algorithm.

4.1 Control Bandwidth Analysis

In a dynamic system, control bandwidth is used to specify speed of digital control. In MPPT-PV system, high control bandwidth is desirable for fast tracking requirement. But there are several limitations on system operating bandwidth no matter how high the performance of the digital controller and measurement devices is. It was mentioned in the book "Control Sensors And Actuators" [35] that "For a system to respond faithfully to a control action (input), the control bandwidth has to be sufficiently small (i.e., input has to be slow enough) in comparison to the dominant (smallest) resonant frequency of the system".

Switching mode dc-dc converters are usually slow systems with relatively large time constants, although they generally operate at very high switching frequencies. This is because that large inductors and capacitors are necessary in such topologies to keep voltage and current ripples at low level. This point implies that the controllers have to update the commanding set-point slowly and smoothly in MPPT systems with switching mode dc-dc converters, because the systems cannot response fast to command changes. Finally, a small but sufficient dither signal, at a low frequency, is superimposed on the power interface to ensure reliable and predictable processing of the MPPT algorithm. The actual system bandwidth needs to be decided by parameter calculation and experimental

results. Otherwise, the control may become unstable if it is operated with a wrong frequency.

This point was also proved in Knopf (1999)'s simulation [12] on the solar powered racing car. The simulation results show serious oscillations of MPPT control with a switching mode converter at a high sampling and control frequency (about 1KHz). In industry, the control bandwidth of MPPT control system could be even lower. The Xantrex product description [36] states "Our Maximum Power Point Tracking (MPPT) software, which samples once a minute, ensures complete harvest of the sun's energy all day long".

4.2 Power Measurements

In terms of power feedback control, the power measurement is essential for the feedback control loop. The power level can be known by sensing the voltage and current and multiplying them together, either with a micro-controller or with an analog multiplier. Either the input or output power of the power conditioner could be measured. Since the initial objective is to operate the photovoltaic array at its maximum power point, many systems measure the power at the photovoltaic array terminals. Another possibility is to maximize the actual usable power: the output power of the power conditioner. In practice the MPPT system is effective with either.

It is widely found that the current measurement is critical for successful MPPT control. If we do some investigation on the basic waveforms of different switching mode DC-DC converter comparatively, the continuous current through inductors is good for instrumentation. In a buck converter, the continuity lies on output current side (Figure 2.10). For boost converter, the current goes continuously in the input side. It is convenient to put current sensor/transducer to measure the continuous current, which is close to DC value. Otherwise, an analog filters with large time constants are required in the signal conditioning circuits and the digital controllers need do digital filtering to get the stable DC values of current condition, which are necessary in power feedback MPPT control systems.

In the MPPT system introduced in section 2.1.3, a buck converter is used as power interface. So the output power will be maximized by the proposed MAHC control

algorithm, which will be described in following sections. This system structure can be illustrated in Figure 4.1

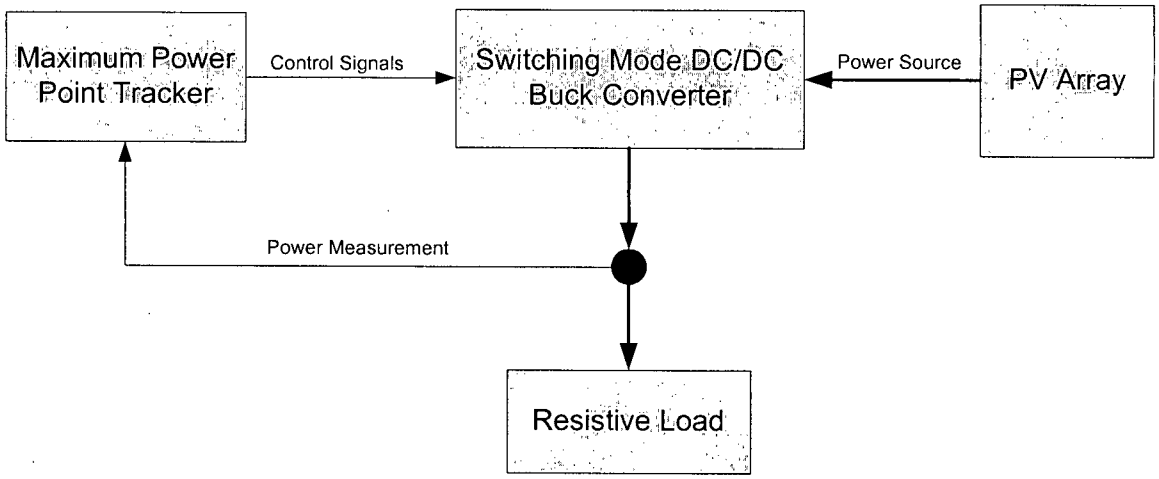

Figure 4.1 System Block Diagram with Power Measurement Located at Converter Output Side

4.3 Issues Related to Adaptive Hill Climbing Method (AHC)

The adaptive hill climbing method (AHC), a simple MPPT control method introduced in section 3.2.4.4, which tracks the maximum power point by comparison of output powers at different operating points is generally used to find the maximum power point. This method developed the direct relationship between the switching duty ratio and the PV system output power. However, this method is not enough to provide the good performances on both tracking stages and steady-state stages.

In [22], it is pointed out that the P&O MPPT algorithm sometimes deviates from MPOP in case of rapidly changing atmospheric conditions, such as broken clouds. This problem could happen with the adaptive hill climbing method as well. In the case of a sudden increase in insolation *Ga* dominating the output power change, the adaptive hill-climbing algorithm may just keep the perturbation in the same direction as the previous one, which could lead the operating point far away from the actual MPOP. This process continues until the increase in insolation slows down or ends.

So it is necessary to solve the drawbacks of AHC by applying the modified AHC for better tracking performance.

4.4 The Modified Adaptive Hill Climbing Method (MAHC)

The Modified Adaptive Hill Climbing Method (MAHC) will be introduced in this section. The modifications of AHC include automatic parameter tuning and control mode switching.

4.4.1 Automatic Parameter Tuning

The issues were discussed in section 4.3 that there was tradeoff between dynamic response and steady state condition due to the selection of "*a*", the incremental step of switching duty ratio. Through analysis, it is ideal to make "*a*" large during transient stage and *"a"* small in steady state. In MAHC, this problem was solved by the automatic tuning of parameter *"a"* on-line. The system control and tuning mechanism is shown in Figure 4.2.

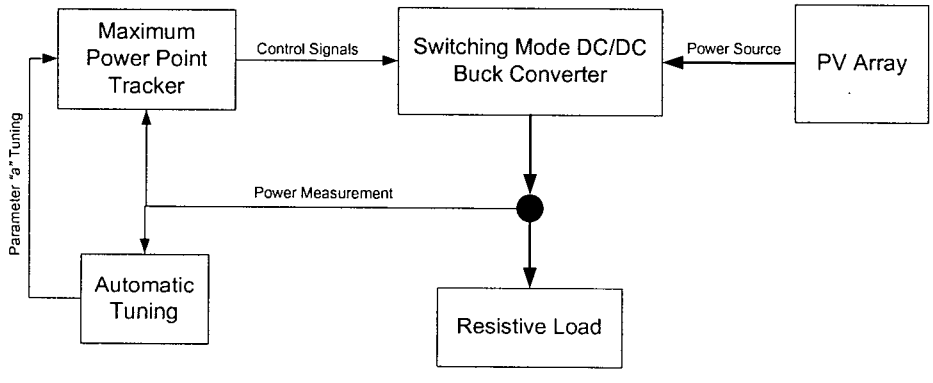

Figure 4.2 Proposed MAHC Control Structure with Automatic Parameter Tuning

In the design, the automatic tuning topology was illustrated as a linear equation:

$$Ta(k) = M \frac{|\Delta P|}{a(k-1)}$$

where $\Delta P = P(k)-P(k-1)$, represents the change of power condition, $a(k-1)$ is the historic value of "*a*", M is constant parameter, and $Ta(k)$ is a tuning index that decides the

next value of "*a*". When power changes in a large range, the tuning index will indicate the controller that the "*a*" needs to be switched to a large value to satisfy the fast response requirement during the transient stage. When the power change is small, the controller assumes that the system enters the steady state and the value of "*a*" becomes small to keep control signal change smoothly. With the automatic tuning, both dynamic and steady-state requirements are considered in the controller design, because the critical parameter is updated and adjusted adaptively.

4.4.2 Control Mode Switching

It was shown that the traditional hill climbing method could cause the operating point deviating from MPOP during the period of rapid insolation changes. This problem could be corrected by switching the control mode. The control algorithm can be demonstrated in flow chart format shown in Figure 4.3.

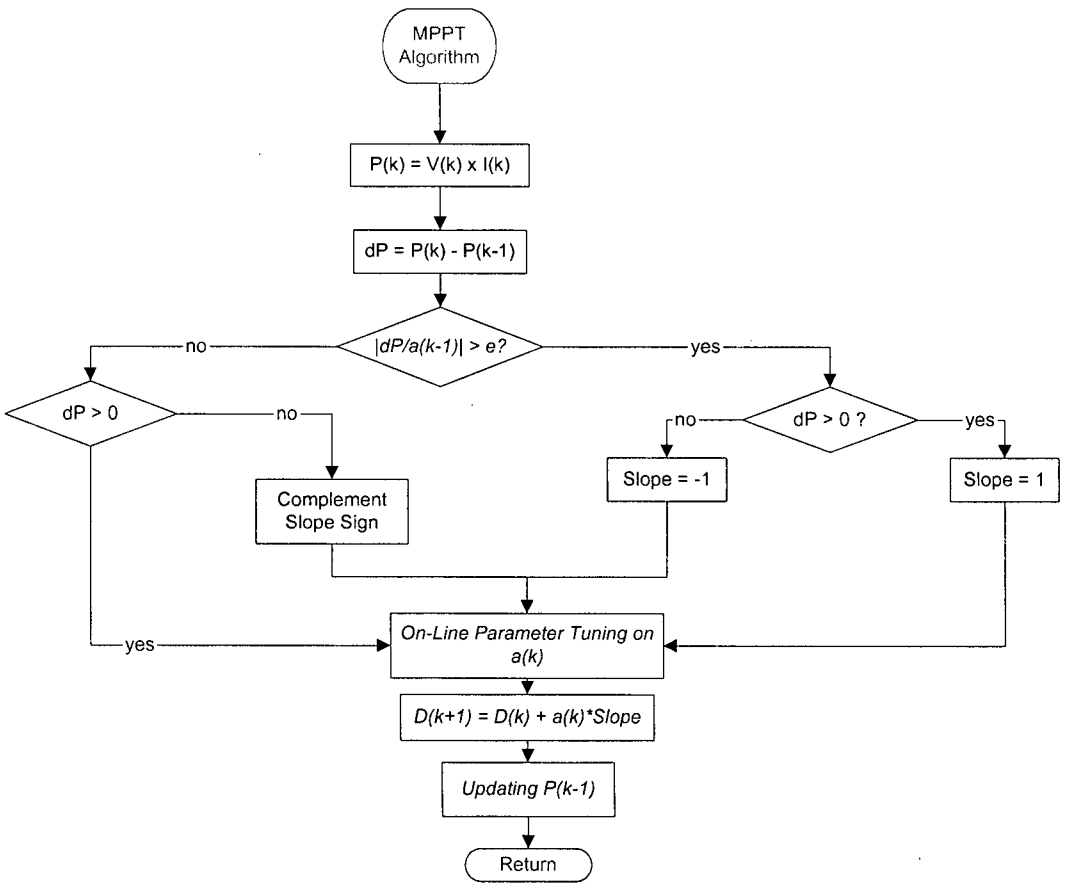

Figure 4.3 Flow Chart of the Modified Adaptive Hill Climbing MPPT Control Algorithm

The switching criterion is defined as $|dP/a(k-1)|$. If the value of $|dP/a(k-1)|$ is larger than the threshold *"e"*, the controller understands that the power variation was mainly caused by the solar insolation, so the increment of duty factor is set to the same direction as *dP*, the change of power condition. The perturbation direction is represented by "*Slope*" in the flow chart (Figure 4.3). If the value of $|dP/a(k-1)|$ is small, the controller assumes that the system control is within the steady state, or the large change on power is caused by the large step of *"a"* only. During this period, the ordinary hill climbing method is adopted. In this control mechanism, there are two important tuning parameters, *"e"* and *"M"*, which make the controller more flexible to deal with different situations. The validity of the presented control and tuning mechanism will be evaluated in simulation and experimental results, demonstrated in following chapters.

Chapter 5 Simulation and Evaluation

This chapter presents how the mathematical models of the proposed PV power system and maximum power point tracking algorithm are implemented and evaluated by using SIMULINK®, a model-based software package for modeling, simulating and analyzing dynamical systems. The effectiveness and advantage of the proposed modified adaptive hill climbing control (MAHC) algorithm is verified by way of simulation results.

5.1 Modeling System Components

The MPPT-controlled photovoltaic power system introduced in section 2.1.3 and the control algorithm proposed in chapter 4 could be simulated as a combination of components as shown in Figure 5.1. Individual block sets represent the actual physical parts of the system. They can be modeled and tested individually and then interconnected later. These models are based on the characteristic equations derived in chapter 2 and chapter 4. Therefore, MPPT techniques and converter types can be combined and their operation can be simulated on solar panels of any desired size under an unlimited variety of operating conditions. The following paragraphs will clarify how the various component block sets for this study were modeled and on which mathematical equations they are based.

5.1.1 Solar Module

The mathematical models of photovoltaic cell and module were introduced in Section 2.2 and were given by Equation 2.1 and Equation 2.2.

The model parameters used in the system simulation are from the PV module SM50-H, manufactured by Siemens Solar Industries. The technical data about this module are listed in Table 5-1.

With Simulink®, the PV module models were constructed by several different blocks and the blocks were integrated together to create one final PV array block, in which the number of modules need be defined in series and in parallel relatively. The final block diagram of the PV array is illustrated in Figure 5.2.

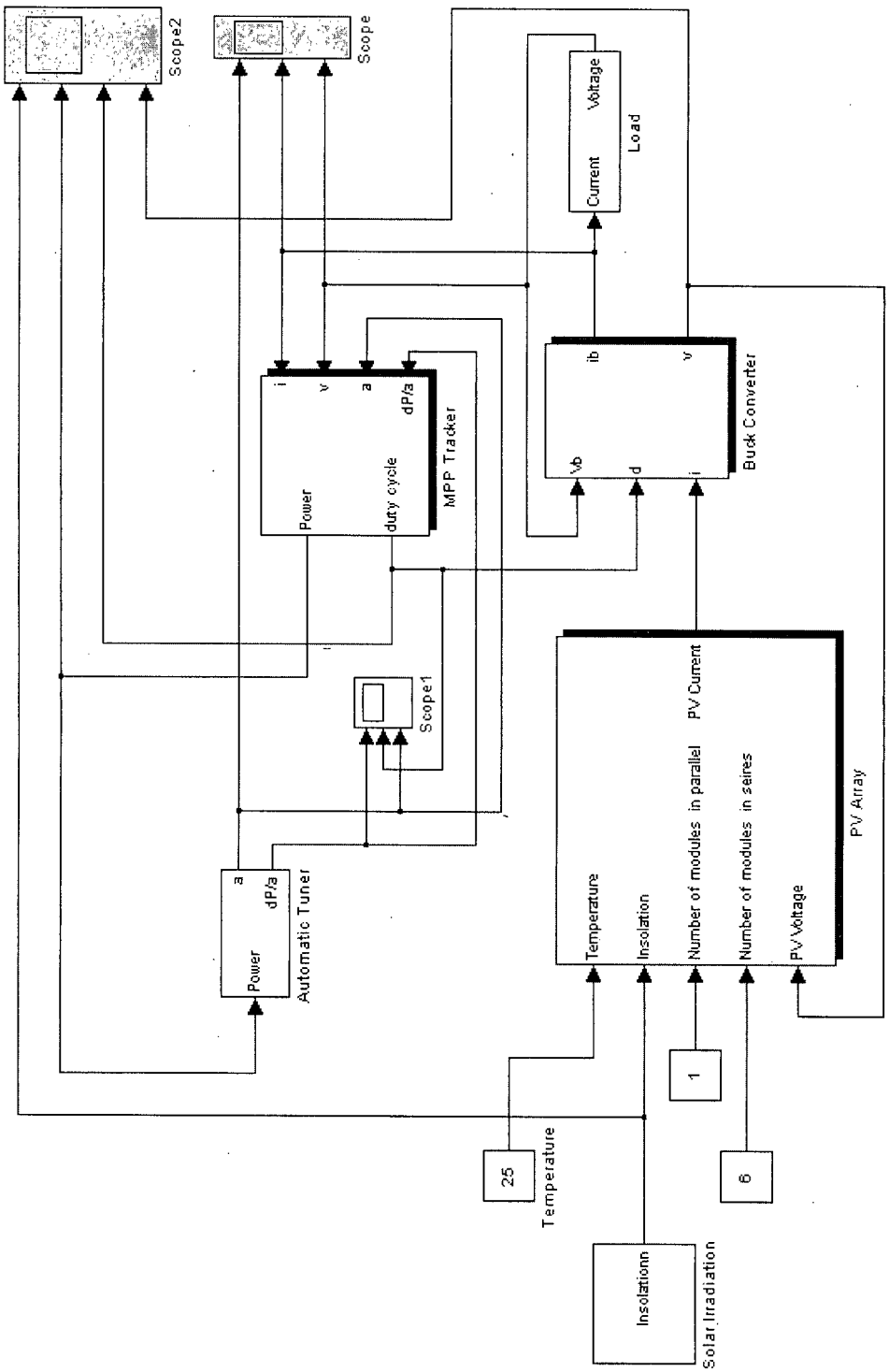

Figure 5.1 Simulink® Model of the Proposed MPPT Control System

Table 5-1 Electrical parameters of solar module SM50-H

Module maximum power rating Pmax [W]	50
Module short circuit current Isc [A]	3.35
Module open circuit voltage Voc[V]	19.8
Number of cells in series Ns	33
Number of cells in parallel Np	1
Temperature coefficient: short-circuit current [mA/°C]	1.2
Temperature coefficient: open-circuit voltage [V/°C]	-0.077

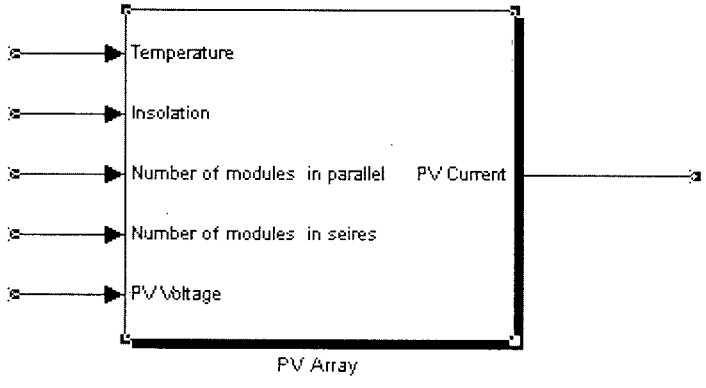

Figure 5.2 The Simulink® Model of a Solar Array

The values of temperature, insolation, number of module in series, and number of modules in parallel are accessible as external variables and changed anytime during the simulation process. This makes it possible to observe and evaluate the system's reaction to sudden changes in the operating conditions, such as variations in irradiation caused by passing sources of shade.

The simulated current-Voltage relation curves of this specific module are shown in Figure 5.3 (b, c, d and e). For good comparison, the output characteristics provided by manufacturer is illustrated in Figure 5.3(a). The parameter tuning is essential to make the mathematical model has similar output feature as the real module. But it is very difficult to make them completely identical with the limited tuning parameters based on such mathematical model. The importance of this simulation model is that it can clearly reflect, the influences on the PV array's output characteristics with the change of temperature and insolation.

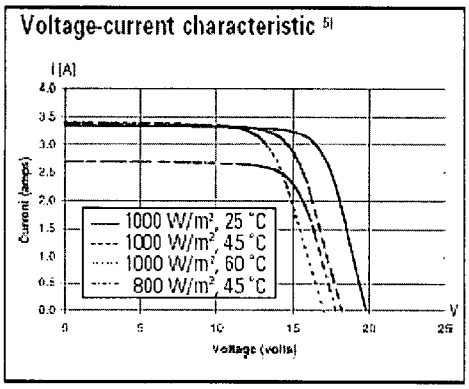

(a) I-V curve (From datasheet of solar module SM50-H)

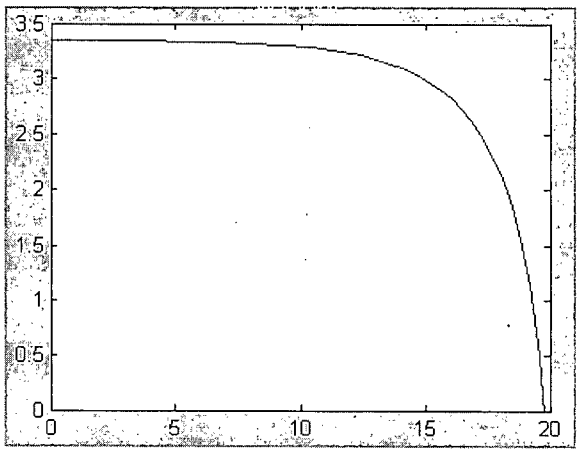

(b) I-V Curve (1000W/m², 25°C)

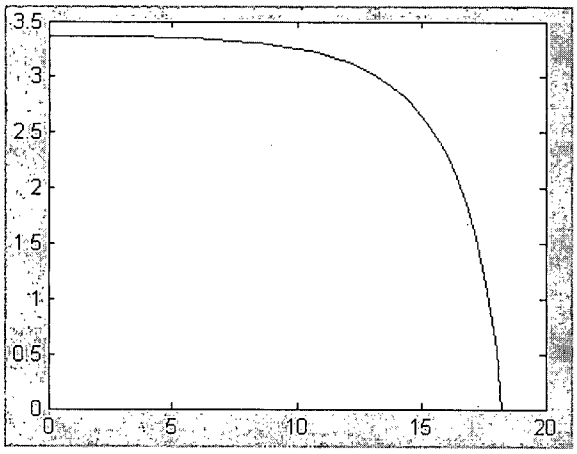

(c) I-V Curve (1000W/m², 45°C)

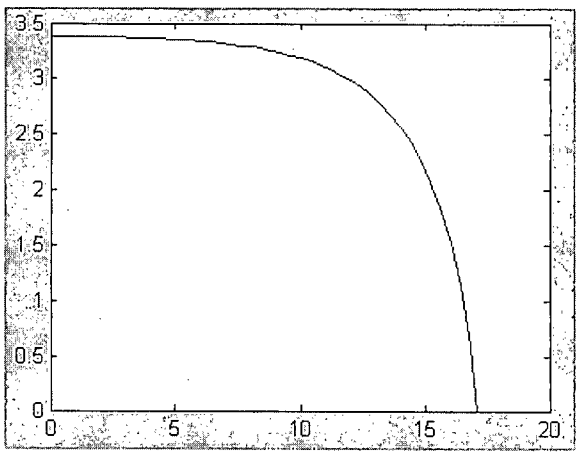

(d) I-V Curve (1000W/m², 60°C)

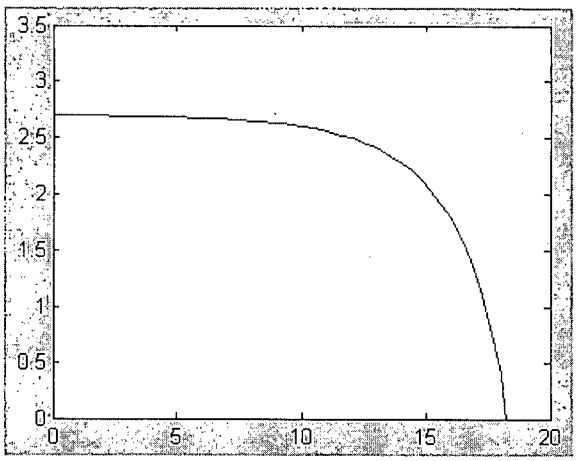

(e) I-V Curve (800W/m², 45°C)

Figure 5.3 Comparisons of PV Module Output Characteristics Between Simulation Results and Real Product Characteristics

5.1.2 The Switched Mode DC-DC Buck Converter

The mathematical modeling method of switching mode dc-dc converter was introduced in section 2.3.2. A simplified Simulink® dc-dc converter model was presented by Knopf's thesis [12] in 1999. In the following paragraphs, a dc-dc buck converter is modeled based on this method.

5.1.2.1 Modeling an Ideal Buck Converter

To further investigate the ideal buck converter and to derive its mathematical model, the equivalent circuit representation for the two different switch states (open and close switch) must be analyzed. Figure 5.4 shows equivalent circuit diagram of a buck converter with the switch closed during time interval *DTs*. Figure 5.5 represents the buck converter with the switch open during the time interval *D'Ts*, where *D'* denotes the complement of the duty cycle *D*, define as

$$D' = 1 - D \tag{5.1}$$

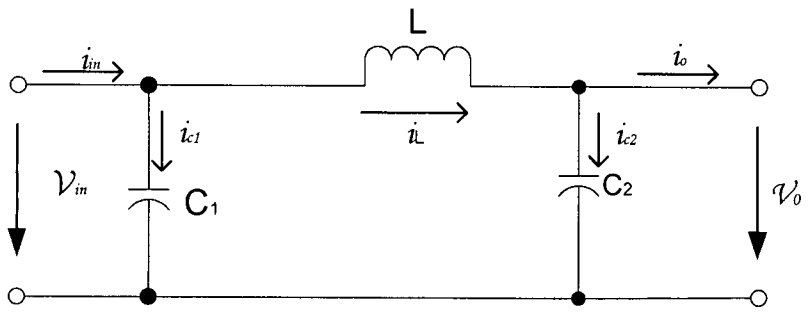

Figure 5.4 Equivalent Circuit of an Ideal Buck Converter at Switch "on" Time

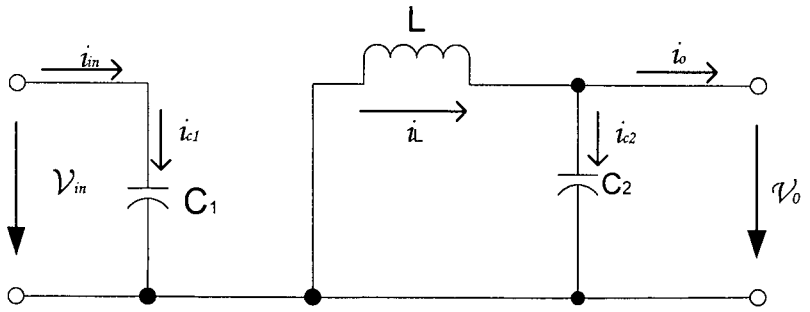

Figure 5.5 Equivalent Circuit of an Ideal Buck Converter at Switch "off" Time

Applying Kirchhoff's law to the circuit in Figure 5.4 (Switch on period) leads to the following set of equations:

$$i_{C1}(t) = C_1 \frac{dv_{in}(t)}{dt} = i_{in}(t) - i_L(t) \tag{5.2}$$

$$i_{C2}(t) = C_2 \frac{dv_o(t)}{dt} = i_L(t) - i_o(t) \tag{5.3}$$

$$v_L(t) = L \frac{di_L(t)}{dt} = v_{in}(t) - v_o(t) \tag{5.4}$$

Using Kirchhoff's law on Figure 5.5 (Switch off period), a second set of equations is obtained:

$$i_{C1}(t) = C_1 \frac{dv_{in}(t)}{dt} = i_{in}(t) \tag{5.5}$$

$$i_{C2}(t) = C_2 \frac{dv_o(t)}{dt} = i_L(t) - i_o(t) \tag{5.6}$$

$$v_L(t) = L \frac{di_L(t)}{dt} = -v_o(t) \tag{5.7}$$

With state variable averaging modeling method mentioned section 2.3.2, the equations (5.2)-(5.7) can be combined together to obtain an averaged system description.

$$\frac{dv_{in}(t)}{dt} = \frac{1}{C_1}\left[i_{in}(t) - Di_L(t)\right] \tag{5.8}$$

$$\frac{dv_o(t)}{dt} = \frac{1}{C_2}\left[i_L(t) - i_o(t)\right] \tag{5.9}$$

$$\frac{di_L(t)}{dt} = \frac{1}{L}\left[Dv_{in}(t) - v_o(t)\right] \tag{5.10}$$

Equations (5.8)-(5.10) can be expressed as forms suited to be implemented in Simulink®.

$$i_L(t) = \frac{1}{D}\left[i_{in}(t) - C_1 \frac{dv_{in}(t)}{dt}\right] \tag{5.11}$$

$$i_o(t) = i_L(t) - C_2 \frac{dv_o(t)}{dt} \tag{5.12}$$

$$v_{in}(t) = \frac{1}{D}\left[v_o(t) + L \frac{di_L(t)}{dt}\right] \tag{5.13}$$

Now the coupled relationship can be easily implemented as a Simulink® simulation model, shown in Figure 5.6.

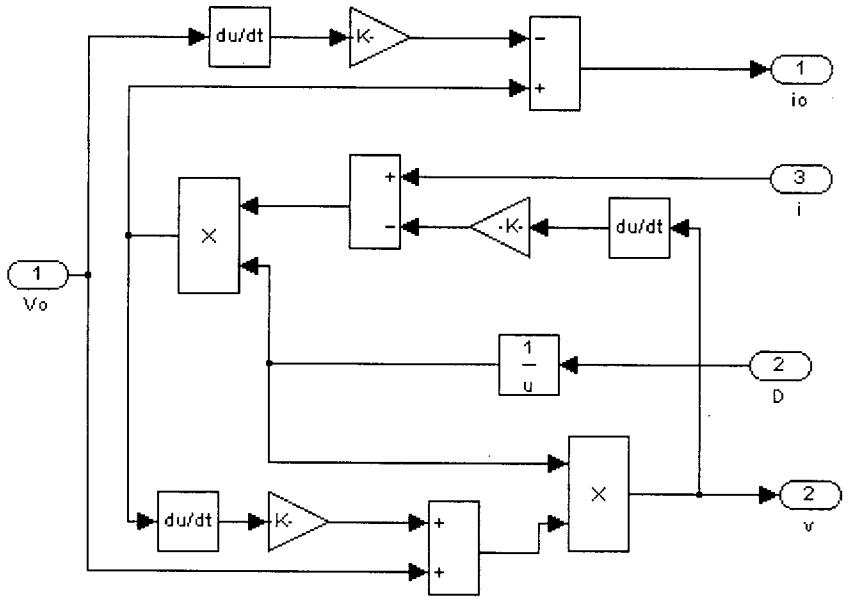

Figure 5.6 Block Diagram of Simulink® Model as a DC/DC Buck Converter

With Simulink®, the simulation model of the switching mode buck converter can be simplified into only one block, shown in Figure 5.7.

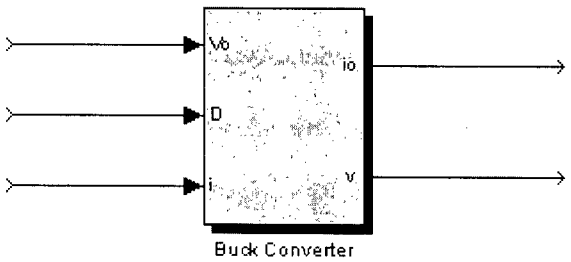

Figure 5.7 One Block Representation of Buck Converter

There are three inputs and two outputs. *D* represents the switching duty cycle from controller, *Vo* and *Io* are the output voltage and output current relatively, and *V* and *I* represent the input voltage and input current.

5.1.3 The MPPT Controller

The modified adaptive hill climbing (MAHC) MPPT controller, which was introduced in chapter 4, was implemented in a similar fashion as the other system components

discussed in the previous sections. The Simulink® model of the proposed method is illustrated in Figure 5.8. It can also be further integrated into one model block shown in Figure 5.9.

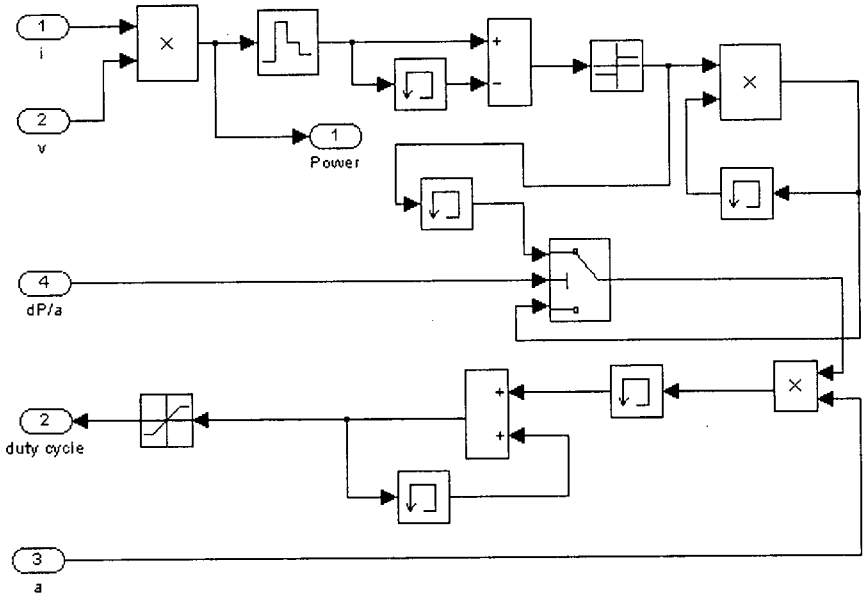

Figure 5.8 Simulink® Model of The Modified Hill Climbing MPPT Controller

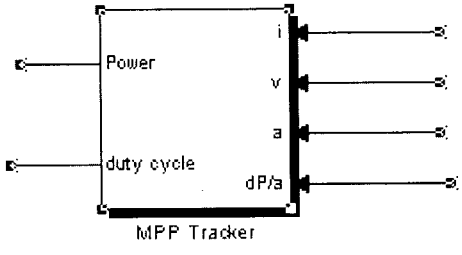

Figure 5.9 One Block Representation of MPP Tracker

There are 4 inputs and 2 outputs. Duty cycle represents the control signal to DC/DC converter. The power output is used for system monitoring. Inputs *i* & *v* is used as power calculation. "a" is the duty cycle implemental step tuned by automatic tuner. "dP/a" represents the criteria switching the control mode to adapt the fast changing of solar insolation. A block set of Zero-Order Hold (ZOH) shown in Figure 5.8 was implemented. It is used to set the sampling period of digital controller.

5.1.4 Automatic Tuner

The Simulink® tuner model is represented in Figure 5.10. A block set of ZOH is also presented to simulate digital control. The tuner monitors the system power conditions and modified the control parameter "a" in real time.

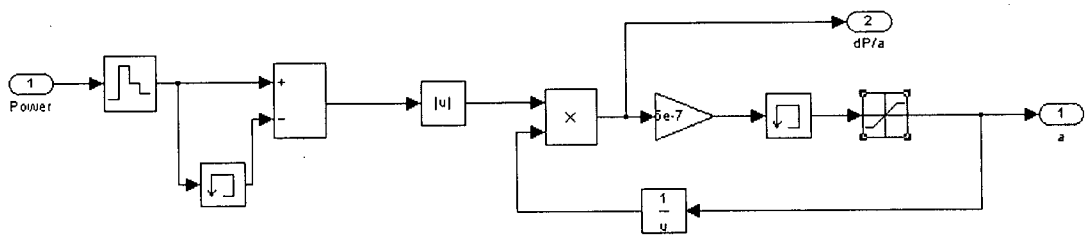

Figure 5.10 Simulink® Model of Proposed Automatic Tuner

With fewer modifications, this controller model can be used for the simulation with standard adaptive hill climbing (AHC) method, which will be used for performance comparison.

5.2 Simulation Results

The simulations provide the valuable opportunity to evaluate various MPPT techniques presented earlier and analyze their behavior under the exact same operating conditions. The main focus will be on the power ripple caused by oscillations around MPP and the fast determination for MPP.

In reality, photovoltaic cell temperature changes slowly, although it shifts V_{MPOP} in a large range. This indicates that its change is not directly related to system dynamic response. So a fixed temperature value is set to 25°C in all upcoming simulations. The PV array is configured to 2.1KW output with 120V open-circuit voltage. The detailed simulation conditions and configuration are summarized in Table 5-2. The only fast changeable variable used in simulation is solar insolation programmed from 990W/m^2 to 510W/m^2 alternatively. This kind of rapidly changing insolation could be caused by mixed, fast moving cloud cover. One case is that the rapidly changing irradiation will be represented by a sequence of rectangular signals, shown in Figure 5.11. Another case is

designed to verify tracking performance with smoothly changing insolation, which is represented by triangular waveform shown in Figure 5.12.

Table 5-2 Table of Simulation Conditions

Temperature:	25°C
Irradiation Range:	0 – 1000W/m^2
PV Module:	Siemens SM50-H
PV Array configuration:	7 modules in parallel 6 modules in series
Maximum Power Output at standard condition:	2100W

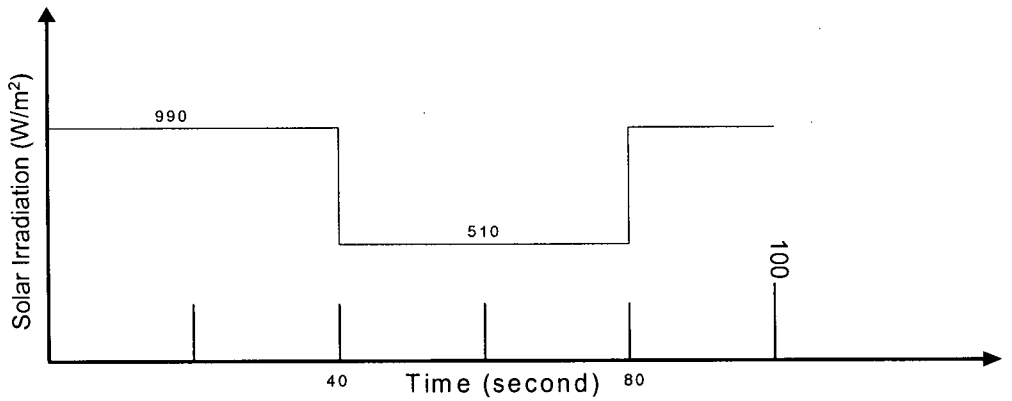

Figure 5.11 Simulated Waveform of the Sudden Change of Solar irradiation

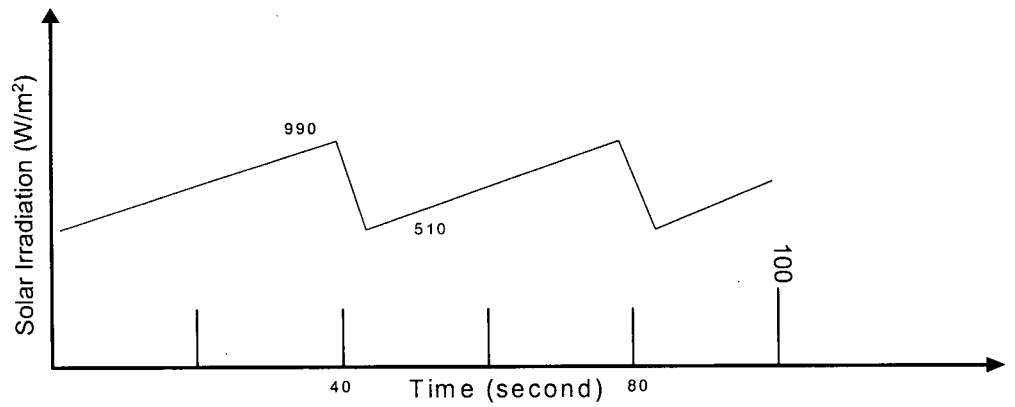

Figure 5.12 Simulated Waveform of the Smooth Change of Solar Irradiation

5.2.1 Adaptive Hill Climbing Method

For better comparisons between standard adaptive hill climbing (AHC) method and the modified one (MAHC), the simulation results of AHC will be presented in this section. Figures (5.13 – 5.16) show the simulated results of maximum power point tracking performance controlled by AHC. The simulations can be described as follows.

At the beginning, the MPPT manages to adjust the duty ratio D very quickly such that a stable maximized power output is reached. The sudden irradiation changes happened at the moments of 40s and 80s. At these moments, the operating power points deviate from peak power point. The MPPT need to re-adjust the control variables to bring the maximum power operating point (MPOP) back.

The first case is designed to evaluate the system response of sudden irradiation change. MPPT controls the PWM input of the dc-dc converter by adjusting its duty ratio D in relatively large increment step of a = 2%. These simulation results demonstrate fast response to instant change of solar irradiation, but large ripples on steady state, as shown in Figure 5.13. At the 40s, the tracking even went to the wrong direction and the deviation was corrected when insolation change was over.

The second case is that MPPT controller outputs duty ratio D in a small increment step of a = 0.4% under sudden irradiation change. The simulation results demonstrate good performance in steady state, but slow response to fast changing environment. The waveforms are shown in Figure 5.14.

The third case is designed to test the system response with smooth irradiation change. The MPPT controls the PWM input of the dc-dc converter by adjusting its duty ratio D by a relatively large increment of a = 2%. The simulation results are shown in Figure 5.15. The MPPT controller can make the system follow the irradiation very fast but is not able to avoid large power ripple due to relatively strong control signals.

The fourth case is that MPPT controller outputs duty ratio D in a small increment of a = 0.4% under smooth irradiation change. The simulation shows unstable control condition (Figure 5.16). The system is completely out of control because the control signals are too weak to dominate the change of power caused by change of solar irradiation. The controller failed to follow the change of irradiation until the irradiation

change slow down. This simulation shows that very small control step can cause control system unstable with adaptive hill climbing control algorithm.

The simulation results illustrate some drawbacks on this standard adaptive hill climbing (AHC) control algorithm. These limitations were presented and analyzed in section 3.2.4.4 and chapter 4 in details. Fixed incremental step "*a*" on duty cycle fails to provide good performance on both transient stage and steady state. In specific cases, the AHC controller can be confused by sudden change of insolation and give wrong control signals. Further simulations presented in following sections show that these problems will be corrected through applying MAHC method.

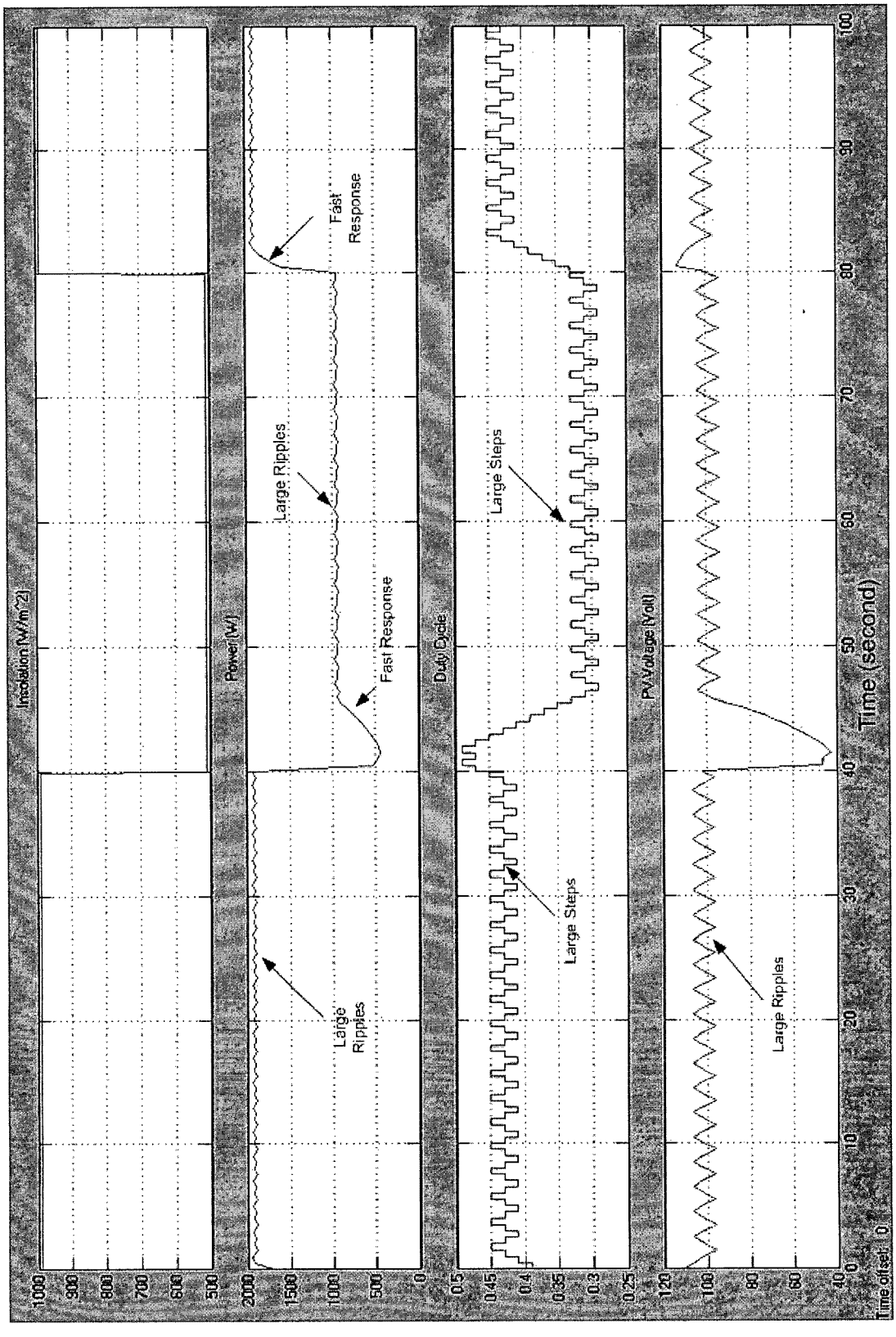

Figure 5.13 Simulation Results of AHC Tracking under Sudden Irradiation Change (a = 2%)

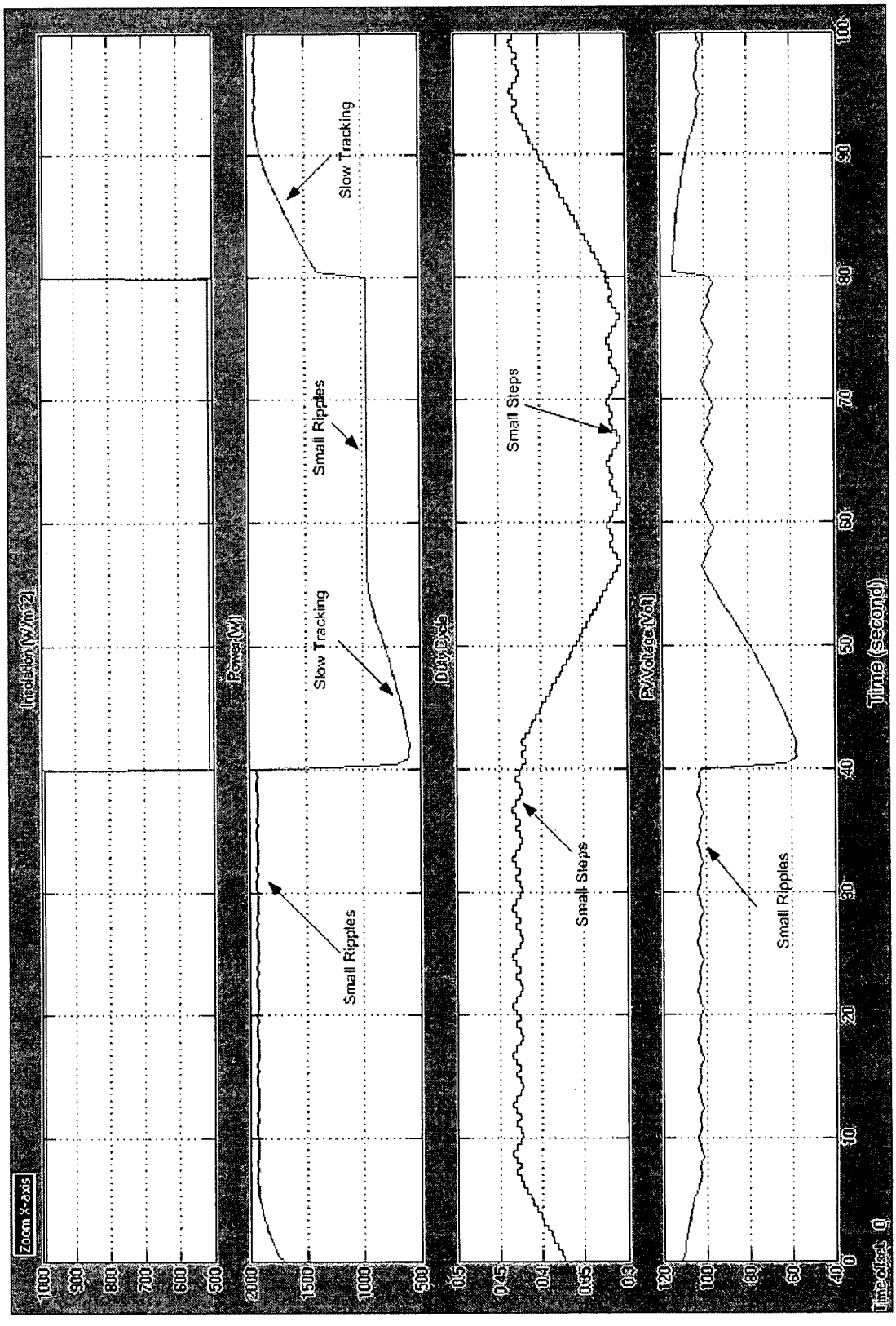

Figure 5.14 Simulation Results of AHC Tracking under Sudden Irradiation Change (a = 0.4%)

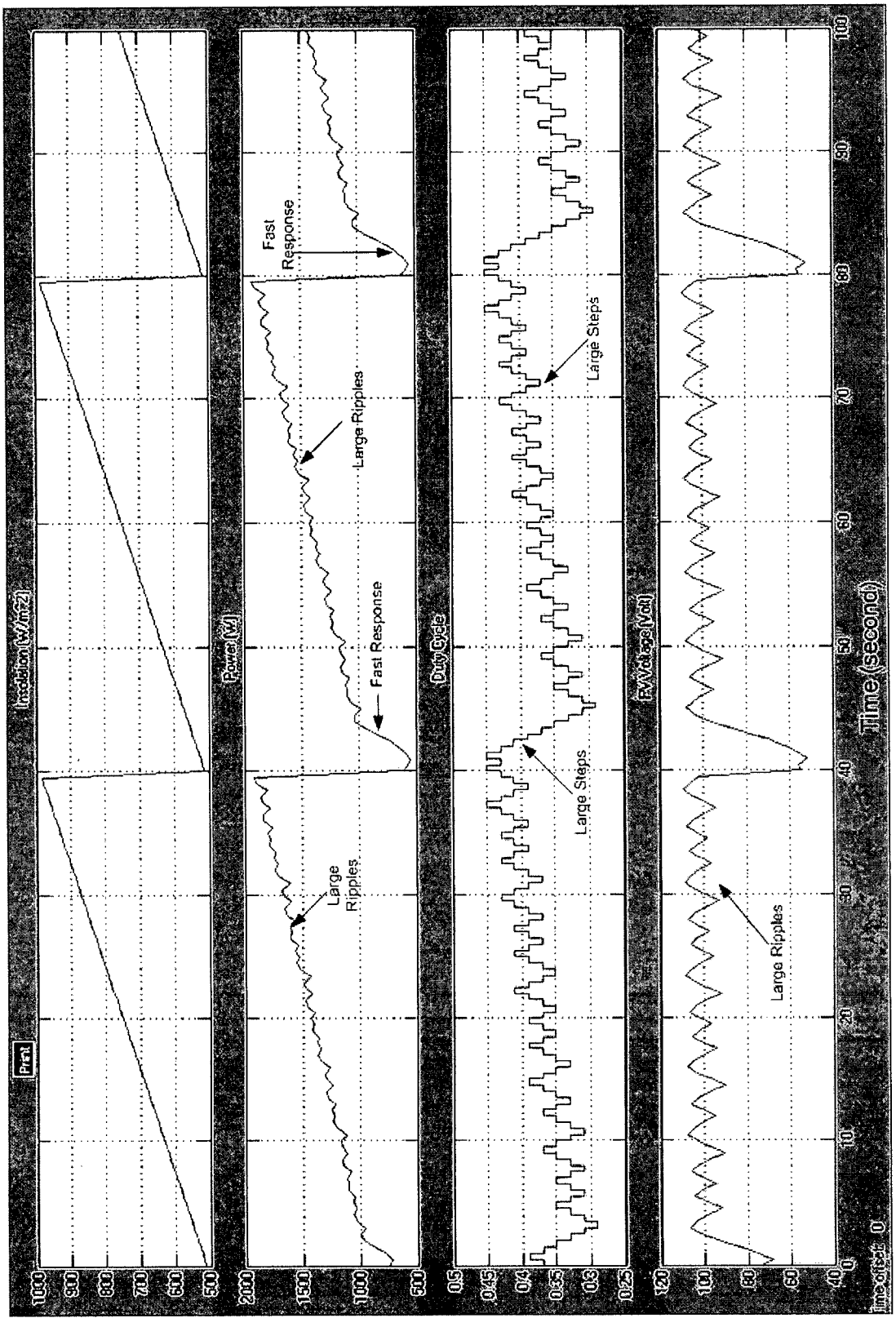

Figure 5.15 Simulation Results of AHC Tracking under Smooth Irradiation Change (a = 2%)

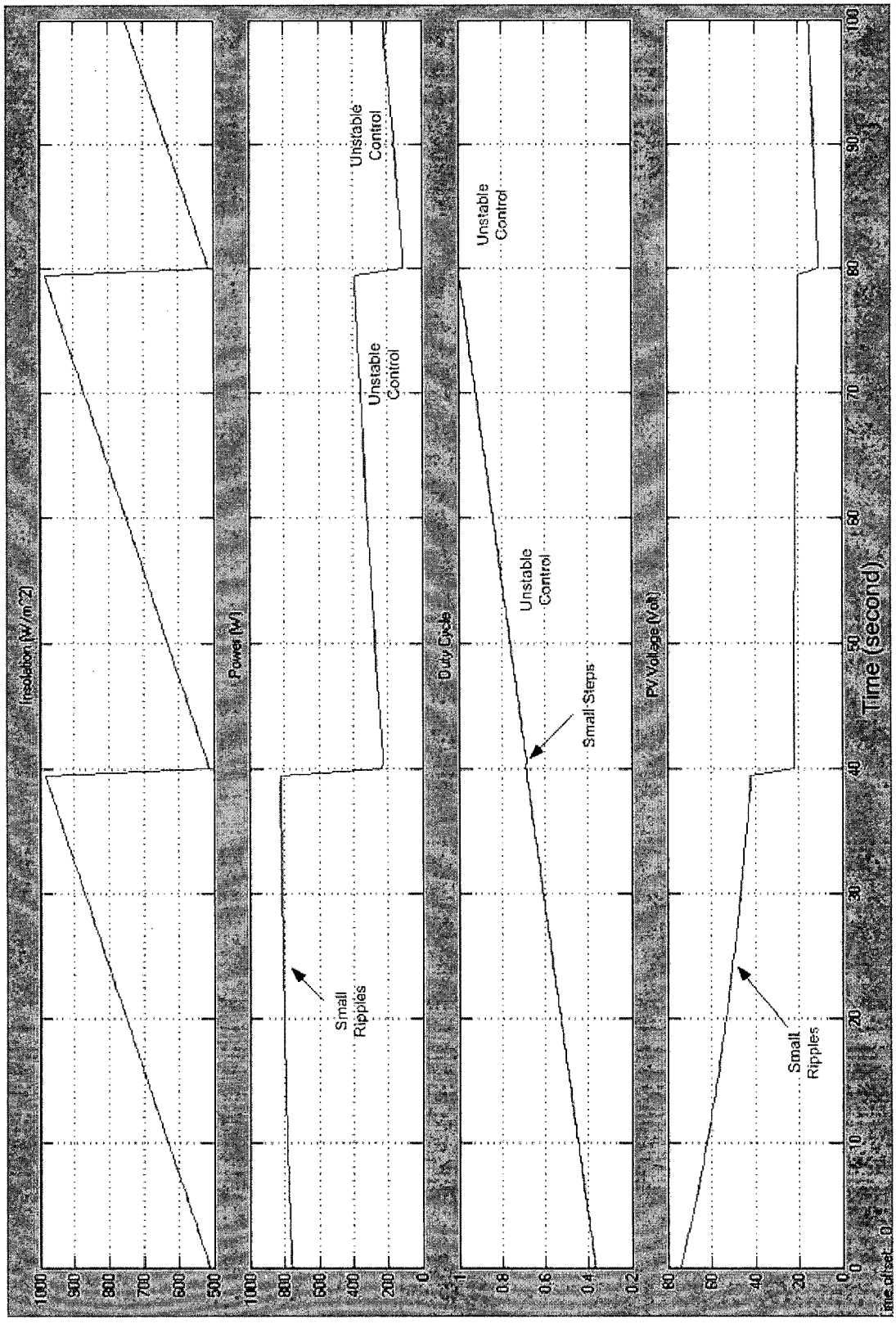

Figure 5.16 Simulation Results of AHC Tracking under Smooth Irradiation Change (a = 0.4%)

5.2.2 The Modified Adaptive Hill Climbing Method

The modified adaptive hill climbing method (MAHC) was introduced in chapter 4. Based on standard adaptive hill climbing method (AHC), it was modified to meet good-performance requirement on both dynamic stage and steady state. In this section, the simulation results based on MAHC control system will be introduced and analyzed. For good comparison, the simulations are under exactly the same conditions as former simulations with AHC control algorithm. Figures (5.17, 5.18) show the simulated results of maximum power point tracking performance by using MAHC method. The simulations can be described as follows.

At the beginning, the MPPT manages to adjust the duty ratio D very quickly such that a stable maximized power output is reached. The sudden irradiation changes happened at the moments of 40s and 80s. At these moments, the operating power points deviate from peak power point. The MPPT need to re-adjust the control variables to bring the maximum power operating point (MPOP) back.

The simulation results show better performance by way of this suggested MPPT technique over standard adaptive hill climbing (AHC) method. The maximum power points in Figure 5.17 were determined quickly and tracked accurately. The controller operates well under dynamically varying insolation. The simulation results also show both good performances on steady state condition and improved performance on low-level power stage. Figure 5.18 shows the good following and tracking performance with smoothly changing insolation, which is represented by triangular waveform.

The improved performance can also illustrated in the comparison tables. In Table 5-3, the tracking time and power ripple are shown and compared under sudden change in irradiation. It is clear that the MAHC gives better overall performance on both dynamic response and steady-state stage.

In Table 5-4, average values of delivered power are presented and compared. These data can be treated as the most direct parameters to evaluate MPPT control systems. The power system with MAHC control algorithm shows best results on power conversion with 1.520KW average power output. With AHC control, the highest value was 1.507KW, when incremental steps of duty cycle were set between 1% and 2%. These results prove the effectiveness of MAHC algorithm in MPPT control system.

Table 5-3 Comparison on Tracking Time and Steady-State Power Ripple

MPPT Algorithm	AHC		MAHC
Incremental Step	*"a" = 2%*	*"a"=0.4%*	"*a*" is adaptive
Tracking Time at 1st Point	7 seconds	20 seconds	8 seconds
Tracking Time at 2st Point	3 seconds	17 seconds	3.5 seconds
Steady-state power ripple	Large	Small	Small

Table 5-4 Comparison on Delivered Power Values

MPPT algorithm	Incremental Step "a"	Average power delivery	Description
AHC	0.04	1439W	
	0.03	1498W	
	0.02	1507W	Optimal parameter for AHC algorithm
	0.01	1507W	Optimal parameter for AHC algorithm
	0.008	1493W	
	0.005	1492W	
	0.003	1463W	Simulations show unstable situation during certain environment
MAHC	Adaptive	1520W	Highest efficiency on power delivery

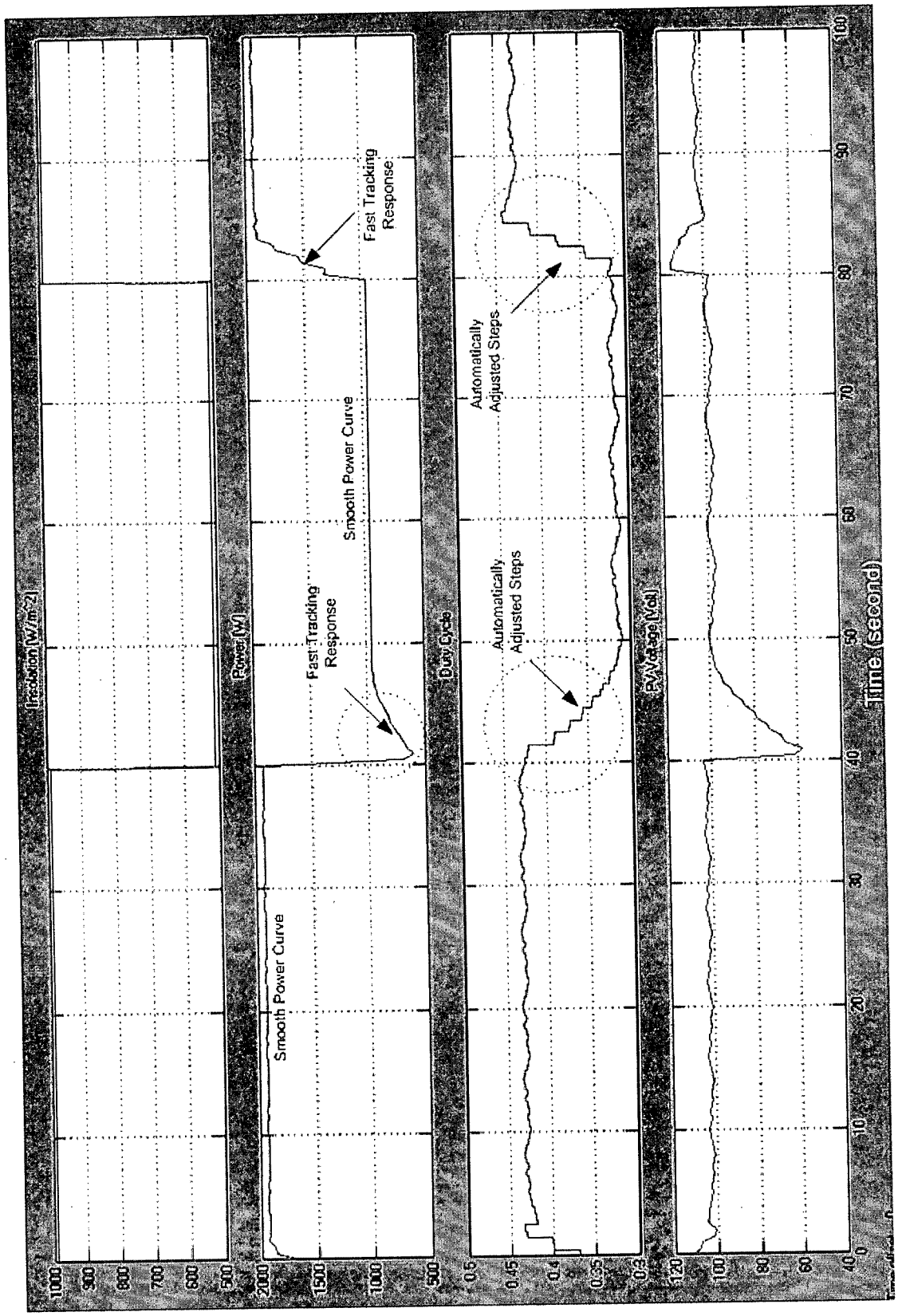

Figure 5.17 Simulation Results of Sudden Insolation Change With MAHC Tracking

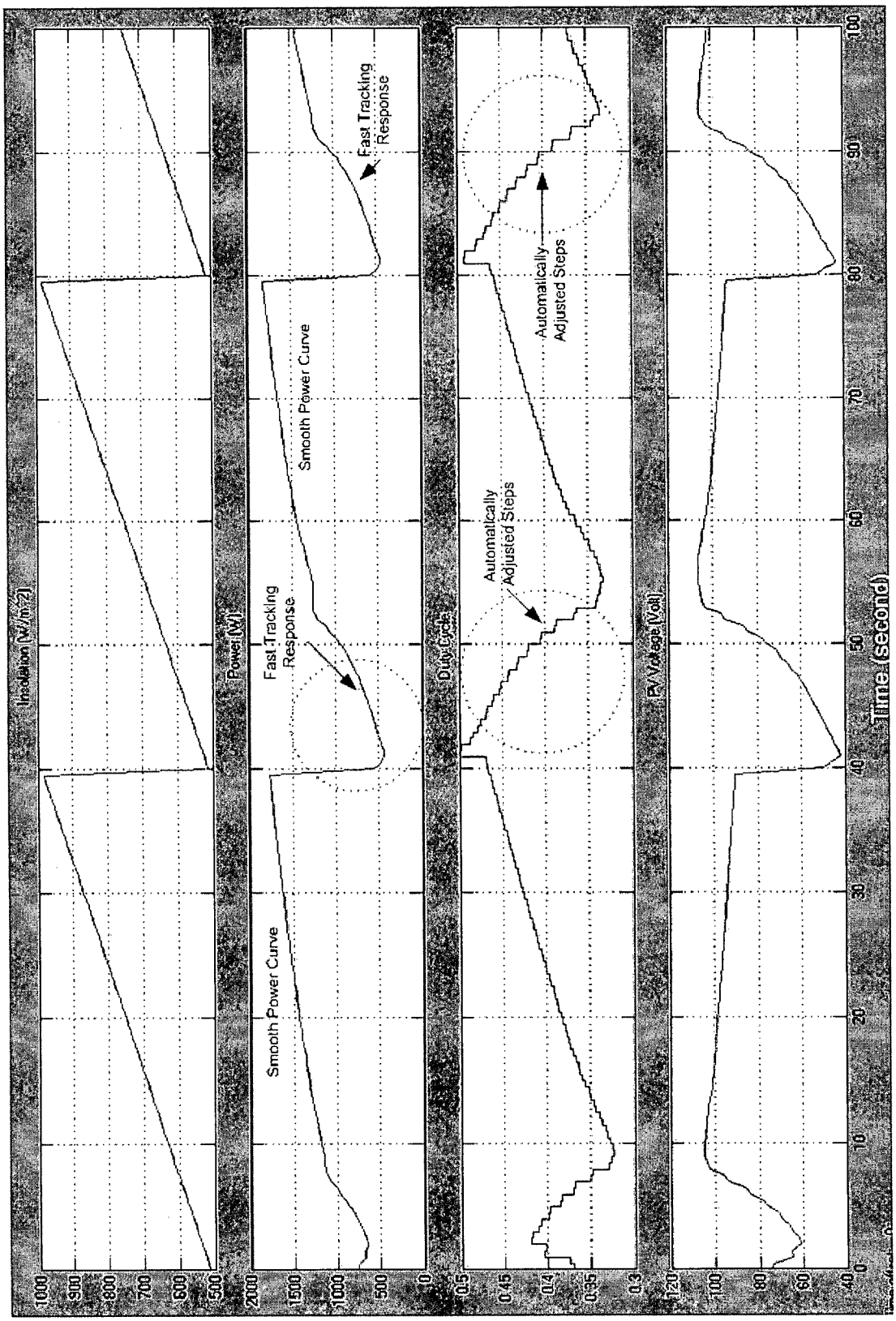

Figure 5.18 Simulation Results of Smooth Insolation Change With MAHC Tracking

Chapter 6 System Design and Evaluation

To evaluate MPPT control algorithm, a DSP-controlled MPPT test system was designed and built. The structure of this system was first introduced in section 2.1.3. In this chapter, the system design and implementation will be described in details. The experimental results are used to illustrate the effectiveness of the proposed MAHC algorithm.

6.1 System Specifications

This photovoltaic power system comprises of two PV panels, one power conditioner (DC/DC converter) and one resistive load. The specifications of this test system are defined as:

- Converter Topology: Buck
- Converter Switching Frequency: 60KHz
- Maximum Power capacity: 64W
- Input Voltage Range: 20-40Vdc
- Output Voltage Range: 10-16Vdc
- Two PV panels are configured in series
- PV Panel* specs
    - Open circuit voltage: 19.6Vdc
    - Manufacturer: SILONEX INC
    - Maximum Power rating: 32W

*The two PV panels used in this system are very old product. No detailed specification is available. The given parameters are based on testing result and estimation.

6.2 System Context

Figure 6.1 shows the structure of this testing system. In this application, the two PV panels are the power source, which delivers electrical power to load and supplies control

circuits. The eZDSP^{TM} LF2407 acts as a digital controller of the whole system, in which control algorithms are implemented. Combining with personal computer (PC), the eZDSP^{TM} LF2407 also provides a physical base for system testing of hardware and software. The converter power board (CPB) is the executive unit for maximum power point tracking by way of power conversion. Linear voltage regulators, transducers and signal conditioners are also located in the CPB. A load is essential for system operation. We use a DC lamp as a resistive load. A useful feature of the lamp is that there is a visible indication of power changes.

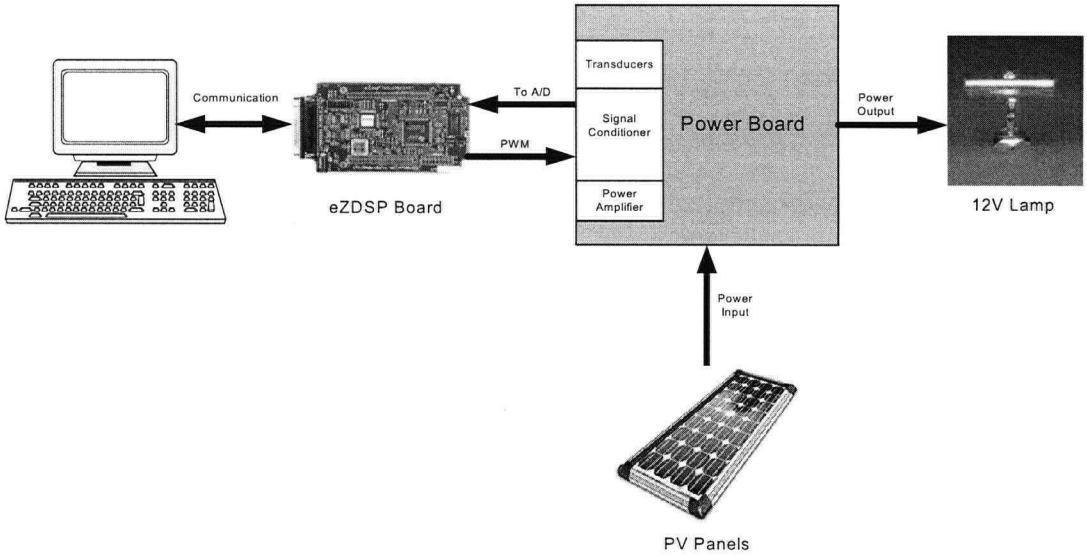

Figure 6.1 MPPT Test Bed System Context Diagram

6.3 Static Relationship

The physical hierarchy of the system is shown in Figure 6.2.

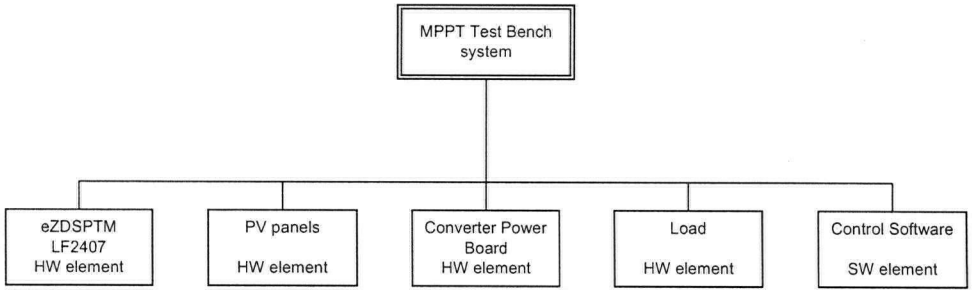

Figure 6.2 System Physical Hierarchy

6.4 Hardware Design

As show in Figure 6.1, the necessary hardware of the system includes an eZDSP^{TM} LF2407 board, a converter power board, two PV panels and a DC load.

6.4.1 eZDSP^{TM} LF2407

The eZDSP^{TM} LF2407 board is shown in Figure 6.3.

6.4.1.1 Overview of the eZDSP^{TM} LF2407

The eZDSP^{TM} LF2407 is a stand-alone card. It is shipped with a TMS320LF2407, 16-bit fix point DSP chip. An onboard JTAG connector provides interface to emulators, operating with other debuggers to provide assembly language and 'C' high level language debug. [37]

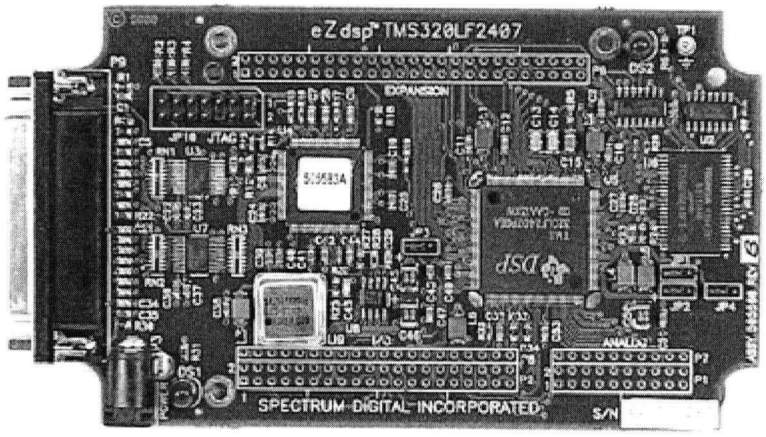

Figure 6.3 eZDSP™ Board

6.4.1.2 Key Features of the eZdsp™ LF2407

The eZdsp^{TM} LF2407 has the following features [37]:

- TMS320LF2407 Digital Signal Processor
- 30 MIPS operating speed

- 64K words onboard program/data RAM
- 32K words on-chip Flash memory
- Onboard 7.3728-MHz oscillator
- 3 Expansion Connectors (analog, I/O, expansion)
- Onboard IEEE 1149.1 JTAG Controller
- 5-volt only operation with supplied AC adapter
- TI Code Composer tools driver
- On board IEEE 1149.1 JTAG emulation connector

6.4.2 Converter Power Board

The converter power board is shown in Figure 6.4. It is a prototype board design and implementation of this test system.

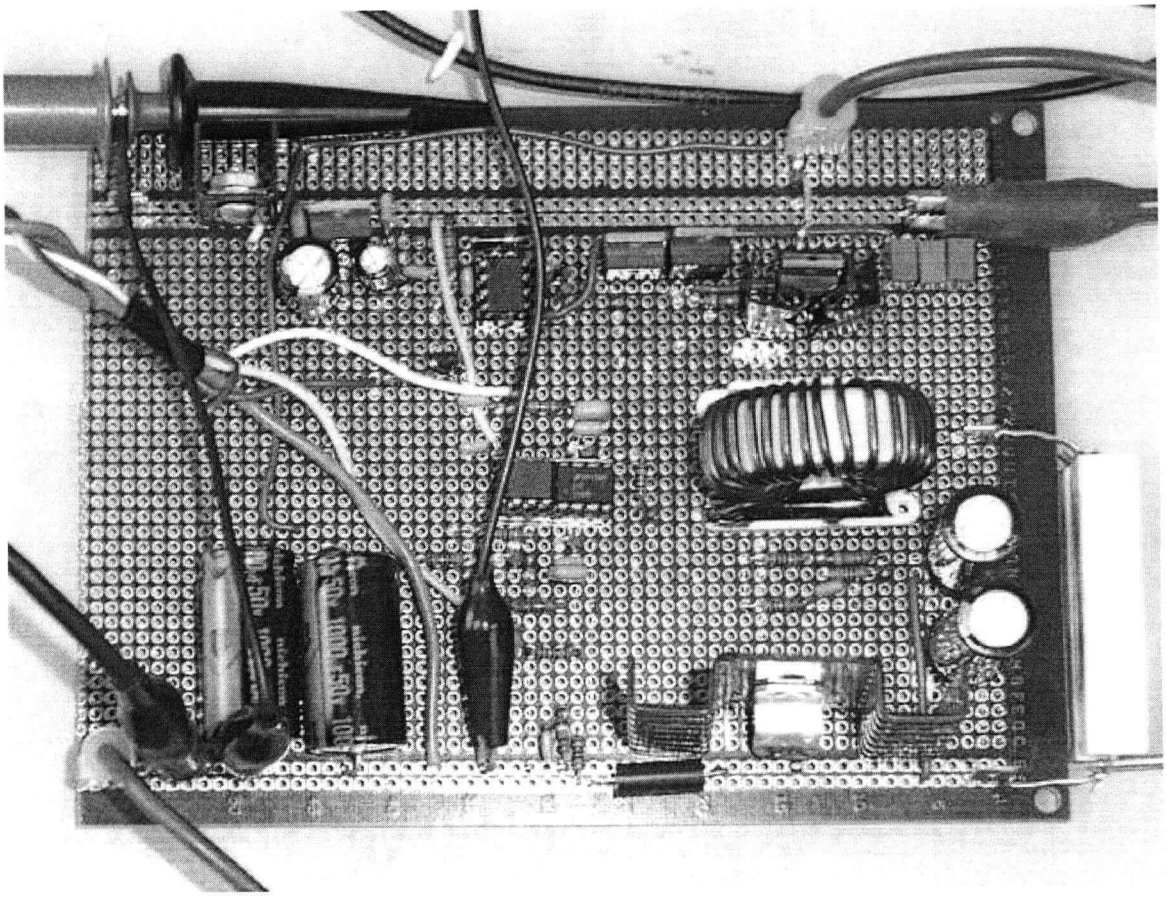

Figure 6.4 Converter Power Board

The structure of CPB is presented in Figure 6.5. It comprises a power unit, a sensing signal conditioning unit, a control signal conditioning unit and voltage regulation unit.

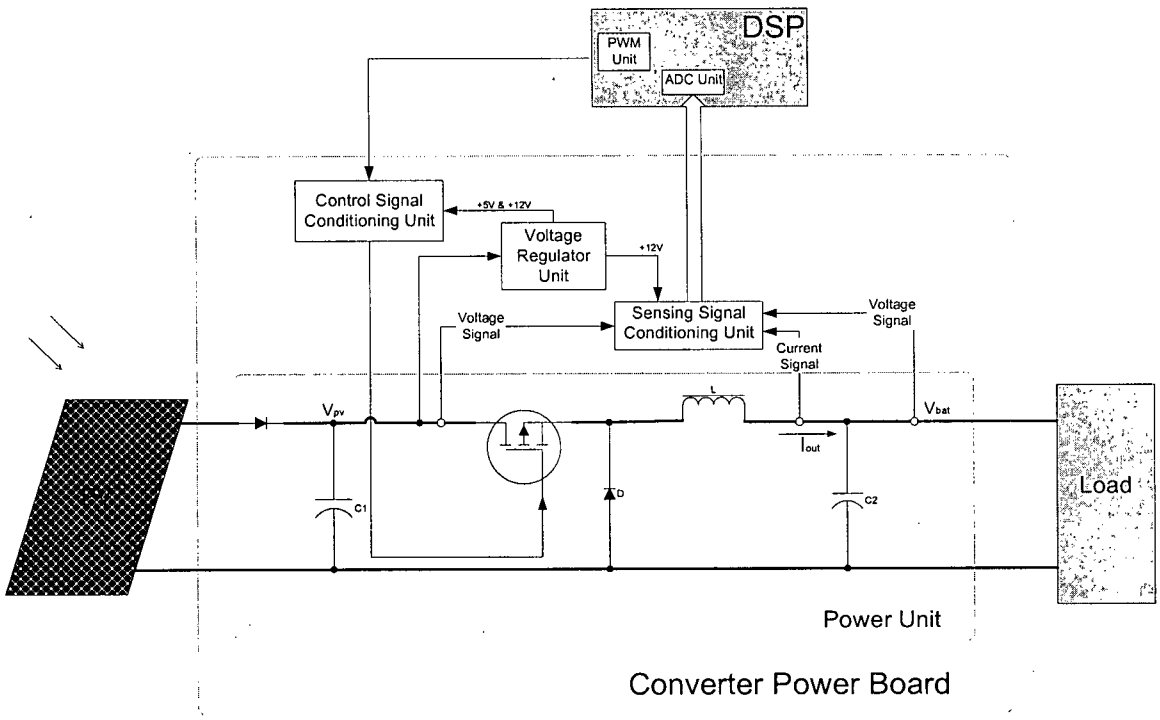

Figure 6.5 Diagram of System Hardware Architecture

6.4.2.1 Power Unit

The power unit can be treated as standard switching-mode DC/DC buck converter (SMDDBC). The only difference is that a blocking diode is included on the input side. The blocking diode is essential for PV usage as we mentioned in Chapter 2. Voltage and current transducers are classified in this unit. Figure 6.6 (b) shows the detailed design of this unit.

6.4.2.2 Sensing Signal Conditioning Unit

The measured feedback signals need to be fed into the signal-conditioning block, which scales and offsets the voltages to the desired levels for the A/D module of DSP. An important factor that we must consider in any practical control system is noise, including external disturbances. Furthermore, weak signal will have to be amplified. So in this unit, signal conditioning methods such as filtering and amplification are implemented in electronic circuitry. There are three sensed signals shown in Figure 6.5. Table 6-1 lists

the detailed descriptions. The detailed circuitry design about this unit is illustrated in Figure 6.6(a).

Table 6-1Signal Measurement Description

Symbols	Descriptions
Vpv	PV voltage or input voltage of DC/DC converter, monitored by system operation
Vbat	Output voltage of DC/DC converter, Which is used in power feedback control loop
Iout	Output Current of DC/DC converter, which is used in power feedback control loop

The input voltage (*Vpv*) of DC/DC converter, the corresponding input voltage (*Vpvo*) to ADC Channel of DSP and the resulting ADC data register values are listed in Table 6-2. The measurement resolution on this signal is 40.28mV.

Table 6-2 Converter Input Voltage Scaling and Level Shifting

Vpv(V)	*Vpvo*(V)	ADCFIFO
0	0	0000h
40	3.2	F800h
41.25	3.3	FFC0h

The output voltage (*Vbat*) of DC/DC converter, the corresponding input voltage (*Vbato*) to ADC Channel of DSP and the resulting ADC data register values are listed in Table 6-3. The measurement resolution on this signal is 25.46mV.

Table 6-3 Converter Output Voltage Scaling and Level Shifting

Vbat(V)	*Vbato*(V)	ADCFIFO
0	0	0000h
20	2.53	C464h
26.07	3.3	FFC0h

The output current (*Iout*) of DC/DC converter, the corresponding input voltage (V*iouto*) to ADC Channel of DSP and the resulting ADC data register values are listed in Table 6-4. The measurement resolution on this signal is 4.13mA.

Table 6-4 Converter Output Current Scaling and Level Shifting

Iout(A)	*Viouto*(V)	ADCFIFO
0	0	0000h
2	1.56	7909h
4.23	3.3	FFC0h

6.4.2.3 Control Signal Conditioning Unit

The DSP controller generates the pulse width modulation (PWM) signals as a control command based on the MPPT calculation. The control signal-conditioning unit collects these commands and converts them to driving signals for switching the MOSFET in the power unit. Electrical isolation between the power MOSFET and the control circuit is often desirable. An optically coupled IC is used for electrical isolation in this system. Because the system uses buck topology with n-channel MOSFET, the MOSFET drive circuit must be floating with respect to the circuit ground. In this case, the "bootstrap" circuit is designed and shown in schematics (Figure 6.6 (a)).

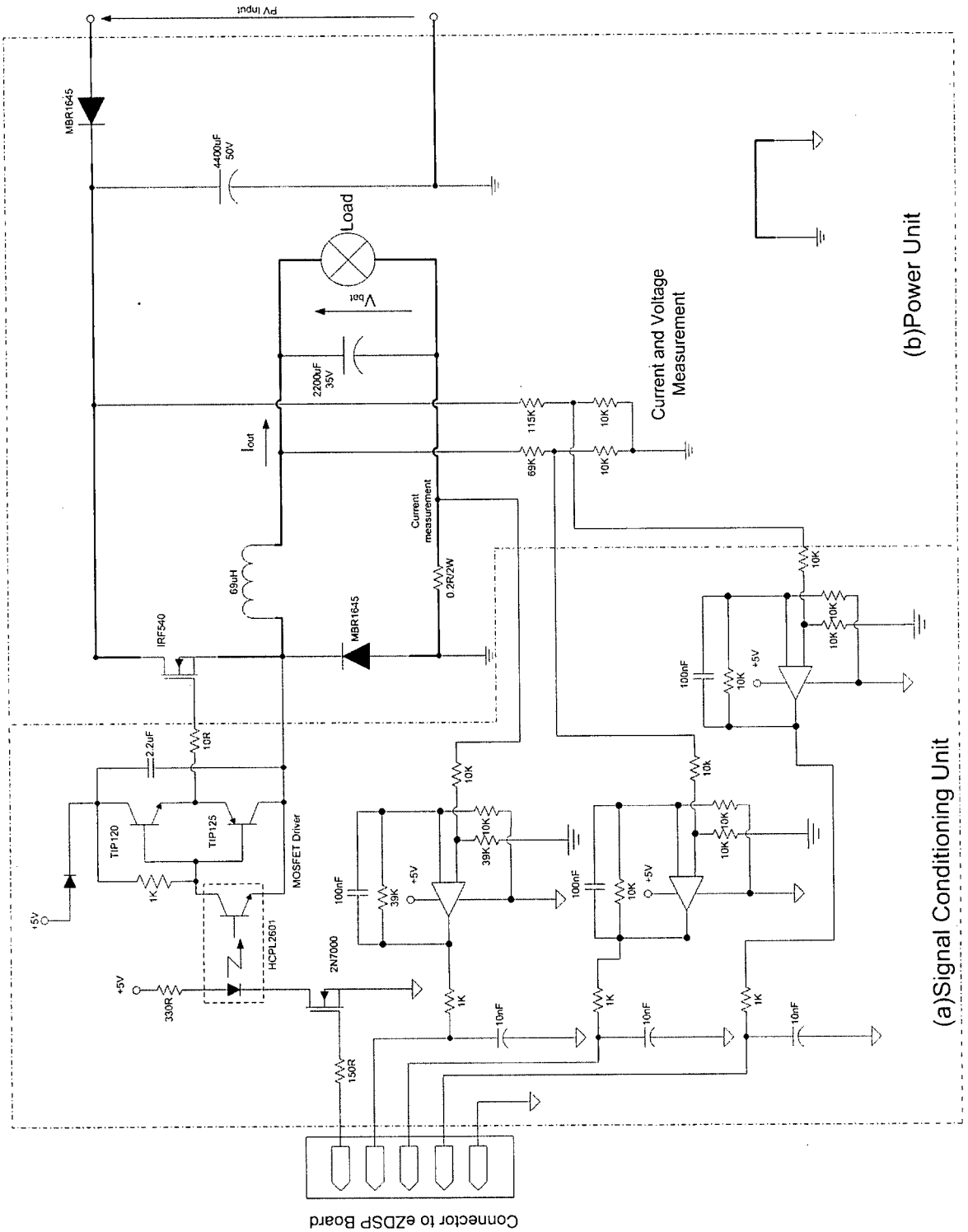

Figure 6.6 Schematics of Converter Power Board

6.5 Software Design

6.5.1 Software Architecture

The language for programming the device is C. The direct benefits of using C in embedded systems design are as follows [38].

- *Programmer won't be overwhelmed by details*
- *It can allow the programmer to spend more time on algorithm design and less time on implementation*

C is a kind of high-level language. Programmers will be able to program and change their control algorithm quickly and easily using C. In this application, the calculation time of each control cycle based on C programming is estimated as 60μs. The maximum control bandwidth is designed to 10Hz, and the maximum sampling frequency is set to 8kHz. So there is not any overhead related real time execution with C programming

6.5.2 Software Flowchart

The flowchart diagram is basically a representation of the relationships between major and minor tasks in the embedded software.

Figure 6.7 is software flow chart of this system. After system initiation, software goes to background loop. Signal sampling and maximum power point tracking calculation are executed in timer interrupt service routine to guarantee fixed control bandwidth.

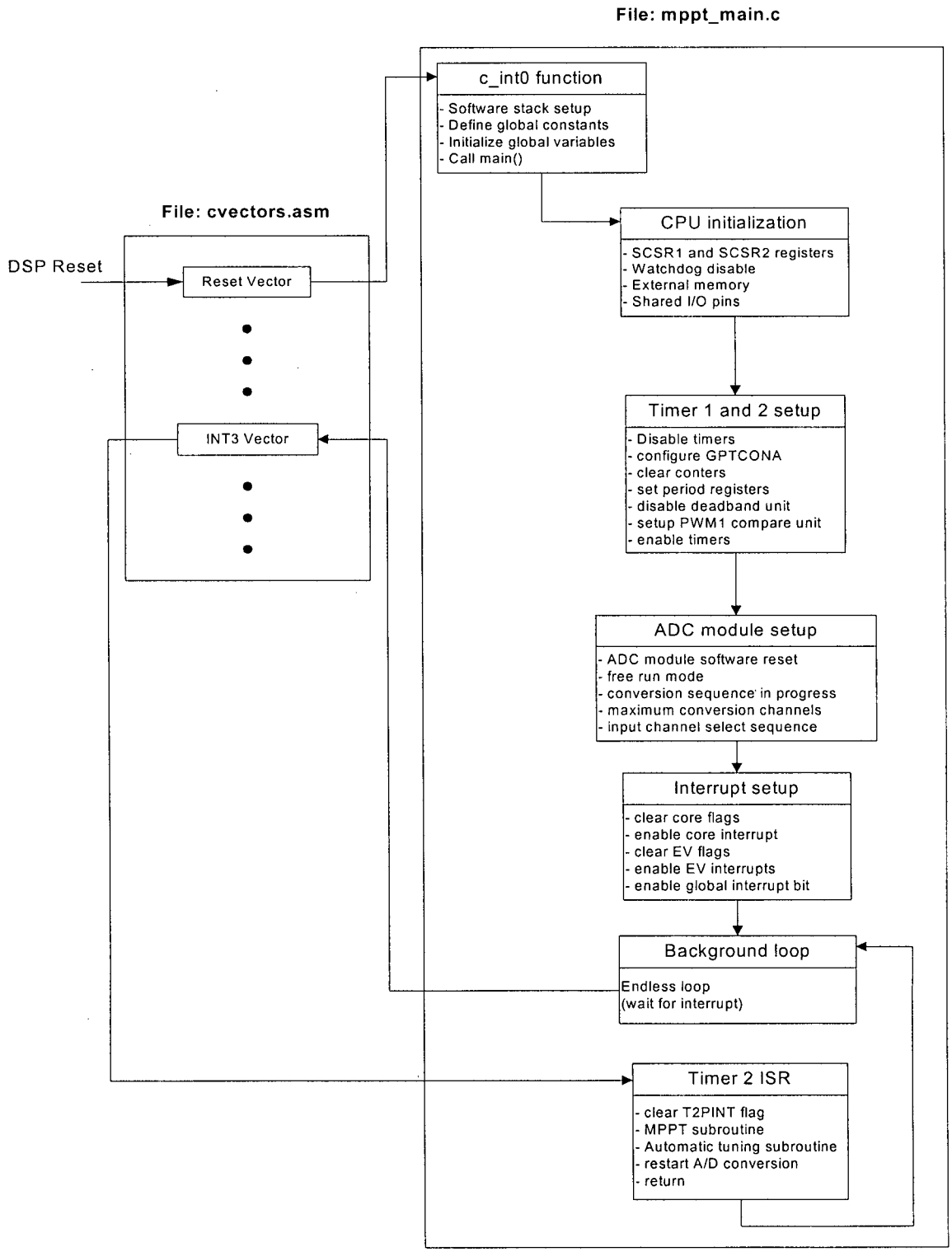

Figure 6.7 Diagram of Software Flow Chart

6.6 Experimental Test

According to the design, the MPPT system tests are carried out to verify the proposed control method.

6.6.1 Test Preparation

To compare the control performance between adaptive hill climbing (AHC) method and the proposed algorithm (MAHC), indoor PV testing using artificial light was first applied in the system test. Indoor testing has advantage in that the same reproducible light spectrum can be used. Therefore, this is a fair method because all MPPT control methods can be tested under the same (or very similar) operating conditions. The insolation can be kept constant. And the difference in photovoltaic device temperature between different experiments was also small. The benefits and drawbacks of artificial light applied in test are summarized in Table 6-5.

Table 6-5 Benefits and Drawbacks of Artificial Light Applied in PV System Test

Advantages	Disadvantages
• Very reproducible light source • Not subject to weather • Able to operate indoors • Good for MPPT performance comparison because test environment can be controlled	• Light spectrum is different from real sunlight • Difficult to give uniform light distribution over a PV panel • Usually not good for high power level test

In this test bed, the configuration of artificial light with PV panels was arranged as Figure 6.8. Three spotlights served as indoor light source. It is able to provide constant insolation to PV modules to create equal test environment for performance comparison.

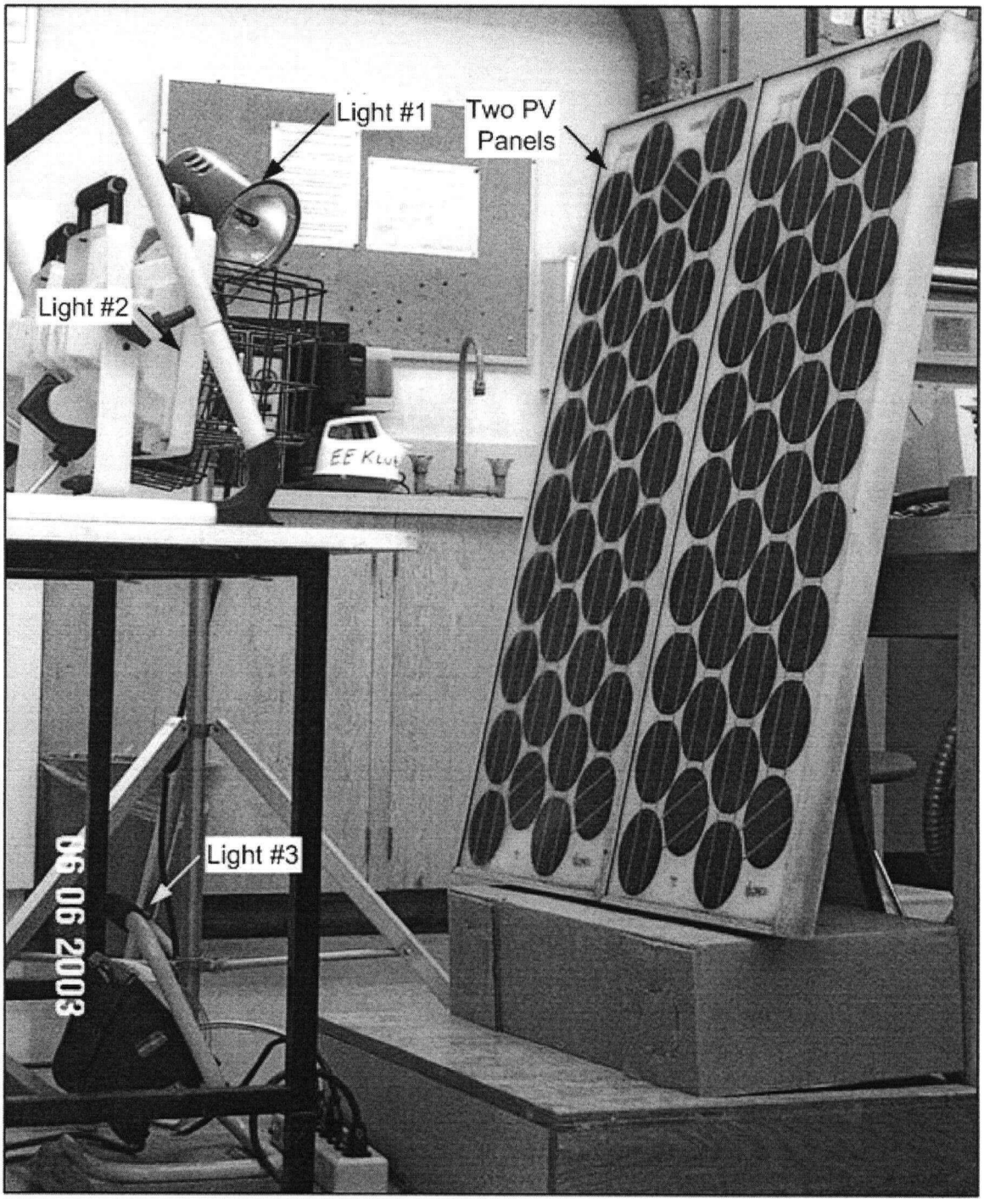

Figure 6.8 Indoor PV Testing Configuration with the Artificial Light as the Power Source

6.6.2 PV Power System Test Procedure

To record the test data accurately, LabVIEW was used as data acquisition system (DAQ). LabVIEW is a product of National Instruments Corporation. It is a graphical development environment specifically designed for measurement and automation applications. With data acquisition, the signals can be logged for a programmable certain period. In the test system, input voltage and output power of converter are two important signals to be monitored. The test procedure was organized as follows:

a) Install the test bed system with artificial lighting kits
b) Setup LabVIEW hardware and software as a DAQ system. The sampling frequency was set to 2 Hz.
c) Turn on the artificial light and monitor the surface temperature of PV panels
d) Implement the algorithm into controller
e) Set incremental step of duty cycle to certain value when AHC algorithm is applied
f) Do several dummy tests until the PV temperature becomes stable
g) Run test software to record the PV modules' output characteristics
h) Start the maximum power point tracking test
i) Record the data of input voltage, output voltage and output current for a certain period time with LabVIEW support
j) Monitor the waveforms of the voltage across diode and PV voltage with oscilloscope
k) Repeating this procedure for different algorithms

6.6.3 Test Results

To prove that the proposed algorithm and control law have better performance, both adaptive hill climbing (AHC) method and the modified adaptive hill climbing (MAHC) algorithm were tested under the same test environment.

6.6.3.1 Step Response Test using Artificial Lights

In this test, the insolation level was controlled constant with artificial lights. During this test, all the spotlights shown in Figure 6.8 were turned on. The test began when the cell temperature was stable.

First, the PV modules' output characteristics were measured. The test results were shown in Figure 6.9, Figure 6.10 and Figure 6.11. Figure 6.9 shows the *Current-Voltage* characteristic of the solar panels. Figure 6.10 illustrates the *Power-Voltage* feature. Figure 6.11 demonstrates the relationship of system output power and switching duty cycle of the buck converter. The recorded maximum power point is about 5.80W, which is clearly shown in Figure 6.10 and Figure 6.11.

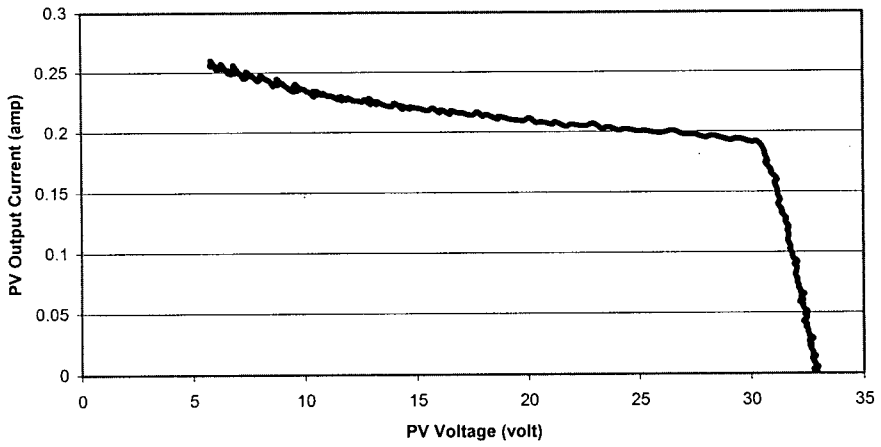

Figure 6.9 Current-Voltage Characteristics of PV Array 's Output Using the Artificial Lights as the Power Source

Second, the tracking performance with AHC control algorithm was test. The steady state performances vary with different values of incremental steps of duty cycle. Similar situations were also shown in simulation results. The experimental plots are shown in Figure B.1, Figure B.2, Figure B.3, Figure B.4, Figure B.5, Figure B.6, Figure B.7 and Figure B.8 of Appendix B.

Figure 6.12 and Figure 6.13 illustrate the tracking performance with MAHC control algorithm. Figure 6.12 illustrates the waveform of PV voltage during 4-minute tracking period. During the first 23.5 seconds, the PV voltage drops quickly to a level of about

30V, where it stabilizes. The plot also presents a detailed look at the signals of the PV voltage, which have the continuous oscillation of the operating point around the point of maximum operating point (V_{MPOP}). This continuous oscillation is fundamental to this kind of control algorithm. Figure 6.13 shows the actual output power signal of DC/DC buck converter. After 23.5 seconds, the output power level was tracked and maximized to about 5.71W, which is 98.45% of the peak power point 5.80W.

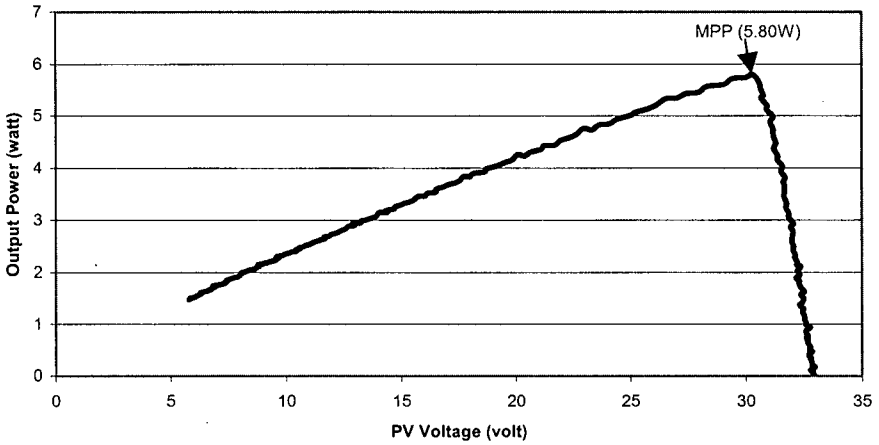

Figure 6.10 Power-Voltage Characteristics of PV Array 's Output By Using the Artificial Lights as the Power Source

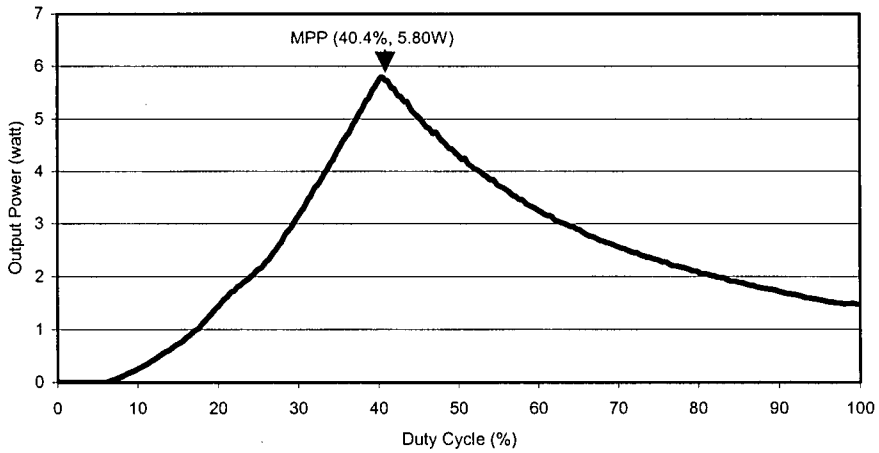

Figure 6.11 The Relationship of Output Power and Switching Duty Cycle of DC/DC Converter With the Artificial Lights as the Power Source

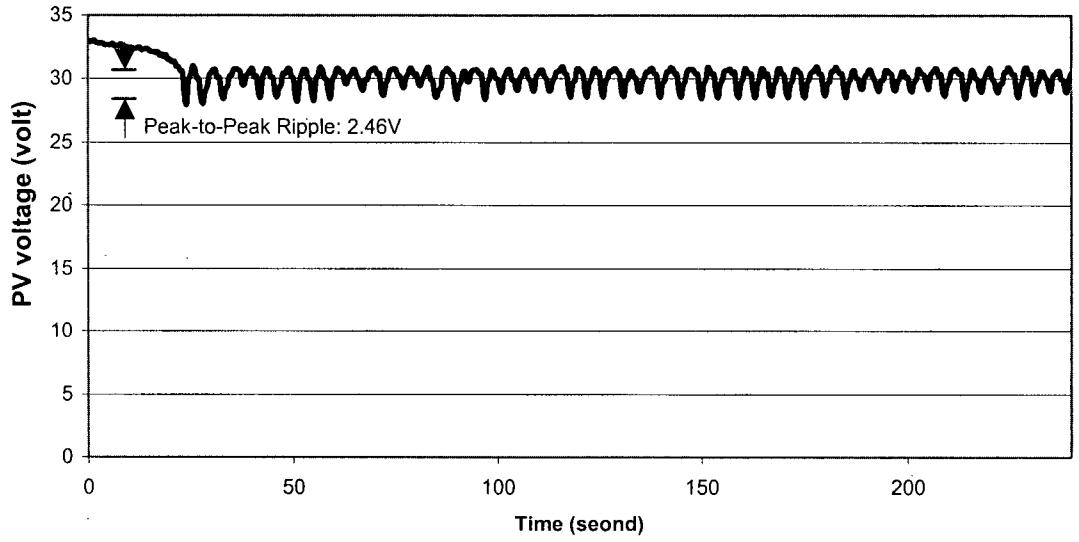

Figure 6.12 Experimental PV Voltage Waveform of MAHC Tracking By Using the Artificial Lights as the Power Source

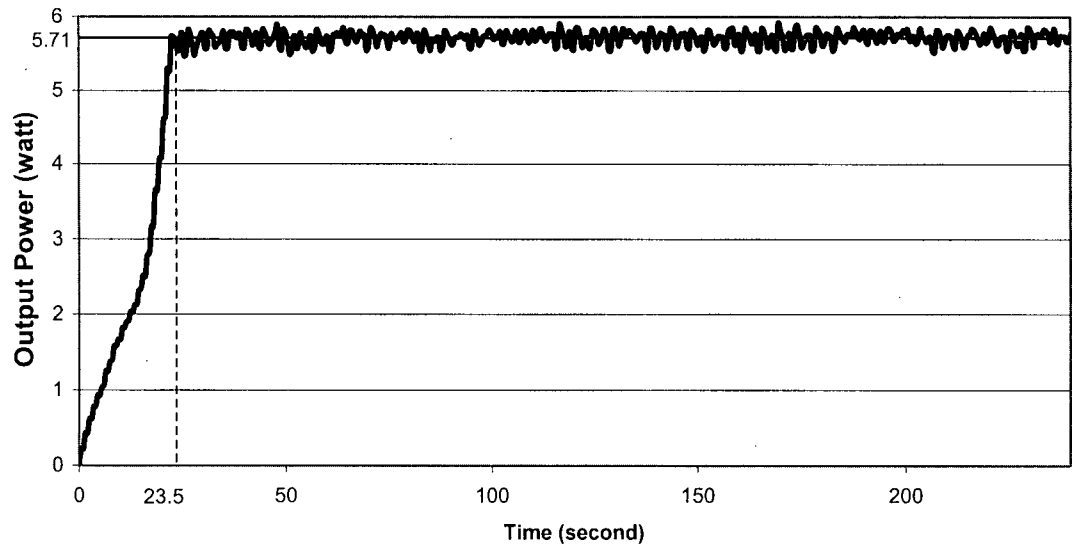

Figure 6.13 Experimental Output Power Waveform of MAHC Tracking Algorithm By Using the Artificial Lights as the Power Source

6.6.3.2 Dynamic Response Test using with Artificial Lights

In this test, the insolation was controlled in two different levels by switching on/off one of the three spotlights. The test schedule is illustrated in Figure 6.14. The initial condition is that all spotlights were turned on. This is called high insolation condition. After one and half minutes, the spotlight #1 shown in Figure 6.8 was turned off. This low insolation stage lasts one minute, until the high insolation returns by switching on spotlight #1 again. This test was designed for dynamic response evaluation.

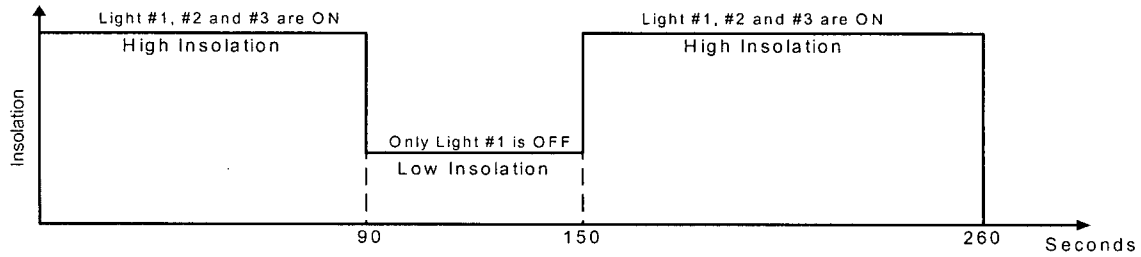

Figure 6.14 Insolation Switching Schedule By Turning ON/OFF the Spotlight

First, the PV modules' output characteristics were measured at the two levels of insolation. The test results were shown in Figure 6.15, Figure 6.16 and Figure 6.17. Figure 6.15 shows the *Current-Voltage* characteristic of the solar panels at two different insolation levels. Figure 6.16 illustrates the *Power-Voltage* feature. Figure 6.17 demonstrates the relationship of output power and switching duty cycle of the buck converter. The recorded maximum power point is about 5.83W at high-level insolation, and the value is around 2.37W at low insolation stage.

Second, the tracking performance with AHC control algorithm was tested. The dynamic response mainly depends on the selection of "a", the incremental step of duty cycle. The test results were shown in Figure B.9, Figure B.10, Figure B.11 and Figure B.12 of Appendix B.

Figure 6.18 and Figure 6.19 illustrate the dynamic tracking performance with MAHC control algorithm. Figure 6.18 illustrates the change of PV voltage during the controlled tracking period. Observation of the output power curves of the proposed system leads to graph shown in Figure 6.19. After the first 23.5 seconds, the PV voltage was stabilized to a level of about 30V, which represents the maximum power operating point. And the

output power stayed at 5.79W, which is 0.01W less than the recorded maximum power point. At the moment of 90 seconds, the insolation was switched to low level by turning off one spotlight. It took 16.5 seconds for the MAHC controller to detect the deviation from current MPOP and readjust the control variables to a new optimal level. The last insolation change happened at the moment of 150 seconds, when the spotlight was switched on again. The MAHC controller spent 6 seconds on re-capturing the new maximum power operating point at higher insolation level.

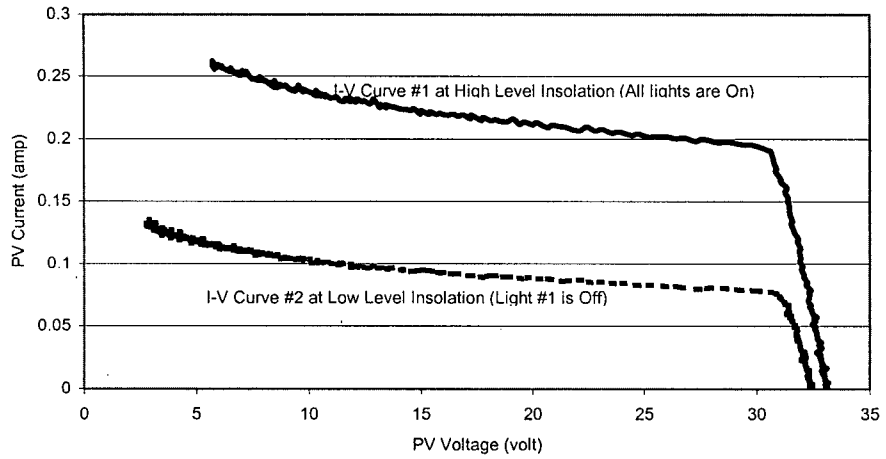

Figure 6.15 Experimental Current-Voltage Relationships of PV Array Output By Using the Artificial Lights as the Power Source

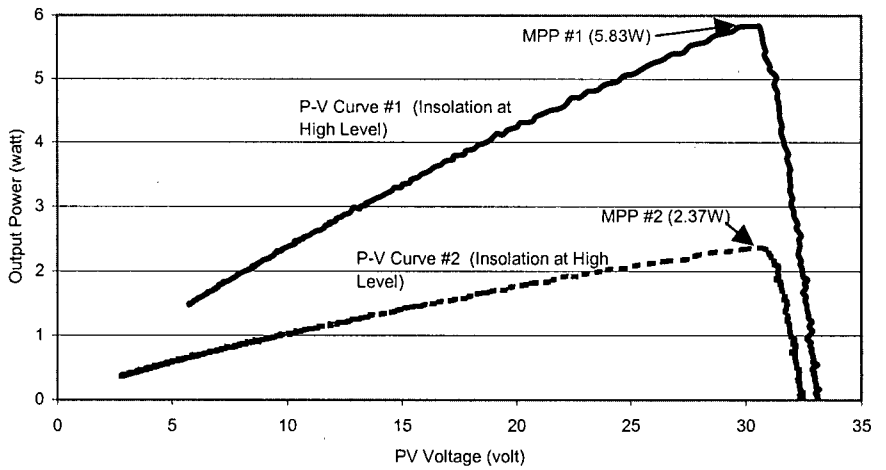

Figure 6.16 Experimental Power-Voltage Relationships of PV Array Output By Using the Artificial Lights as the Power Source

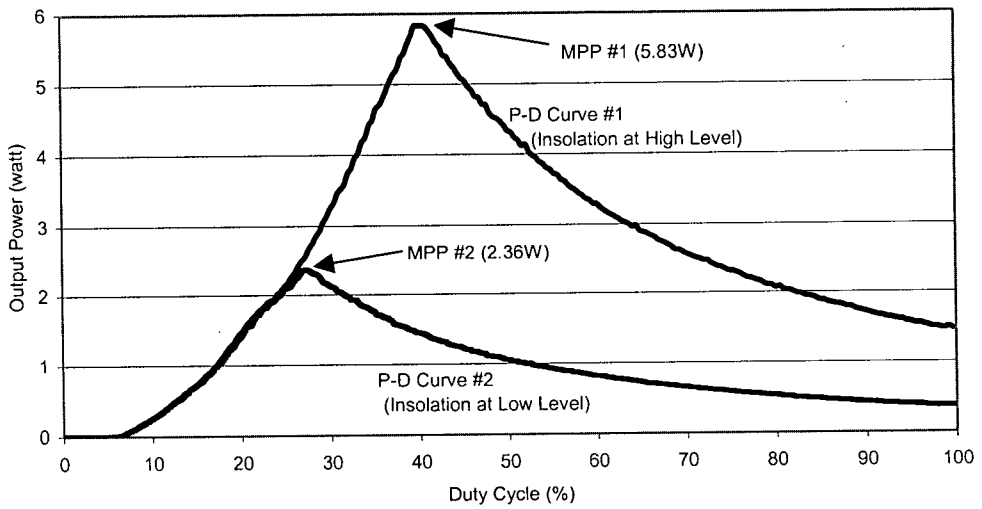

Figure 6.17 The Relationship of Output Power and Switching Duty Cycle of DC/DC Converter By Using the Artificial Lights as the Power Source

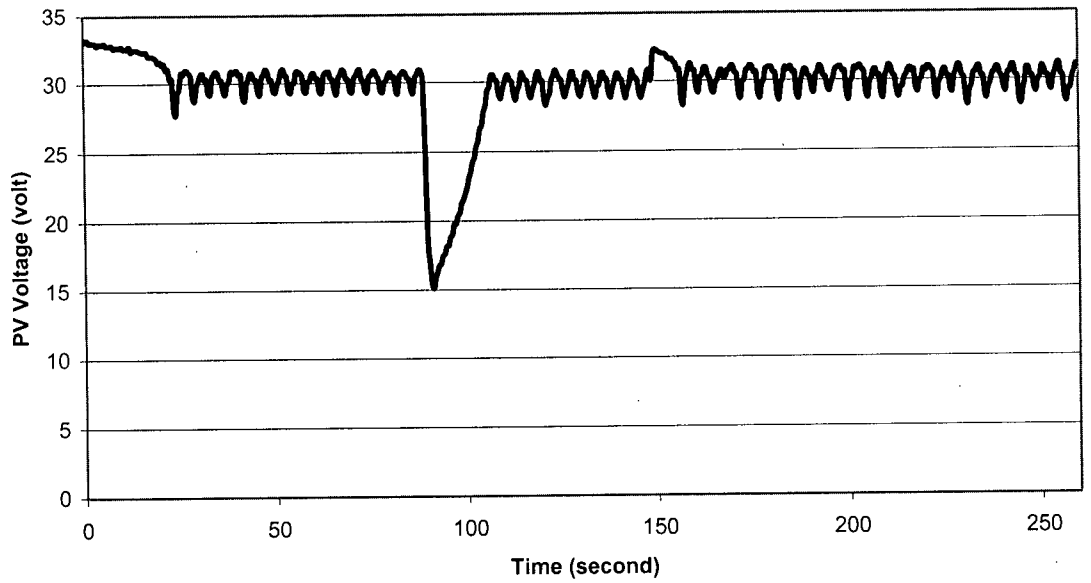

Figure 6.18 Experimental PV Voltage Waveform of MAHC Tracking Method By Using the Artificial Lights as the Power Source

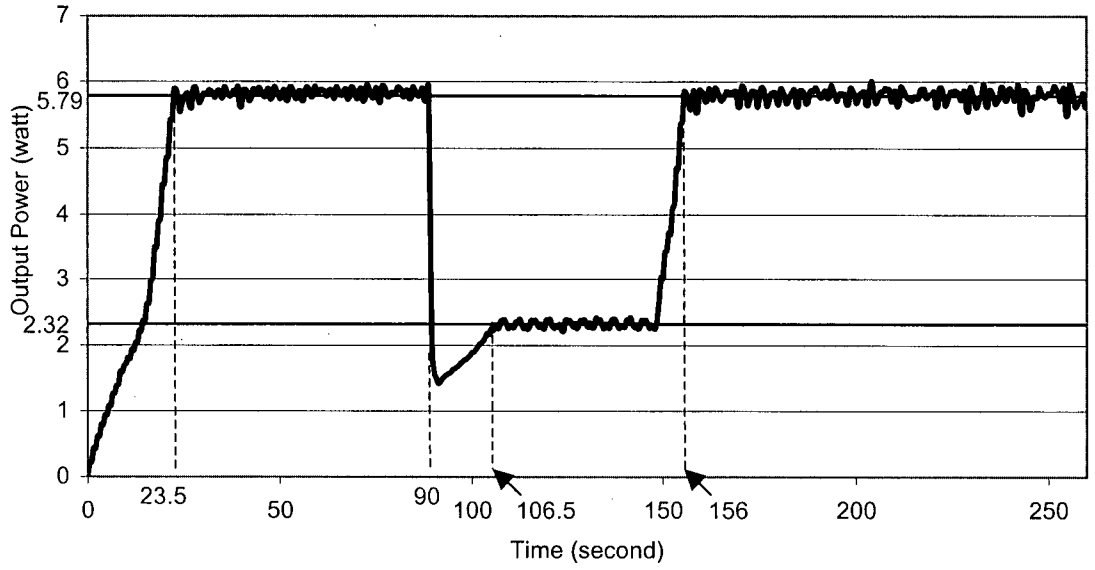

Figure 6.19 Experimental Output Power Waveform of MAHC Tracking Method By Using the Artificial Lights as the Power Source

6.6.3.3 10-minute Sunlight Test

The validity of the proposed MAHC controller was examined in natural solar insolation for 10 minutes. These tests were done from 3:00PM to 3:30PM in June 11, 2003. The weather condition is partially cloudy with 19°C in temperature.

First, the PV modules' output characteristics were measured. The test results were shown in Figure 6.20, Figure 6.21 and Figure 6.22. Figure 6.20 shows the *Current-Voltage* characteristic of the solar panels. Figure 6.21 illustrates the *Power-Voltage* feature. Figure 6.22 demonstrates the relationship of output power and switching duty cycle of the buck converter. The recorded maximum power point is 32.33W, which is clearly marked in Figure 6.21 and Figure 6.22.

Figure 6.23 and Figure 6.24 illustrate the tracking performance with MAHC control algorithm. Figure 6.23 illustrates the change of PV voltage during 10-minute tracking period. Figure 6.24 shows the output power curve. It is noticed that the PV voltage curve was kept almost constant due to steady maximum power operating point. The output power varied in a small range because of minor insolation change. The averaged value of

delivered power is 33.02W, which is 99.04% of the recorded maximum power level. Figure 6.25 shows the waveforms of PV voltage and voltage signals across the diode of DC/DC buck converter, which was captured by a two-channel oscilloscope.

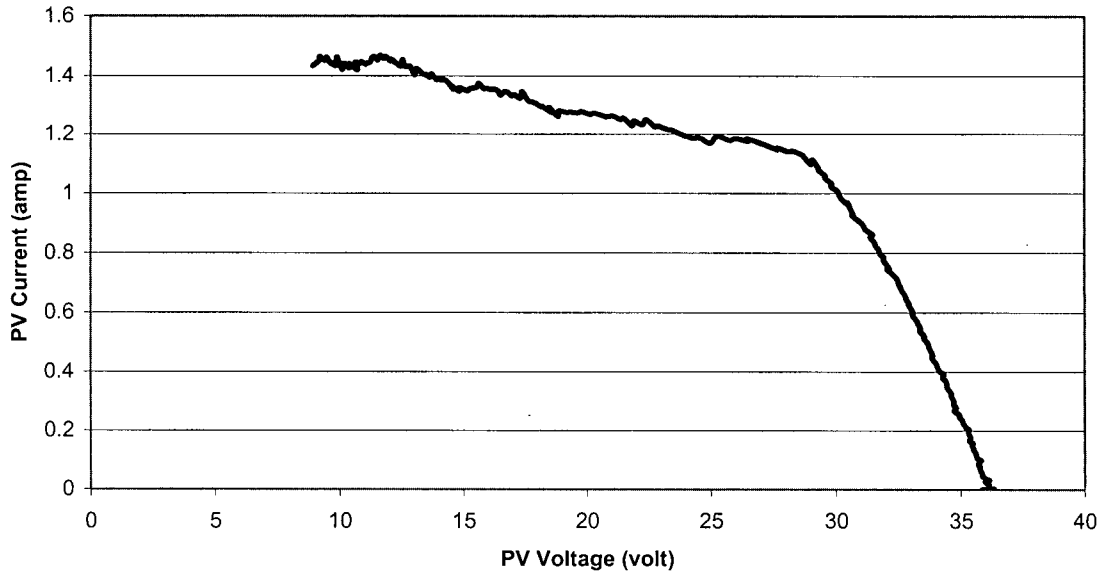

Figure 6.20 Experimental Current-Voltage Curve of PV Output In Natural Sunlight

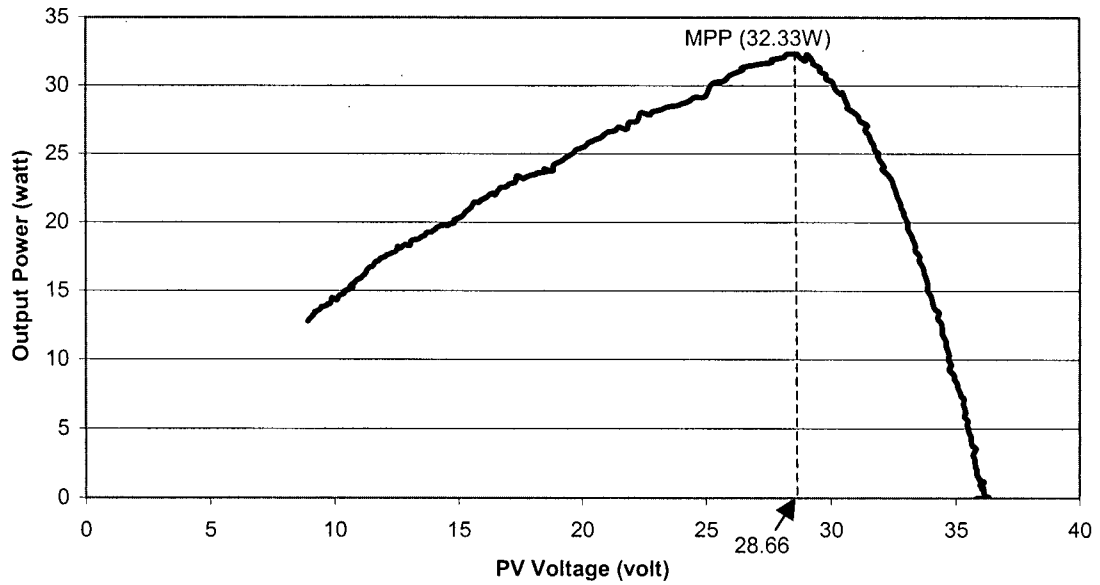

Figure 6.21 Experimental Power-Voltage Curve of PV Output In Natural Sunlight

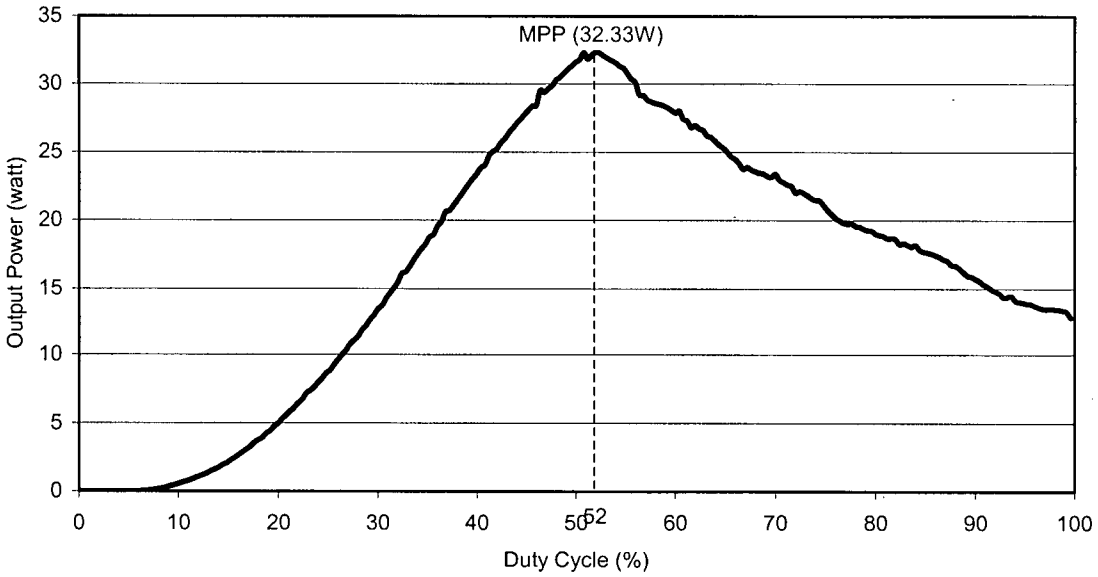

Figure 6.22 The Relationship Curve of Output Power and Switching Duty Cycle of DC/DC Converter By Using Natural Sunlight as the Power Source

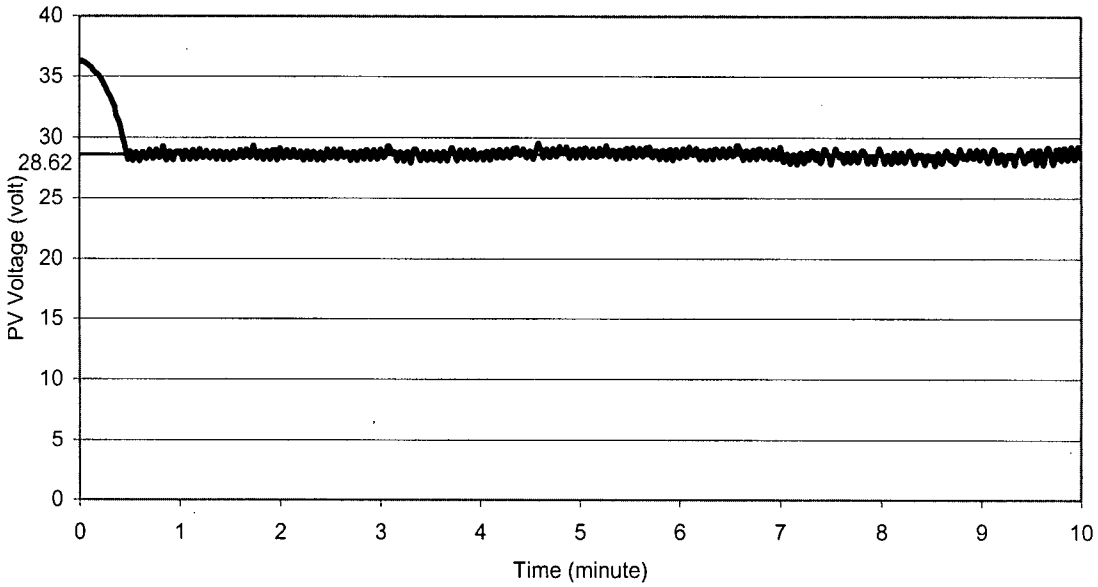

Figure 6.23 Experimental PV Voltage Waveform of MAHC Tracking Algorithm By Using Natural Sunlight as the Power Source

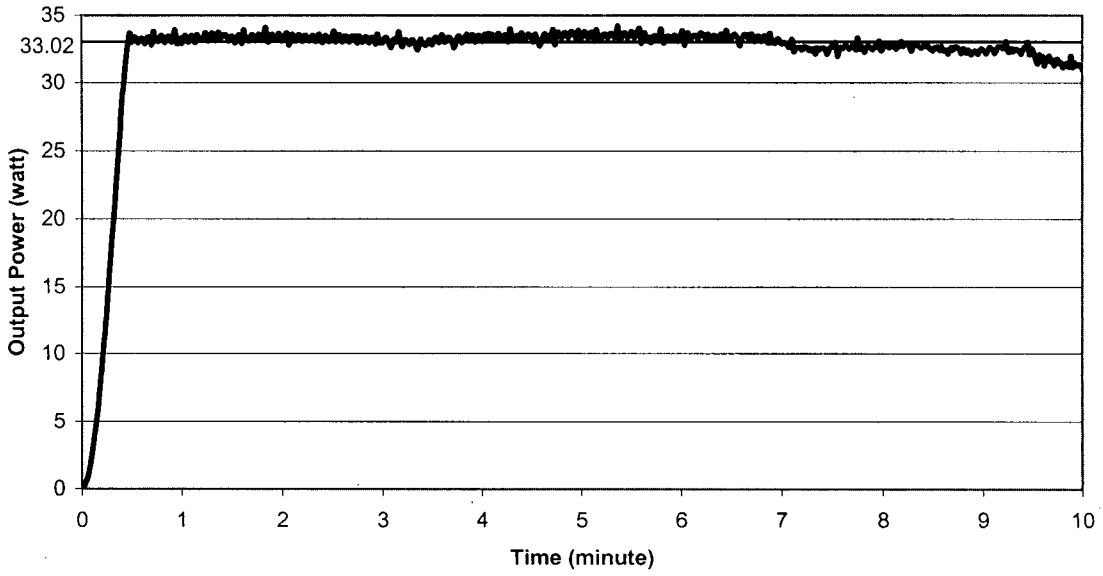

Figure 6.24 Experimental Output Power Waveform of MAHC Tracking Algorithm By Using Natural Sunlight as the Power Source

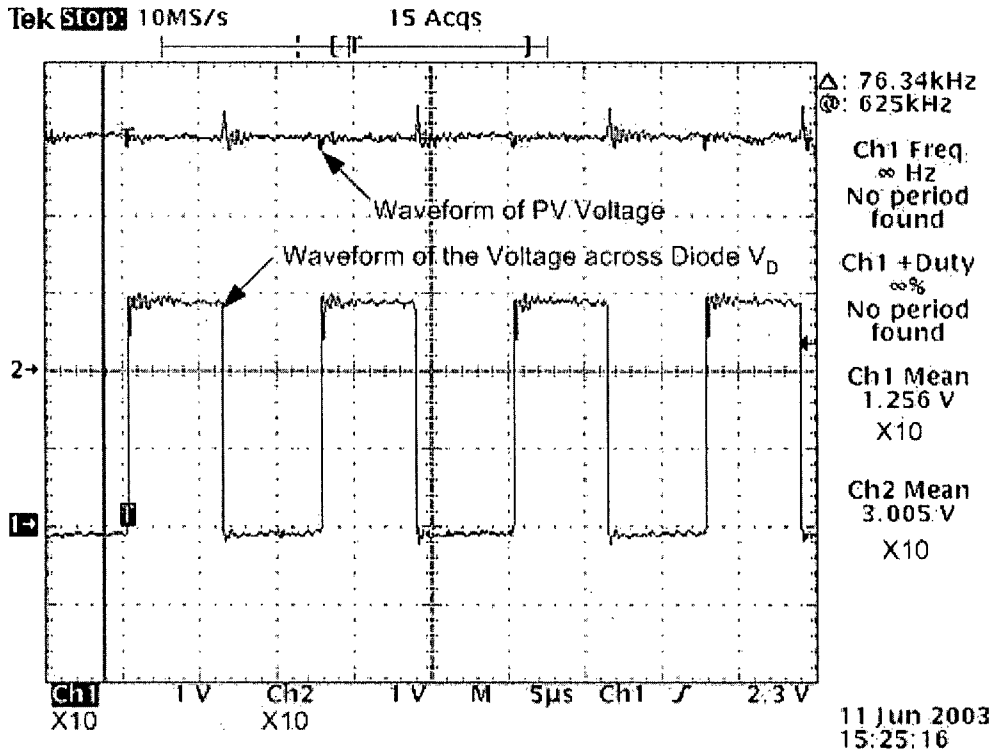

Figure 6.25 Voltage Waveforms Captured by Oscilloscope During MAHC-PV System Test In Natural Sunlight

6.6.4 Data Analysis

The performance comparison between AHC and MAHC algorithm is based on steady-state performance and dynamic response.

6.6.4.1 Step Response Performance

The PV Voltage ripple level, average delivered power and steady-state error during steady state period are summarized in Table 6-6. The values of 100% rise time that represents the speed of response of a control system were also illustrated. It is noticed that AHC controller with small incremental step of duty cycle demonstrates very good steady state performance. The MAHC control shows similar steady state performance as the AHC when the incremental step of duty cycle was equal to 1.2% (a = 1.2%), but the tracking speed is 5 seconds faster. These results show the system controlled by the modified adaptive hill climbing control algorithm can provide better steady-state performance than the traditional AHC algorithm without loss of dynamic response.

Table 6-6 Comparison of Step Response Performance

Control Algorithm	*Peak-to-Peak Ripple Level of PV Voltage (volt)*	*Average Output Power (watt)*	*Steady State Error (watt)*	*100% Rise Time (second)*
AHC (a = 0.8%)	1.75	5.75	0.05	39.5
AHC (a = 1.2%)	2.33	5.70	0.10	28.5
AHC (a = 1.6%)	2.13	5.61	0.19	20.5
AHC (a = 2%)	4.70	5.54	0.27	16.5
MAHC	2.46	5.71	0.09	23.5

6.6.4.2 Dynamic Response

During the test of dynamic response, insolation levels were changed in three regions. First, the insolation was switched from zero to high level. Second, the insolation level was switched from high to low by switching off one spotlight. The third one is that the insolation level was switched back to high by turning on the light #1. So there are three rise times were recorded. The experimental waveforms of MAHC control algorithm were shown in Figure 6.18 and Figure 6.19. The comparison results were summarized in Table 6-7. Although AHC with large value of incremental step of duty cycle gives better

dynamic response, it shows large steady-state error shown in Figure B.11 and Figure B.12 of Appendix B. The AHC with small value of incremental step of duty cycle shows better steady state performance, but tracking speed is slow. These features are illustrated in Figure B.9 and Figure B.10. These statistical results prove MAHC shows better performance in dynamic response without losing steady state performance. This is because MAHC automatically adjusts the incremental step to satisfy the requirements of both fast dynamic response and good steady-state.

Table 6-7 Comparison of Tracking Time

Control Algorithm	*Region I (High Insolation)*		*Region II (low Insolaiton)*		*Region III (high Insolation)*	
	First 100% Rise Time (second)	*Average Output Power (watt)*	*Second 100% Rise Time (second)*	*Average Output Power (watt)*	*Third 100% Rise Time (second)*	*Average Output Power (watt)*
AHC (a = 0.8%)	39.5	5.80	20	2.35	14	5.80
AHC (a = 1.2%)	28.5	5.78	16.5	2.32	10.5	5.78
AHC (a = 1.6%)	21.5	5.73	14	2.30	10	5.73
AHC (a = 2%)	16.5	5.71	10	2.28	5	5.71
MAHC	23.5	5.79	16.5	2.32	6	5.79

Chapter 7 Conclusions

The output characteristics of photovoltaic array are nonlinear and changed with cell temperature and solar irradiation. Maximum power point tracking control in the design of PV systems is essential to draw peak power from solar array to meet the load requirement. So the efficiency, dynamic and steady-state characteristics of PV power systems are chiefly influenced by the performance of MPPT controllers.

In this thesis, different techniques followed in tracking the maximum power point of PV arrays were investigated and analyzed. The comparison of some major algorithms is summarized in Appendix A. The simple tracking method, adaptive hill climbing, uses the fact that PV output power has direct relationship with the switching mode DC/DC converter's switching duty ratio. In general, this simple control algorithm has difficulty in providing good performances on both tracking stages and steady-state stages, because a constant value is applied to the control parameter. Furthermore, in some cases the controller can make wrong decision to move the operating point far from the maximum power point instead of close to it. A modified maximum power point tracking algorithm, MAHC, which is proposed in Chapter 4, was further developed based on the previous research and detailed analysis of the characteristics of PV power systems. Automatic tuning on parameter and control mode switching were implemented in the proposed control method. The improved tracking performance of this method was verified through computer simulation and experimental test. By comparing the experimental performances, shown in Table 6-6, the MAHC control shows 10% better steady state performance than the AHC when the incremental step of duty cycle was equal to 1.2% (a = 1.2%), and the tracking speed is 17.5% faster.

Mathematical models were used to simulate the PV array in the evaluation of the algorithms performances under rapid varying atmospheric conditions in the time domain. The proposed experimental system utilizing a step down converter based on a DSP control was constructed and the experimental tests were carried out. The simulation and experiment results show different performance between traditional adaptive hill climbing MPPT control algorithm and the proposed MPPT control algorithm. The tracking

efficiency of the MAHC algorithm was confirmed by bother simulation and experimental results.

7.1 Limitations on Simulation Method

The control algorithms were evaluated with SIMULINK® based on mathematical models of the PV array and ideal DC/DC buck converter. There is no doubt that simulation on the PV module can show similar output characteristics with the effect of insolation and temperature. But the mathematical model used, which is represented by a current source in parallel with an ideal p-n junction, provides limited parameters for tuning to simulate the real features about different kind of PV products. Furthermore, switching mode DC/DC converters are non-linear systems with high switching frequencies comparing to their large values of inherent time constants. In this thesis, the modeling is based on state variable averaging modeling method, which was introduced in section 2.3.2. Its validity is restricted to the small-signal, low-frequency-domain, and continuous conduction mode. The dynamic analysis of switching dc-dc converters can also be performed using the discrete time domain method, which is widely used in computer simulation. But the time domain simulation requires a heavy numerical computation, which has to be carried out for each switching cycle.

7.2 Limitations on Parameter Tuning

In practical digital embedded control systems, the resolution of PWM duty cycle is limited by the capability of microcontroller or DSP. These limitations come from the system clock, the PWM timer size and the requirement of switching frequency on power converters.

7.3 Temperature Effect

Besides insolation, another important factor influencing the characteristics of a photovoltaic array is the cell temperature (shown in Figure 2.5 and Figure 3.1). The variation of cell temperature primarily depends on the insolation level, environmental temperature and cell conducting loss. Since a sudden increase or decrease in temperature

usually seldom happen and a minor variation of cell temperature does not influence the PV output power dramatically, both the system simulation and experiment don't show the impact of temperature on this PV power system. In reality, the continuous solar radiation on PV cells' surface and conduction through photovoltaic cells will cause a gradual increase in cell temperature. This will reduce the PV output power and shift the maximum power operating points to different values until a thermal balance is reached. The power feedback MPPT methods are usually good enough to deal with this slow variation. During the system test, it was noticed that the open-circuit voltage of the PV array was about 35.9 volt at the beginning of test with turning on all artificial lights and the voltage was reduced and stabilized to about 33 volt after several cycle tests. So all the experimental data were recorded only after several dummy tests until a balanced and almost identical testing environment is created.

7.4 Future Study

In this thesis, the parameter-tuning index was represented by a simple linear equation. In reality, this relation is non-linear. This is why a limited tuning range was selected. Fuzzy logic or other non-linear tuning solution may be applied in the future for more effective on-line tuning. More accurate modeling methods for the PV module and DC/DC switching mode converter will be another challenge to achieve improved simulation results. A programmable PV simulator will be very helpful for further study in this area.

References

[1] Gaia Energy Centre Web Site, http://www.gaiaenergy.co.uk/exhibition/solar.htm

[2] Sustainable Energy Technologies web site, http://www.sustainableenergy.com/SET-FAQ/SET-FAQPV.html

[3] FSEC Web site, http://www.fsec.ucf.edu/pvt/pvbasics/

[4] DayStar Technologies Web Sit, http://www.daystartech.com/whatpv.htm

[5] Anca D.Hansen, Poul Sorensen, Lars H. Hansen and Henrik Bindner, "Models for a Stand-Alone PV System", *Technical Report of Riso National Laboratory*, Roskilde, December 2000

[6] Underwriters Laboratories, Inc., *UL Standard 1703, Flat-Plate Photovoltaic Modules and Panels*, Northbrook, IL, 1993

[7] "Switching Regulators", http://www.national.com/appinfo/power/files/f5.pdf, pp. 34-35

[8] Walt Kester, and Brian Erisman, "SWITCHING REGULATORS", http://www.analog.com/UploadedFiles/Associated_Docs/, pp. 10-15.

[9] R. D. Middlebrook, and S. Cuk, "A General Unified Approach to Modeling Switching-Converter Power Stages", *Records of IEEE Power Electronics Specialists Conference - 1976*, pp. 18-34.

[10] D.P. Hohm and M.E. Ropp, "Comparative study of maximum power point tracking algorithms using an experimental, programmable, maximum power point tracking test bed", *Conference Records of the Twenty-Eighth IEEE Photovoltaic Specialists Conference*, vol.1, Sept. 2000, pp. 1699 –1702

[11] Yongji, H. and Deheng, L., "A new method for optimal output of a solar cell array", *Proceedings of the IEEE International Symposium on Industrial Electronics*, vol.1, May 1992, pp. 456 –45

[12] Hannes Knopf, *Analysis, Simulation, and Evaluation of Maximum Power Point Tracking (MPPT) Methods For A solar Powered Vehicle*, Master's Thesis, Electrical and Computer Engineering, Portland State University, 1999

[13] H.D Maheshappa, J. Nagaraju, and M.V. Krishna Murthy, "An improved maximum power point tracker using a step-up converter with current locked loop", *Renewable Energy*, vol.13, 1998, no.2, pp.195-201

[14] W. Swiegers and J.H.R. Enslin, "An integrated maximum power point tracker for photovoltaic panels", *Proceedings of IEEE International Symposium on Industrial Electronics* (ISIE '98), vol.1, July 1998, pp. 40 –44

[15] Lyon van de Merwe, Gawie J. van de Merwe, "Maximum power point tracking-implementation strategies", Proceedings of 1998 IEEE International Symposium on Industrial Electronics (ISIE'98), vol.1, 1998, pp. 214-217

[16] Chihchiang Hua and Chihming Shen, "Study of maximum power tracking techniques and control of DC/DC converters for photovoltaic power system", *Records of 29t IEEE Power Electronics Specialists Conference* (PESC'98), vol. 1, May 1998, pp. 86 –93

[17] H.E.-S.A. Ibrahim, F.F. Houssiny, H.M.Z. El-Din, and M.A. El-Shibini, "Microcomputer controlled buck regulator for maximum power point tracker for DC pumping system operates from photovoltaic system", *Proceedings of 1999 IEEE International Fuzzy Systems Conference* (FUZZ-IEEE '99), vol. 1, Aug. 1999, pp. 406 –411

[18] A.M.A. Mahmoud, H.M. Mashaly, S.A. Kandil, H. El Khashab, and M.N.F. Nashed, "Fuzzy logic implementation for photovoltaic maximum power tracking", *Proceedings of 9th IEEE International Workshop on Robot and Human Interactive Communication*, Sept. 2000, pp. 155 –160

[19] C.R. Sullivan and M.J. Powers, "A high-efficiency maximum power point tracker for photovoltaic arrays in a solar-powered race vehicle", *Proceedings of 24th IEEE Power Electronics Specialists Conference* (PESC '93), vol.1, June 1993, pp. 574 –580

[20] Chihchiang Hua, Jongrong Lin, and Chihming Shen, "Implementation of a DSP-controlled photovoltaic system with peak power tracking", *IEEE Transactions on Industrial Electronics*, vol. 45, no. 1, Feb. 1998, pp. 99 –107

[21] Mao-Lin Chiang, Chih-Chiang Hua, and Jong-Rong Lin, "Direct power control for distributed PV power system", *Proceedings of 2002 Power Conversion Conference* (PCC-Osaka 2002), vol.1, April 2002, pp. 311 –315

[22] K.H. Hussein, I. Muta, T. Hoshino, and M. Osakada, "Maximum photovoltaic power tracking: an algorithm for rapidly changing atmospheric conditions", *IEE Proceedings on Generation, Transmission and Distribution,* vol. 142, no. 1, Jan. 1995, pp. 59 –64

[23] Chih-Chiang Hua and Jong-Rong Lin, "Fully digital control of distributed photovoltaic power systems", *Proceedings of IEEE International Symposium on Industrial Electronics* (ISIE 2001), vol. 1, June 2001, pp. 1-6

[24] J.H.R. Enslin "Maximum power point tracking: a cost saving necessity in solar energy systems", *Proceedings of 16th Annual Conference of IEEE Industrial Electronics Society* (IECON'90), vol.2, Nov. 1990, pp. 1073 –1077

[25] T. Senjyu and K. Uezato, "Maximum power point tracker using fuzzy control for photovoltaic arrays", *Proceedings of the IEEE International Conference on Industrial Technology*, vol.1, Dec. 1994, pp. 143 –147

[26] E. Koutroulis, K. Kalaitzakis, and N.C. Voulgaris, "Development of a microcontroller-based, photovoltaic maximum power point tracking control system", *IEEE Transactions on Power Electronics*, vol. 16, no.1, Jan. 2001, pp. 46 –54

[27] S.S.M. Wolf and J.H.R. Enslin, "Economical, PV maximum power point tracking regulator with simplistic controller", *Proceedings of 24th IEEE Power Electronics Specialists Conference* (PESC '93), vol.1, June 1993, pp. 581 –587

[28] Ziyad M. Salameh, Fouad Dagher, and William A. Lynch, "Step-down maximum power point tracker for photovoltaic systems", *Solar Energy*, Vol.1, 1991, pp279-282

[29] J.H.R. Enslin and D.B. Snyman, "Simplified feed-forward control of the maximum power point in PV installations", *Proceedings of the 1992 International Conference on Power Electronics and Motion Control*, vol.1, Nov. 1992, pp. 548 –553

[30] M. Veerachary, T. Senjyu, K. Uezato, "Voltage-based maximum power point tracking control of PV system'', *IEEE Transactions on Aerospace and Electronic Systems*, vol. 38, no. 1, Jan. 2002, pp. 262 –270

[31] N. Kasa, T. Iida, G. Majumdar, "Robust control for maximum power point tracking in photovoltaic power system", *Proceedings of the 2002 Power Conversion Conference* (PCC-Osaka 2002), vol.2, April 2002, pp. 827 –832

[32] N. Patcharaprakiti, and S. Premrudeepreechacharn, "Maximum power point tracking using adaptive fuzzy logic control for grid-connected photovoltaic system", *Proceedings of 2002 IEEE Power Engineering Society Winter Meeting*, vol. 1, Jan. 2002, pp. 372 –377

[33] Sun Xiaofeng, Wu Weiyang, Wang Baocheng, and Wei Xiaogui, "A research on photovoltaic energy controlling system", *Proceedings of the Fifth International Conference of Electrical Machines and Systems* (ICEMS 2001), vol.1, Aug. 2001, pp. 542 –545

[34] Xiaofeng Sun, Weiyang Wu, Xin Li, and Qinglin Zhao, "A research on photovoltaic energy controlling system with maximum power point tracking", *Proceedings of the 2002 Power Conversion Conference* (PCC-Osaka 2002), vol.2, April 2002, pp. 822 –826

[35] Clarence W. De Silva, *Robot Control Sensors and Actuators*, Prentice Hall, January 1989, pp.30

[36] Xantrex Technology Grid Tie Web Site, http://tracegridtie.com/products/gridtie/suntie.html

[37] Spectrum Digital Inc., *eZdsp™ LF2407 Technical Reference*, August 2001

[38] Kirk Zurell, *C Programming for Embedded Systems: Apply C to 8-Bit Microprocessors for Efficient Development,* R&D Books, March 2000

Appendix A. Summary of Major MPPT Control Techniques

MPPT Algorithms	VOLTAGE FEEDBACK METHOD	POWER FEEDBACK METHOD		
		Perturbation and Observation method (P&O)	*Incremental Conductance Method (IncCond)*	*Adaptive Hill Climbing Method (AHC)*
Principle	• Regulating PV array voltage to an 'optimal' level • Voltage feedback control	• Keep dP/dV =0 • Discrete solution	• Keep dP/dV = 0 • dI/dV=-I/V • Control mode switching • Digital solution	• Keep dP/dD = 0 (D is switching duty cycle of converter or inverter) • Digital solution
Advantage	• Simple feedback structure • Easy to implement • Analog control is available	• Simple • Easy to implement	• Good tracking performance during sudden environment change • Improved steady state performance	• Stability • Simple • Easy to implement
Disadvantage	• Tracking is not accurate	• Difficult to balance the performance trade-off between steady-state and dynamic response • Some tracking problems on sudden change on insolation	• More complicated mechanism • Some tuning issues	• Difficult to balance the performance trade-off between steady-state and dynamic response • Some tracking problems on sudden change on insolation

Appendix B. Additional Experimental Plots

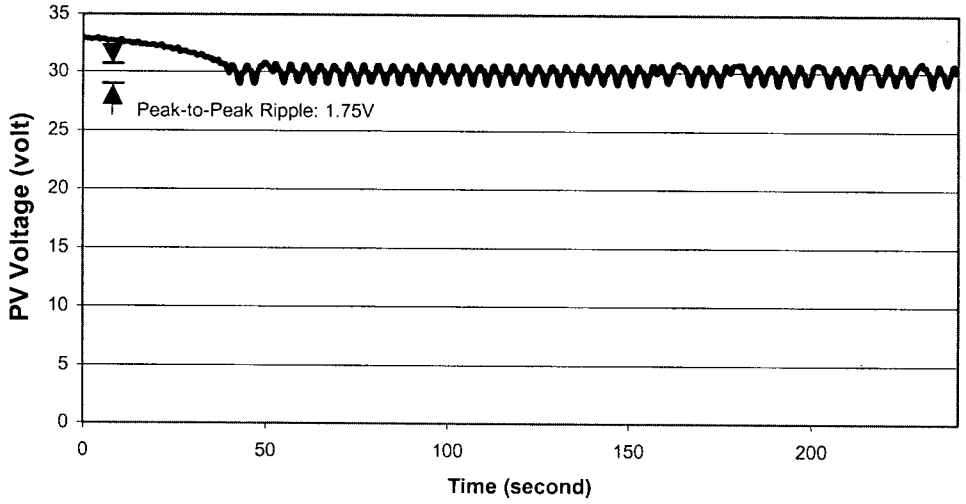

Figure B.1 Experimental PV Voltage Waveform of AHC Tracking Algorithm with a = 0.8%

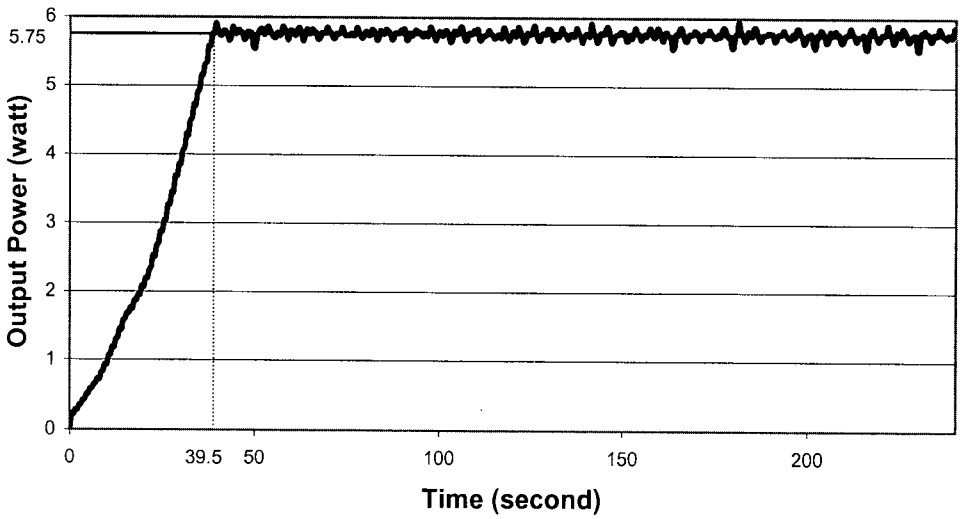

Figure B.2 Experimental Output Power Waveform of AHC Tracking Algorithm with a = 0.8%

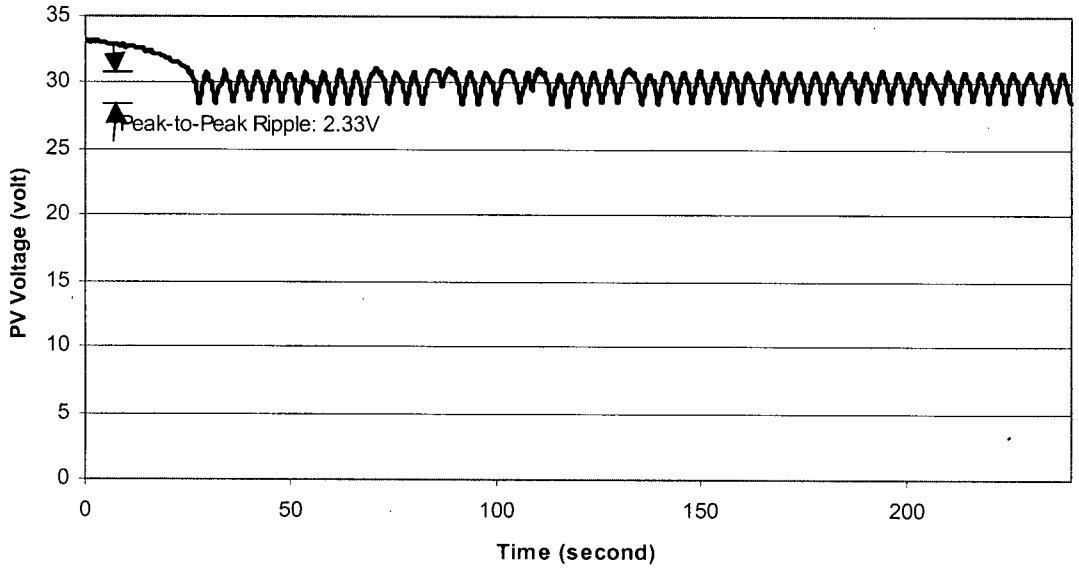

Figure B.3 Experimental PV Voltage Waveform of AHC Tracking Algorithm with a = 1.2%

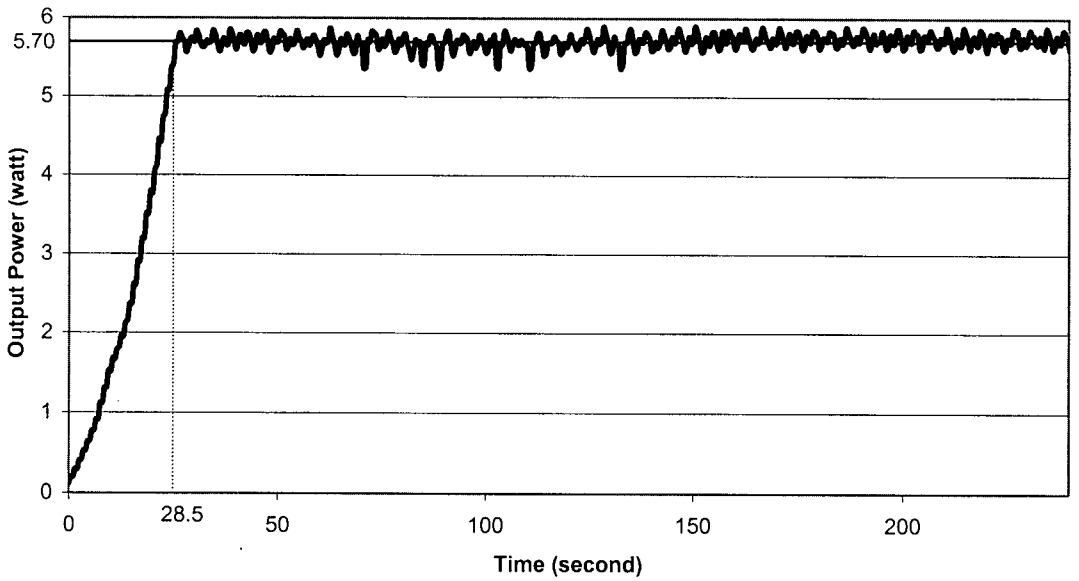

Figure B.4 Experimental Output Power Waveform of AHC Tracking Algorithm with a = 1.2%

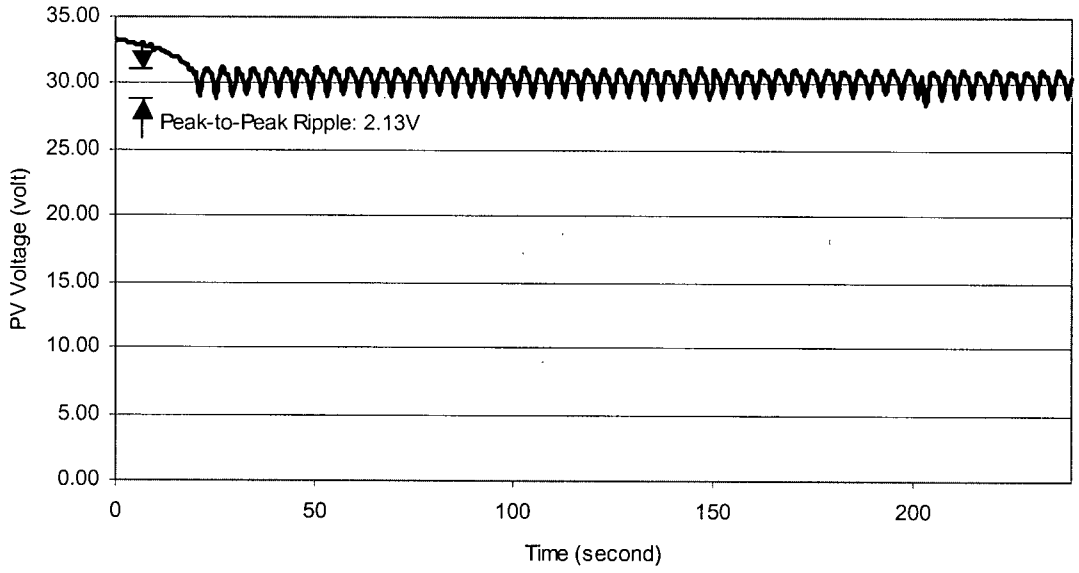

Figure B.5 Experimental PV Voltage Waveform of AHC Tracking Algorithm with a = 1.6%

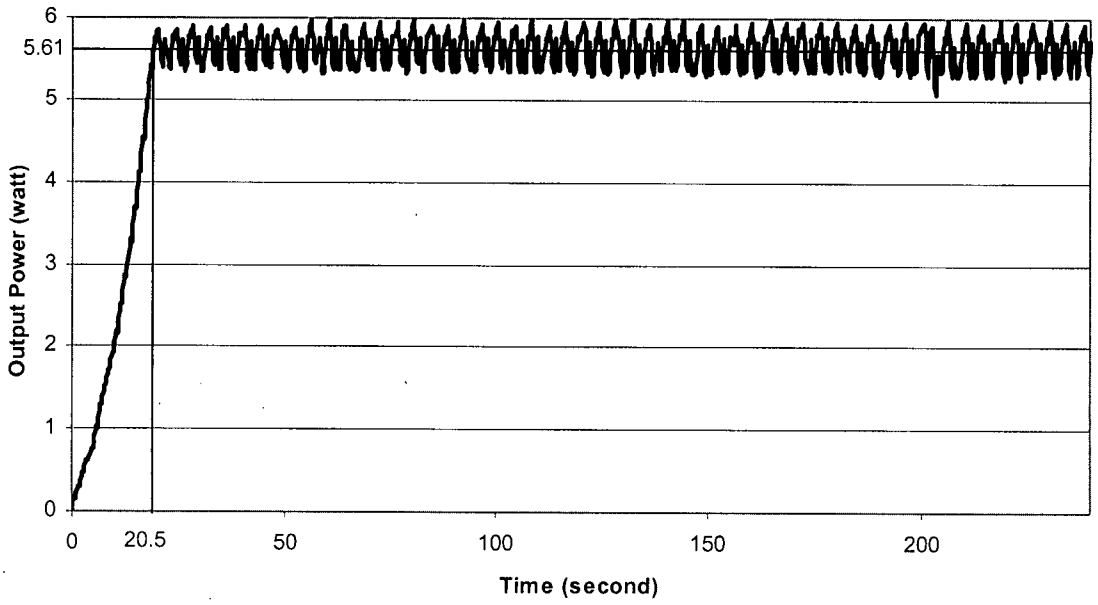

Figure B.6 Experimental Output Power Waveform of AHC Tracking Algorithm with a = 1.6%

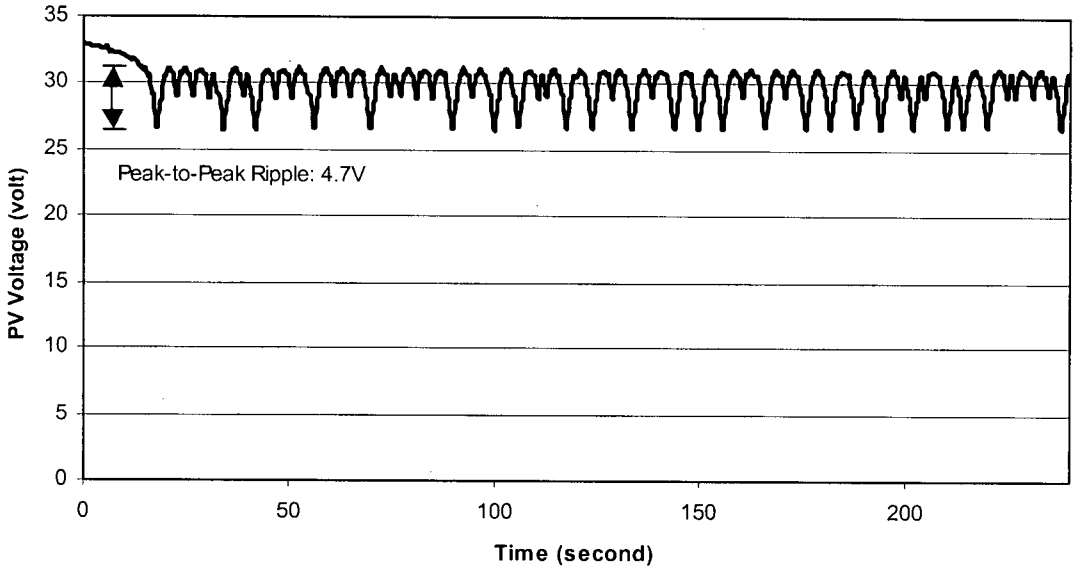

Figure B.7 Experimental PV Voltage Waveform of AHC Tracking Algorithm with a = 2.0%

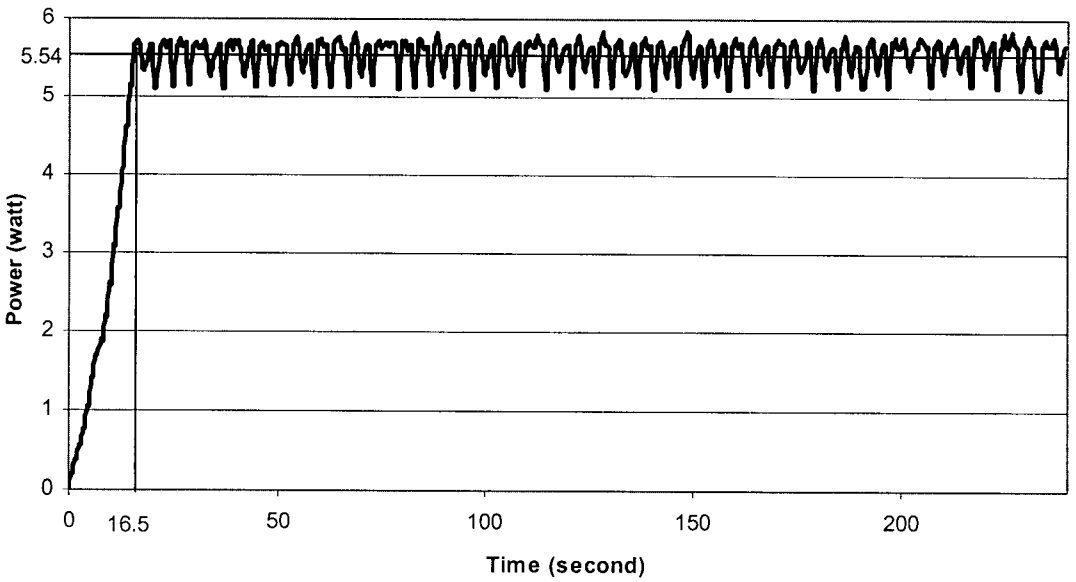

Figure B.8 Experimental Output Power Waveform of AHC Tracking Algorithm with a = 2.0%

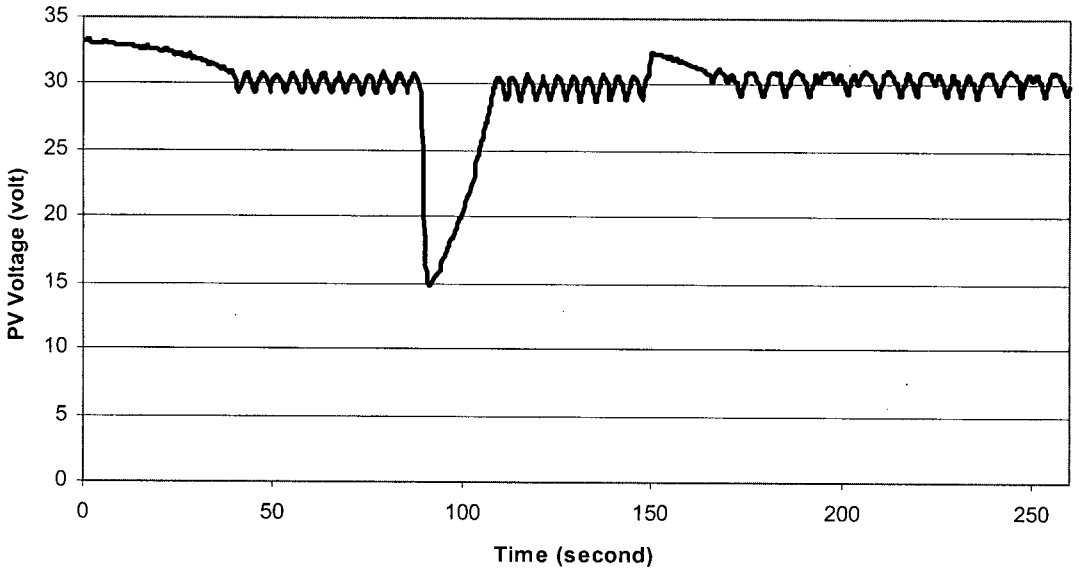

Figure B.9 Experimental PV Voltage Waveform of AHC Tracking Algorithm with a = 0.8%

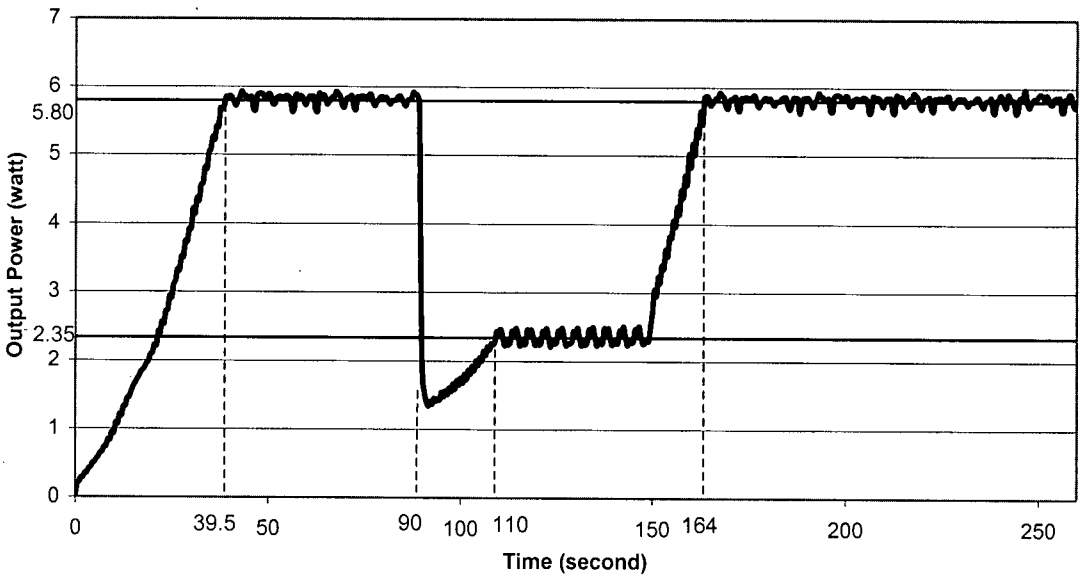

Figure B.10 Experimental Output Power Waveform of AHC Tracking Algorithm with a = 0.8%

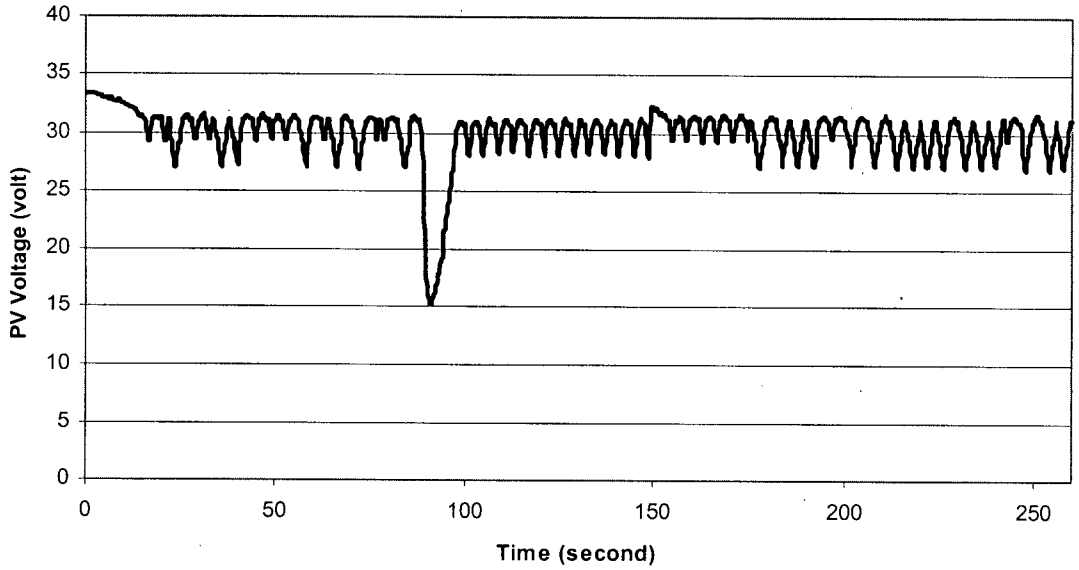

Figure B.11 Experimental PV Voltage Waveform of AHC Tracking Algorithm with a = 2.0%

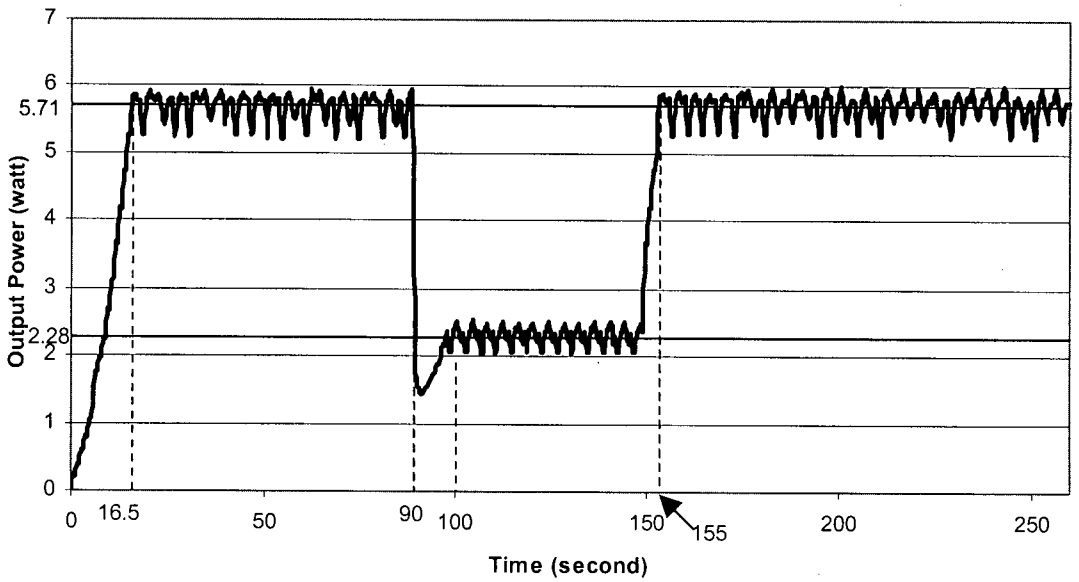

Figure B.12 Experimental Output Power Waveform of AHC Tracking Algorithm with a = 2.0%